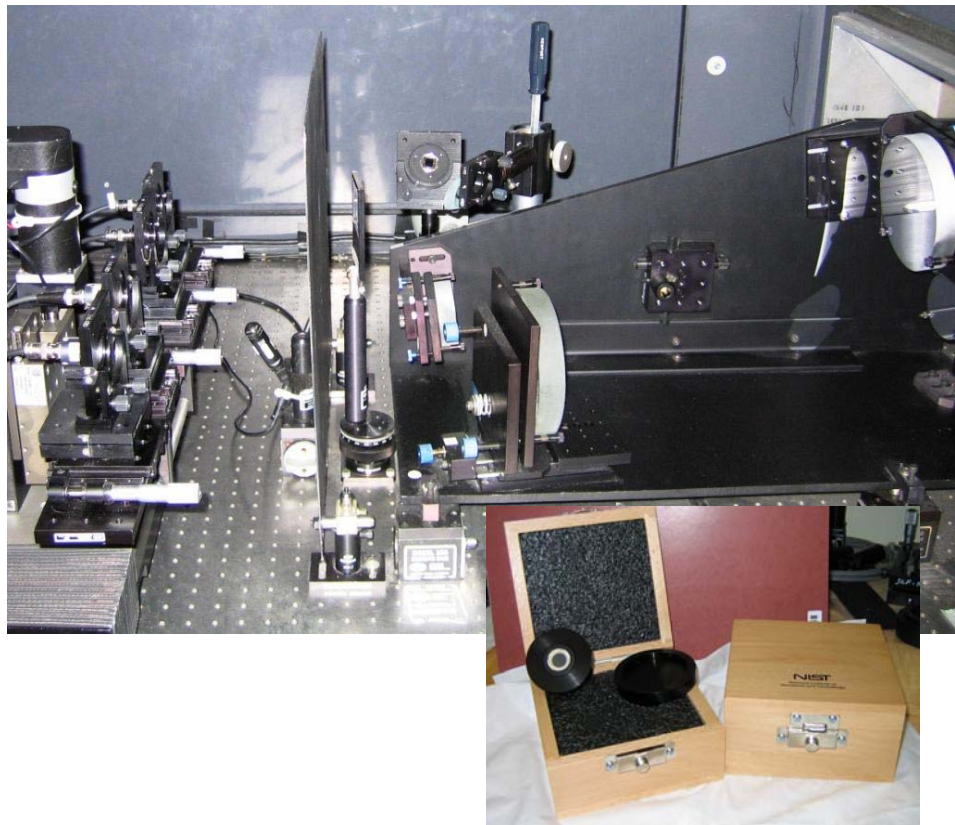


NIST Special Publication 250-41 (2008)

Spectroradiometric Detector Measurements: Ultraviolet, Visible, and Near-Infrared Detectors for Spectral Power

Thomas C. Larason
Jeanne M. Houston



NIST Special Publication 250-41 (2008)

**Spectroradiometric Detector
Measurements:
Ultraviolet, Visible, and Near-Infrared
Detectors for Spectral Power**

Thomas C. Larason
Jeanne M. Houston
*Optical Technology Division
Physics Laboratory
National Institute of Standards and Technology
Gaithersburg, MD 20899-8441*

Supersedes NIST Special Publication 250-41 (1998)

Revised October 2008



U.S. Department of Commerce
Carlos M. Gutierrez, Secretary

National Institute of Standards and Technology
Patrick Gallagher, Deputy Director

Certain commercial entities, equipment, or materials may be identified in this document in order to describe an experimental procedure or concept adequately. Such identification is not intended to imply recommendation or endorsement by the National Institute of Standards and Technology, nor is it intended to imply that the entities, materials, or equipment are necessarily the best available for the purpose.

National Institute of Standards and Technology Special Publication 250-41
Natl. Inst. Stand. Technol. Spec. Publ. 250-41, 119 pages (October 2008)
CODEN: NSPUE2

Preface

The calibration and related measurement services of the National Institute of Standards and Technology (NIST) are intended to assist the makers and users of precision measuring instruments in achieving the highest possible levels of accuracy, quality, and productivity. NIST offers over 300 different calibrations, special tests, and measurement assurance services. These services allow customers to directly link their measurement systems to measurement systems and standards maintained by NIST. NIST offers these services to the public and private organizations alike. They are described in NIST Special Publication (SP) 250, *NIST Calibration Services Users Guide*.

The Users Guide is supplemented by a number of Special Publications (designated as the “SP 250 Series”) that provide detailed descriptions of the important features of specific NIST calibration services. These documents provide a description of the: (1) specifications for the services; (2) design philosophy and theory; (3) NIST measurement system; (4) NIST operational procedures; (5) assessment of the measurement uncertainty including random and systematic errors and an error budget; and (6) internal quality control procedures used by NIST. These documents will present more detail than can be given in NIST calibration reports, or than is generally allowed in articles in scientific journals. In the past, NIST has published such information in a variety of ways. This series will make this type of information more readily available to the user.

This document, SP 250-41 (2008), NIST Measurement Services: Spectroradiometric Detector Measurements, is a revision of SP250-41 (1998). It covers the calibration and special test of spectral radiant power responsivity for photodetectors from 200 nm to 1800 nm (Service ID numbers 39071S - 39081S in SP 250, NIST Calibration Services Users Guide). Inquiries concerning the technical content of this document or the specifications for these services should be directed to the authors or to one of the technical contacts cited.

NIST welcomes suggestions on how publications such as this might be made more useful. Suggestions are also welcome concerning the need for new calibration services, special tests, and measurement assurance programs.

Belinda L. Collins
Director
Technology Services

Katharine B. Gebbie
Director
Physics Laboratory

Abstract and Key Words

The National Institute of Standards and Technology supplies calibrated photodiode standards and special tests of photodetectors for spectral radiant power responsivity for the wavelengths from 200 nm to 1800 nm. The scale of spectral radiant power responsivity is based solely on detector measurements traceable to the Primary Optical Watt Radiometer (POWR), the reference absolute cryogenic radiometer maintained by the National Institute of Standards and Technology's Optical Technology Division. Solid-state transfer standard detectors are used to transfer the optical power unit, the optical watt, from this cryogenic radiometer to working standard detectors used in monochromator-based facilities where routine measurements are performed. A description of current measurement services is given along with the procedures, equipment, and techniques used to perform these calibrations. Detailed estimates and procedures for determining the uncertainties of the reported values are also presented.

Key Words: calibration; detector; measurement; photodiode; photodetector; power responsivity; quantum efficiency; radiometry; spectral; standard; uncertainty

TABLE OF CONTENTS

1. INTRODUCTION.....	1
2. NIST SPECTRORADIOMETRIC DETECTOR MEASUREMENT SERVICE.....	4
2.1 Description of Measurement Services	4
2.2 Measurement Limitations	7
2.3 How to Order Calibrations.....	8
2.4 Technical Contacts.....	9
3. MEASUREMENT THEORY	10
3.1 Measurement Equation	10
3.1.1 Approximations.....	13
3.2 Substitution Method.....	15
3.2.1 General Substitution Method.....	15
3.2.2 Photodetector Substitution.....	16
3.2.3 Substitution Method with Monitor	17
3.2.4 Measurement Equation Applied to the SCFs.....	17
4. EQUIPMENT DESCRIPTION	20
4.1 Visible to Near-Infrared Spectral Comparator Facility (Vis/NIR SCF).....	20
4.1.1 Vis/NIR Source and Input Optics	21
4.1.2 Vis/NIR Monochromator	22
4.1.3 Vis/NIR Shutter and Output Optics	22
4.1.4 Vis/NIR Translation Stages - Detector Positioning.....	22
4.1.5 Vis/NIR Working Standards.....	22
4.1.6 Beam Splitter and Monitor Detector.....	23
4.1.7 Alignment Lasers	23
4.1.8 Enclosure	23
4.2 Ultraviolet Spectral Comparator (UV SCF)	23
4.2.1 UV Source and Input Optics.....	24
4.2.2 UV Monochromator.....	25
4.2.3 UV Shutter and Output Optics.....	25
4.2.4 UV Translation Stages - Detector Positioning.....	25
4.2.5 UV Working Standards.....	25
4.2.6 Beam Splitter and Monitor Detector.....	26
4.2.7 Alignment Lasers	26
4.2.8 Enclosure	26
4.3 Electronics	26
4.3.1 Electronics - Signal Measurement	26
4.3.2 Electronics - Auxiliary Equipment	28
5. SPECTRAL POWER RESPONSIVITY SCALE REALIZATION.....	29
5.1 The Spectral Power Responsivity Scale Measurement Chain	29
5.2 Cryogenic Radiometry	30
5.3 Calibration of Transfer Standards with a Cryogenic Radiometer.....	32
5.4 Calibration of the Working Standards	35

5.4.1	Calibration of the Visible Si Working Standards (Vis WS)	36
5.4.2	Calibration of the Ultraviolet Working Standards (UV WS)	37
5.4.3	Calibration of the Near-IR InGaAs Working Standards (IGA WS)	38
6.	CALIBRATION PROCEDURES AND COMPUTER AUTOMATION	40
6.1	Spectral Radiant Power Responsivity	40
6.1.1	Calibration Procedures	40
6.1.2	Quantum Efficiency	42
6.2	Spatial Uniformity	43
6.2.1	Measurement Method and Calibration Procedure	44
6.2.2	Limitations	46
6.3	Computer Automation	47
6.3.1	Computer Automated Equipment	47
6.3.2	Computer Calibration Programs	49
7.	UNCERTAINTY EVALUATION	51
7.1	Uncertainty Calculation from the Measurement Equation	51
7.2	Uncertainty Components in Test Detector Calibration	53
7.2.1	Wavelength Uncertainty of the Monochromator	54
7.2.2	Effect of Bandpass	54
7.2.3	Ambient Temperature	56
7.2.4	Long-term Stability	56
7.2.5	Measurement Reproducibility	57
7.2.6	DVM Uncertainty	57
7.2.7	Spectral Stray-light	57
7.2.8	Other Components	58
7.3	Transfer from Cryogenic Radiometer to Working Standards	59
7.3.1	Visible Silicon Working Standards (Vis WS) Uncertainty	59
7.3.2	Near-Infrared InGaAs Working Standards (IGA WS) Uncertainty	61
7.3.3	Ultraviolet Silicon Working Standards (UV WS) Uncertainty	63
7.4	Transfer from Working Standards to Customer Detectors	65
7.4.1	UV Silicon Customer Detector Example Uncertainty	67
7.4.2	Visible Silicon Customer Detector Example Uncertainty	68
7.4.3	Near-Infrared Customer Detector Example Uncertainties	70
7.4.4	Filtered Detector Example Uncertainty (Photometer)	76
7.5	Spatial Uniformity Measurement Uncertainty	78
8.	QUALITY SYSTEM	79
8.1	Control Charts	79
8.2	Interlaboratory Comparisons	80
8.2.1	CCPR K2.a (NIR) 900 nm to 1650 nm	81
8.2.2	CCPR K2.b (Visible) 400 nm to 950 nm	81
8.2.3	CCPR K2.c (UV) 200 nm to 450 nm	82
8.3	Changes in the Spectral Power Responsivity Scale	82
8.3.1	UV Scale (200 nm to 500 nm)	82
8.3.2	Visible Scale (350 nm to 1100 nm)	83
8.3.3	NIR Scale (700 nm to 1800 nm)	84

9.	CHARACTERISTICS OF PHOTODIODES AVAILABLE FROM NIST	85
9.1	Hamamatsu S1337-1010BQ	85
9.2	Hamamatsu S2281	87
9.3	OSI Optoelectronic UV-100	87
9.4	Detector Mounting Fixture Mechanical Drawings	89
10.	FUTURE WORK	91
11.	ACKNOWLEDGMENTS	92
12.	REFERENCES.....	93
APPENDIX A: SAMPLE CALIBRATION REPORT		A-1
APPENDIX B: BIBLIOGRAPHY		B-1

LIST OF FIGURES

Figure 2.1. The expanded uncertainties ($k = 2$) for spectral power responsivity measurements.....	5
Figure 3.1. The geometry for detector spectral power responsivity measurements	11
Figure 3.2. Block diagram of photodetector substitution method	16
Figure 3.3. Block diagram of photodetector substitution method with monitor.....	17
Figure 4.1. Visible to Near-Infrared Spectral Comparator Facility (Vis/NIR SCF)	20
Figure 4.2. The spectral power typically incident on the detectors	21
Figure 4.3. Ultraviolet Spectral Comparator Facility (UV SCF).....	24
Figure 4.4. Electronic block diagram of the Vis/NIR SCF.....	27
Figure 4.5. NIST SCF precision transimpedance (I/V) amplifier circuit	27
Figure 5.1. Calibration chain for the spectral power responsivity measurements.....	29
Figure 5.2. The construction of the NIST Primary Optical Watt Radiometer (POWR).....	31
Figure 5.3. The NIST L-1 ACR used in Spectral Irradiance and Radiance Responsivity Calibrations using Uniform Sources (SIRCUS).....	31
Figure 5.4. Comparison of POWR and the L-1 ACR measurements	32
Figure 5.5. Trap detector arrangement of photodiodes.....	33
Figure 5.6. Optical configuration for the SIRCUS facility.....	34
Figure 5.7. SIRCUS laser wavelengths used to calibrate the transfer standards.....	35
Figure 5.8. The calibration chain for the visible working standards (Vis WS).....	36
Figure 5.9. The calibration chain for the ultraviolet working standards (UV WS).....	37
Figure 5.10. The calibration chain for the InGaAs working standards (IGA WS).....	38
Figure 5.11. The 1999 calibration chain for the InGaAs working standards (IGA WS).....	39
Figure 6.1. Typical signals from Hamamatsu S1337 and monitor photodiodes.....	41
Figure 6.2. Spectral responsivities of typical Si, InGaAs, and Ge photodiodes.....	42
Figure 6.3. Quantum efficiencies of typical Si, InGaAs, and Ge photodiodes.....	43
Figure 6.4. Spatial uniformities of typical Hamamatsu S1337 and S2281 photodiodes	45
Figure 6.5. Spatial uniformities of typical OSI Optoelectronics UV-100 and EG&G Judson Ge photodiodes	46
Figure 6.6. Vis/NIR SCF computer control block diagram.....	48
Figure 7.1. Error due to effect of bandpass for UV photodiode	55
Figure 7.2. Visible WS uncertainty	61
Figure 7.3. Near-Infrared IGA WS uncertainty.....	63
Figure 7.4. Ultraviolet WS uncertainty.....	64
Figure 7.5. Combined uncertainties for spectral power responsivity working standards.....	66
Figure 7.6. Example customer UV Si photodiode uncertainty	68
Figure 7.7. Example customer Si photodiode uncertainty.....	70
Figure 7.8. Example customer InGaAs photodiode uncertainty.....	73
Figure 7.9. Example customer TE cooled Ge photodiode uncertainty	75

Figure 7.10. Example customer photometer uncertainty	77
Figure 8.1. Control chart example for a NIST Visible Working Standard (Vis WS).....	80
Figure 8.2. NIST difference from KCRV in CCPR K2.b (Visible) Key Comparison	81
Figure 8.3. Change in the UV spectral power responsivity scale (UV WS) from 2001 to 2005 and expanded uncertainty ($k = 2$)	82
Figure 8.4. Change in the visible spectral power responsivity scale (Vis WS) from 2005 to 2006 and expanded uncertainties ($k = 2$).....	83
Figure 8.5. Change in the NIR spectral power responsivity scale (IGA WS) from 1999 to 2006 and expanded uncertainties ($k = 2$).....	84
Figure 8.6. Change in the NIR spectral power responsivity scale (Ge WS) from 1996 to 1999 and expanded uncertainties ($k = 2$).....	84
Figure 9.1. Temperature coefficient of silicon Hamamatsu S1226 and S1337 photodiodes.....	86
Figure 9.2. Linearity of Hamamatsu S1337-1010BQ at 633 nm.....	86
Figure 9.3. Linearity of UDT Sensors UV100 at 442 nm.....	88
Figure 9.4. Responsivity dependence on bias voltage of UDT Sensors UV100 at 442 nm	88
Figure 9.5. Mechanical diagram of OSI Optoelectronics UV-100 and Hamamatsu S2281 mounting fixture	89
Figure 9.6. Photograph of a sample NIST issued photodiode in mounting fixture, cap, and wooden storage box.....	90

LIST OF TABLES

Table 2.1. NIST spectroradiometric detector measurement services	4
Table 2.2. NIST spectral power responsivity relative expanded ($k = 2$) uncertainties for typical UV, visible, and NIR photodiodes.	5
Table 7.1 Uncertainty components in photodetector calibration.....	53
Table 7.2. Visible working standard uncertainty (transfer from Vis Trap and Ge TS).....	60
Table 7.3. Near-Infrared InGaAs working standard uncertainty (transfer from Vis WS, IGA TS, and pyroelectric detector).....	62
Table 7.4. UV working standard uncertainty (transfer from UV TS and Vis Trap).....	64
Table 7.5 Relative combined standard uncertainties for NIST spectral power responsivity working standards for the UV, visible, and NIR spectral regions.....	66
Table 7.6. Example uncertainty for customer OSI Optoelectronics UV-100 silicon photodiode	67
Table 7.7. Example uncertainty for customer Hamamatsu S1337-1010BQ or S2281 silicon photodiode	69
Table 7.8. Example uncertainty for customer InGaAs photodiode	72
Table 7.9. Example uncertainty for customer TE cooled Ge photodiode.....	74
Table 7.10. Example uncertainty for customer photometer.....	76
Table 7.11. Photodetector spatial uniformity measurement repeatability uncertainty	78

1. Introduction

This document describes the National Institute of Standards and Technology (NIST) Measurement Service for spectral radiant power responsivity in the ultraviolet (UV), visible, and near-infrared (NIR) spectral regions (200 nm to 1800 nm). This Measurement Service provides calibrated silicon photodiodes (200 nm to 1100 nm) and calibrated customer-supplied photodetectors in the 200 nm to 1800 nm spectral region. This document supersedes NIST Special Publication 250-41 (1998), "Detector Measurements: Part I - Ultraviolet Detectors and Part II - Visible to Near-Infrared Detectors."

The theory, measurement system, operation, and transfer standards of the Spectroradiometric Detector Measurement Service are described in this publication. The traceability of the spectral radiant power responsivity scale to the NIST reference absolute cryogenic radiometer and detailed uncertainty estimates are discussed. Also presented are the spectral radiant power responsivity measurement services provided by NIST and the quality system that complies with ISO/IEC 17025 [1].

The material presented in this document describes the equipment and procedures for the Spectroradiometric Detector Measurement Service as they exist at the time of publication. NIST is continually evaluating and improving the equipment, procedures, and services it offers. The discussions in this document will be primarily directed at the procedures developed to measure the spectral radiant power responsivity of photodiodes supplied by NIST to customers. The procedures for characterizing customer supplied detectors are based on the procedures developed for the NIST-furnished devices.

Note: This document follows the NIST policy of using the International System of Units (SI). Only units of the SI and those units recognized for use with the SI are used. Equivalent values in other units may be given in parentheses following the SI values. The mechanical drawings in Sec. 9.4 were originally prepared in English units and are presented without converting the values shown to SI units.

Background

Many radiometric, photometric, and colorimetric applications require the determination of the spectral radiant power responsivity of photodetectors. The spectral radiant power responsivity is the ratio of the signal from the photodetector (amperes or volts) to the spectral radiant flux (watts) incident on the photodetector. The spectral radiant power responsivity is often referred to as spectral power responsivity or simply, spectral responsivity. Calibration of the spectral power responsivity of photodetectors has been a service provided by the Optical Technology Division and its predecessors for over 30 years.

Various techniques have been employed to determine photodetector spectral power responsivity [2, 3]. In the late 1970's a room-temperature electrical substitution radiometer (ESR), also known as an electrically calibrated radiometer (ECR), was used in conjunction with lasers [4, 5]

as the detector scale base. Relative uncertainties were reported on the order of 1 % to 3 %¹ over the spectral range from 390 nm to 1100 nm [6].

Note: This document conforms, to the ISO Guide to the Expression of Uncertainty in Measurement [7], and follows the NIST policy [8-10] to use an expanded uncertainty with $k = 2$ for the results of calibrations. Also, note that uncertainty components are listed as standard uncertainties and expanded uncertainty is used for the final results of calibrations.

A major advance came in the early 1980's with the silicon photodiode self-calibration techniques [11, 12] and the subsequent introduction of 100 % quantum efficient (QE) photodiodes [13] and their use as the basis for detector calibrations. These photodiodes were used in the development of the United Detector Technologies (UDT) QED-200² trap detector, which is a light-trapping device, constructed of three, windowless, UV inversion-layer silicon photodiodes. The QED-200 had a limited spectral range (usually 400 nm to 750 nm) where it operated with 100 % QE, and suffered from limited dynamic range due to the relatively high reverse-bias voltage used. The spectral power responsivity was transferred to customers at this time by the Detector Response Transfer and Intercomparison Program (DRTIP). Customers would rent a radiometer from NIST and transfer the detector scale to their working standard(s). The scale relative uncertainty ranged from 0.6 % to 4 %¹ over the spectral range from 250 nm to 1100 nm [14].

A second generation trap detector (very similar to the then commercially available Graseby Optronics QED-150³) was later used as the basis for the NIST spectral radiant power responsivity scale [15]. Both second generation trap detectors are constructed with a different type of silicon photodiode (Hamamatsu S1337-1010). They do not have 100 % QE, but the QE could be measured with the QED-200, and extrapolated with high accuracy over a large spectral range from 400 nm to 900 nm [16]. Relative uncertainties were reported on the order of 0.2 % to 0.7 %¹ over the spectral range from 250 nm to 1100 nm (between 200 nm and 250 nm, the relative uncertainty was reported as 3.5 %¹). The next advance came in the late 1980's when cryogenic ESRs were reported with improved uncertainties over the 100 % QE detector-based measurements [17-19]. The use of cryogenic ESRs in detector-based radiometry is discussed in Refs. [20, 21].

In the 1990's NIST improved and expanded the spectral responsivity measurements it provided to its customers. The most significant change was to base the measurements on the NIST High Accuracy Cryogenic Radiometer [22]. At the time, the HACR was the U.S. primary standard for optical power. Today, a second generation reference cryogenic radiometer, the Primary Optical

¹Expanded uncertainty with $k = 2$, converted from the originally stated uncertainty in "3 standard deviation estimate" or "3 σ " used by NBS at the time.

²Certain commercial equipment, instruments, or materials are identified in this paper to foster understanding. Such identification does not imply recommendation or endorsement by the National Institute of Standards and Technology, nor does it imply that the materials or equipment identified are necessarily the best available for the purpose.

³The QED 200 was originally manufactured by UDT Instruments; a part of United Detector Technology. UDT Instruments was sold and became Graseby Optronics in Orlando, FL. UDT Instruments is now a part of Belfort Instruments with headquarters in San Diego, CA (<http://www.udtinstruments.com/>).

Watt Radiometer (POWR), is the U.S. primary standard for optical power [23]. The spectral responsivity scale [24] is transferred by various detectors, including second generation silicon photodiode trap detectors, to working standards used with the NIST Visible to Near-Infrared [25] and Ultraviolet Spectral Comparator Facilities (hereafter referred to as the Vis/NIR SCF and UV SCF respectively in this document) where the Spectroradiometric Detector Calibration Service measurements are performed. The next generation trap detectors, sometimes referred to as “tunnel-trap” detectors, [26] have external quantum efficiencies (EQE) (equal to Internal QE times its reflection loss, defined to be 1-reflectance) equal to 0.998 within 0.1 % between 500 nm and 900 nm [27].

2. NIST Spectroradiometric Detector Measurement Service

This section describes the photodetector calibrations and measurements offered by the Optical Technology Division. A complete listing of the calibration services offered by NIST can be found in the NIST Calibration Services Users Guide NIST Special Publication 250 (NIST SP 250) on the NIST Calibration Services web page:

<http://ts.nist.gov/calibrations>.

The NIST Calibration Fee Schedule (SP 250 Appendix Fee Schedule) lists the current cost for all NIST calibration services. The Fee Schedule is typically updated in January and can be found on the above web page.

2.1 Description of Measurement Services

There are two types of measurement services provided by NIST: Fixed Services and Special Tests. Fixed services (Service ID numbers ending in the letter C) have fixed measurement conditions and NIST issues a calibration report to the customer. Special tests (Service ID numbers ending in the letter S) have no fixed measurement conditions; these services are for unique customer-supplied test items.

The present spectral range for photodetector power responsivity measurements is from 200 nm to 1800 nm. Table 2.1 lists the services offered along with typical measurement ranges and the typical uncertainties of customer-supplied devices. All services listed are provided routinely. The relative expanded uncertainties of the Spectroradiometric Detector Measurement Service are listed in Table 2.2 and plotted in Fig. 2.1. See Sec. 7 for a detailed uncertainty explanation.

Table 2.1. NIST spectroradiometric detector measurement services

Service ID number	Item of test	Range	Relative expanded uncertainty ($k = 2$)
39071C	Ultraviolet Silicon Photodiodes (OSI Optoelectronics UV-100)	200 nm to 500 nm	0.3 % to 4 %
39072C	Retest of Ultraviolet Silicon Photodiodes (UDT Sensors UV100 or OSI Optoelectronics UV-100)	200 nm to 500 nm	0.3 % to 4 %
39073C	Visible to Near-Infrared Silicon Photodiodes (Hamamatsu S2281)	350 nm to 1100 nm	0.2 % to 3 %
39074C	Retest of Visible to Near-Infrared Silicon Photodiodes (Hamamatsu S1337-1010BQ or S2281)	350 nm to 1100 nm	0.2 % to 3 %
39075S	Special Tests of Near-Infrared Photodiodes	700 nm to 1800 nm	0.5 % to 4.6 % [†]
39077C	UV to Near-Infrared Silicon Photodiodes (Hamamatsu S2281)	200 nm to 1100 nm	0.2 % to 4 %
39078C	Recalibration of UV to Near-Infrared Silicon Photodiodes (Hamamatsu S1337-1010BQ or S2281)	200 nm to 1100 nm	0.2 % to 4 %
39080S	Special Tests of Radiometric Detectors	200 nm to 1800 nm	0.2 % to 13 % [†]
39081S	Special Tests of Photodetector Responsivity Spatial Uniformity	200 nm to 1800 nm	0.0024 % to 0.05 % [†]

[†]Depends on photodetector and signal level.

Table 2.2. NIST spectral power responsivity relative expanded ($k = 2$) uncertainties for typical UV, visible, and NIR photodiodes.

Wavelength [nm]	Relative expanded uncertainty ($k = 2$) [%]		
	UV	Visible	NIR
200	3.8		
250	1.5		
300	0.80		
350	0.86	0.72	
400	0.74	0.38	
450	0.36	0.24	
500	0.26	0.22	
550		0.20	
600		0.20	
650		0.20	
700		0.20	0.50
750		0.20	0.48
800		0.20	0.48
850		0.20	0.56
900		0.20	0.62
950		0.20	0.66
1000		1.2	0.66
1050		2.0	0.64
1100		3.0	0.62
1150			0.64
1200			0.62
1250			0.58
1300			0.52
1350			0.48
1400			0.48
1450			0.44
1500			0.42
1550			0.42
1600			0.5
1650			0.8
1700			1.9
1750			3.2
1800			4.6

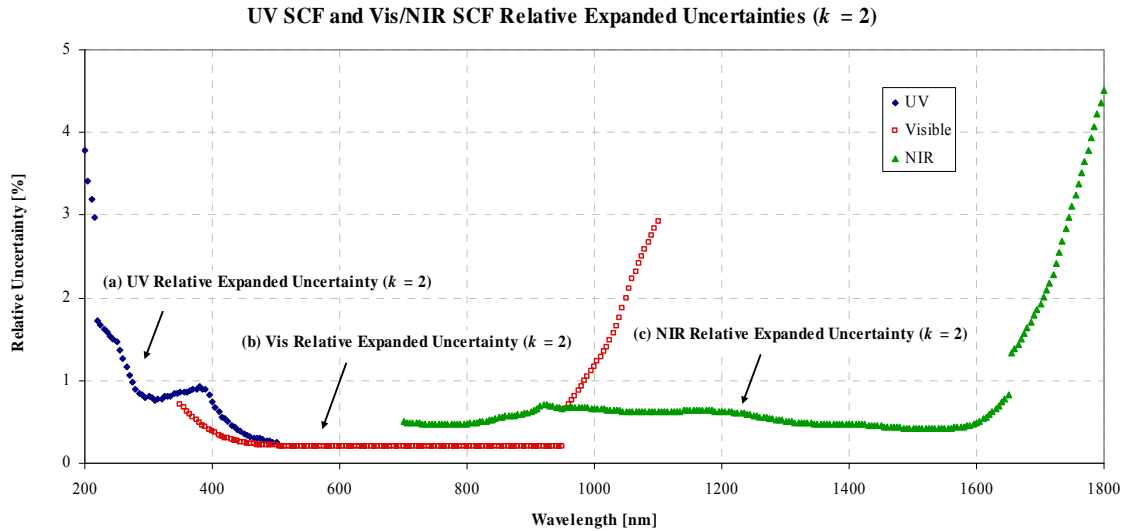


Figure 2.1. The relative expanded uncertainties ($k = 2$) for NIST spectral power responsivity measurements in the (a) UV, (b) visible, and (c) NIR. Three different detector types are used as working standards for the UV, visible, and NIR regions.

Descriptions of each Service ID number are provided below.

39071C - UV Silicon Photodiodes

NIST will supply customers with an OSI Optoelectronics⁴ model UV-100 windowed silicon photodiode characterized in the ultraviolet (UV) spectral region. The UV silicon photodiode includes the measured spectral power responsivity [A/W]⁵ from 200 nm to 500 nm in 5 nm steps. The 1 cm² photosensitive area of the photodiodes is underfilled for the measurements with a beam of diameter ≈ 1.5 mm. The spectral power responsivity is measured at radiant power levels of less than 20 μ W. The relative expanded uncertainty ranges from 0.3 % to 4 %, depending on the wavelength. The spatial uniformity of responsivity over the photosensitive area is also measured at 350 nm.

39072C - Recalibration of UV Silicon Photodiodes

Recalibration of UV silicon photodiodes previously supplied by NIST (under 39071C) is performed by measuring spectral responsivity from 200 nm to 500 nm.

39073C - Visible to Near-Infrared Silicon Photodiodes

NIST will supply customers with a Hamamatsu model S2281 windowed silicon photodiode characterized in the visible to near-IR spectral region. The spectral power responsivity of the photodiode is measured from 350 nm to 1100 nm in 5 nm steps. The 1 cm² photosensitive area of the photodiodes is underfilled for the measurements with a beam of diameter ≈ 1 mm. The spectral responsivity is measured at radiant power levels of less than 1 μ W. The relative expanded uncertainty ranges from 0.2 % to 3 %, depending on the wavelength. The spatial uniformity of responsivity over the photosensitive area is also measured at 500 nm.

39074C - Recalibration of Visible to Near-Infrared Silicon Photodiodes

Recalibration of visible to near-infrared silicon photodiodes previously supplied by NIST (under 39073C) is performed by measuring spectral power responsivity from 350 nm to 1100 nm.

39075S - Special Tests of Near-Infrared Photodiodes

Special tests of customer-supplied near-infrared photodiodes are performed by measuring spectral power responsivity from 700 nm to 1800 nm. A beam of diameter ≈ 1 mm is centered on and underfills the photosensitive area. The spectral power responsivity is measured at radiant power levels of less than 1 μ W. The relative expanded uncertainty ranges from 0.5 % to 4.5 % or greater, depending on the wavelength and the individual item measured. Customers should communicate with one of the technical contacts listed in Sec. 2.4 to discuss details before submitting a formal request.

39077C - UV to Near-Infrared Silicon Photodiodes

NIST will supply customers with a Hamamatsu model S2281 windowed silicon photodiode characterized in the visible to near-IR spectral region. The spectral power responsivity of the photodiode is measured from 200 nm to 1100 nm in 5 nm steps. The 1 cm² photosensitive area

⁴ OSI Optoelectronics in Hawthorne, CA. acquired UDT Sensors, Inc. (<http://www.udt.com/>).

⁵ For clarity, the coherent SI unit is given in brackets for many quantities used in this publication. Of course, SI multiples and submultiples of these units may also be used.

of the photodiodes is underfilled for the measurements with a beam of diameter ≈ 1 mm. The spectral power responsivity is measured at radiant power levels of less than $1 \mu\text{W}$. The relative expanded uncertainty ranges from 0.2 % to 4 %, depending on the wavelength. The spatial uniformity of responsivity over the photosensitive area is also measured at 500 nm.

39078C - Recalibration of UV to Near-Infrared Silicon Photodiodes

Recalibration of UV to near-infrared silicon photodiodes previously supplied by NIST (under 39077C) are performed by measuring spectral power responsivity from 200 nm to 1100 nm

39080S - Special Tests of Radiometric Detectors

Special tests of radiometric detectors in the ultraviolet, visible, and near-infrared regions of the spectrum can be performed. Detector characteristics that can be determined in this special test include spectral responsivity and quantum efficiency (electrons per photon). For example detector responsivity can be measured between 200 nm and 1800 nm at power levels less than $4 \mu\text{W}$. The relative expanded uncertainty ranges from 0.2 % to 13 % or greater, depending on the wavelength and the individual item measured. Since special tests of this type are unique, details of the tests should be discussed with one of the technical contacts listed in Sec. 2.4 before submitting a formal request.

39081S - Special Tests of Photodetector Responsivity Spatial Uniformity

Special tests consisting of measuring the relative changes in responsivity across the photosensitive area (spatial uniformity) can be performed for customer-supplied photodetectors. The uniformity is typically measured at a single wavelength in 0.5 mm spatial increments with a beam diameter of ≈ 1.5 mm in the 200 nm to 400 nm spectral region at power levels less than $20 \mu\text{W}$, and a beam of diameter ≈ 1 mm in the 400 nm to 1800 nm spectral region at power levels less than $1 \mu\text{W}$. The relative expanded uncertainty ranges from 0.0024 % to 0.05 % or greater, depending on the wavelength and the individual item measured. Customers should communicate with one of the technical contacts listed in Sec. 2.4 to discuss details before submitting a formal request.

2.2 Measurement Limitations

There are a few limitations on the types of photodetectors that can be measured in the NIST calibration services. Because of the beam size of the comparators, the detector's active area must be greater than 3 mm in diameter. Due to the monochromator flux level, an amplifier gain of 10^5 V/A to 10^7 V/A is typically required; thus the photodiode dynamic impedance (shunt resistance) must be greater than 10 k Ω . (See Sec. 6.1.1 for more detail.)

Physical size and weight are limited by the translation stages used in the UV SCF and Vis/NIR SCF. Detector packages submitted for testing are limited in size to approximately 20 cm by 20 cm by 20 cm and 2 kg.

The photodetector signal (output current) connection must be clearly identified and preferably provided by a 50 ohm coaxial Bayonet Neill Concelman connector (BNC) connector. The radiometer or photometer must have an analog output voltage. Instruments without an analog output, having only digital display (or analog meter) and/or only digital interface, will not be accepted.

2.3 How to Order Calibrations

- 1) Reference the Service ID number(s) on the purchase order.

Details of Service ID numbers 39075S, 39080S, and 39081S should be discussed with one of the technical contacts listed in Sec. 2.4 prior to submitting a formal request.

- 2) Purchase orders should be sent to:

**Calibration Services
National Institute of Standards and Technology
100 Bureau Drive, Stop 2300
Gaithersburg, MD USA 20899-2300**

Phone number: (301) 975-2092
FAX number: (301) 869-3548
E-mail: calibrations@nist.gov
Web page: <http://ts.nist.gov/calibrations>

- 3) Include the following information on your purchase order:

- A) Service ID number(s)
- B) Manufacturer, model, and serial number of the test item(s)
- C) User's name (technical contact), phone number, and email address
- D) Name and mailing address of the person to receive the calibration report(s)
- E) Billing address
- F) Shipping address
- G) Instructions for return shipment (the fee quoted does not include shipping costs)
[Note: If nothing is stated, NIST will return by common carrier, collect, and uninsured.]

- 4) The cost for special tests is based on the actual labor and material costs involved and customers are responsible for all shipping costs.
- 5) NIST policy requires that non-US customers prepay for calibration services. Please contact Calibration Services to arrange for prepayment.
- 6) Please see the NIST Calibration Services web page (<http://ts.nist.gov/calibrations>) for a complete list of NIST calibration policies.
- 7) All test items should be shipped to the following address:

**Jeanne Houston or Thomas Larason
NIST
Building 221 / Room B208
100 Bureau Drive, Stop 8441
Gaithersburg, MD USA 20899-8441**

2.4 Technical Contacts

For technical information or questions contact:

Jeanne Houston	(301) 975-2327	email: jeanne.houston@nist.gov
Thomas Larason	(301) 975-2334	email: thomas.larason@nist.gov
or fax	(301) 869-5700	

Technical information can also be found on the following web page:

<http://physics.nist.gov/photodiode>

3. Measurement Theory

This section describes the theory and the mathematical basis for the measurement methods used for the services outlined in this publication. The measurement equation is presented and the generalizing assumptions are discussed. The measurement equation is then used in estimating the uncertainties in Sec. 7. The calibration method, detector substitution, is described first in general and then in detail.

3.1 Measurement Equation

Developing the measurement equation is fundamental to understanding the physics and optics involved with the measurement. This derivation provides an analytical foundation for the measurement process and the associated assumptions and approximations. The measurement equation is also fundamental to the analysis of the uncertainty of the measurement. In essence, the detector comparator instrument is similar to a spectroradiometer but compares the response of detectors rather than the irradiance of sources. Thus, the measurement equation developed for a general spectroradiometer can be adapted to detector spectral responsivity measurements.

The measurement equation presented here for spectral responsivity is developed following the general procedure described in chapter 5 of the Self-Study Manual on Optical Radiation Measurements [28] and is similar to the development of Eq. (7.18) in Ref. [29] for spectral irradiance when using a monochromator-based spectroradiometer. The measurement equation for spectral responsivity is:

$$V(A, \Delta\lambda, \lambda_0) = \iint_{\Delta\lambda A} E_\lambda(x, y, \lambda_0, \lambda) \cdot s(x, y, \lambda) \cdot dA \cdot d\lambda, \quad (3.1)$$

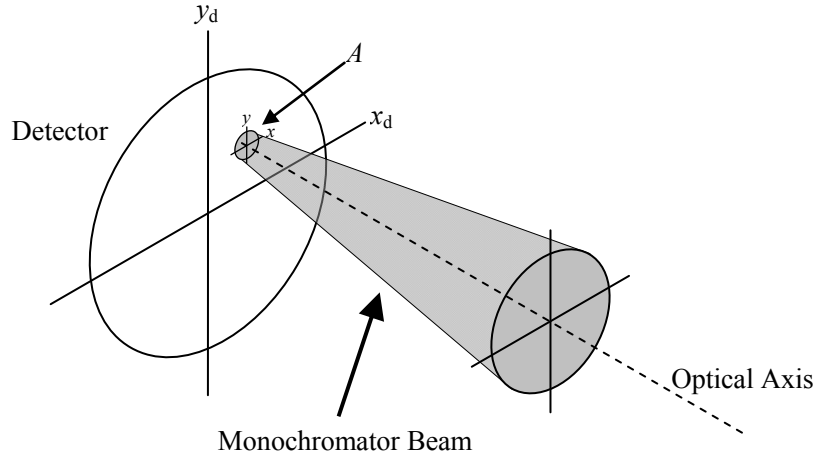
where $V(A, \Delta\lambda, \lambda_0)$ is the output signal (typically in volts or amperes); $E_\lambda(x, y, \lambda_0, \lambda)$ is the spectral irradiance function in λ of the comparator system at detector position x, y for a wavelength setting of λ_0 ; $s(x, y, \lambda)$ is the spectral radiant power responsivity of the detector; A is the area of the radiant power beam at the detector (See Fig. 3.1.); and $\Delta\lambda$ is the wavelength interval for which the value of E_λ is not zero (i.e., the full-width bandpass). This equation is equivalent to Eq. (7.1) [29], with some minor changes in the notation, where A and $\Delta\lambda$ are left symbolically in V to indicate that V depends on how these elements are chosen.

To simplify the analysis, the responsivity s is assumed uniform throughout A , so,

$$s(x, y, \lambda) = s(\lambda). \quad (3.2)$$

Thus, the responsivity s is no longer dependent on position (x, y) and can be removed from the area integral:

$$V(A, \Delta\lambda, \lambda_0) = \int_{\Delta\lambda} s(\lambda) \cdot \int_A E_\lambda(x, y, \lambda_0, \lambda) \cdot dA \cdot d\lambda. \quad (3.3)$$



$$\Phi_{D,\lambda}(\lambda_0, \lambda) = \int_A E_\lambda(x, y, \lambda_0, \lambda) \cdot dA$$

Figure 3.1. The geometry for detector spectral power responsivity measurements.

The area integral of irradiance gives the spectral radiant power function of the comparator system at the detector:

$$\Phi_{D,\lambda}(\lambda_0, \lambda) = \int_A E_\lambda(x, y, \lambda_0, \lambda) \cdot dA = \tau(\lambda) \cdot \Phi_\lambda(\lambda_0, \lambda), \quad (3.4)$$

where $\Phi_\lambda(\lambda_0, \lambda)$ is the output power from the monochromator and $\tau(\lambda)$ is the transmittance of the optics (and atmosphere) between the monochromator and the detector (See Fig. 3.2.).

Considering only the spectral dependence of the signal for any given A , the measurement equation can be written:

$$V(\Delta\lambda, \lambda_0) = \int_{\Delta\lambda} s(\lambda) \cdot \tau(\lambda) \cdot \Phi_\lambda(\lambda_0, \lambda) \cdot d\lambda. \quad (3.5)$$

Equation (3.5) is the power (or flux) equivalent to Eq. (7.1b) [29]. Introducing the slit-scattering function $z(\lambda_0 - \lambda)$ to the measurement equation allows the spectral radiant power function of the monochromator $\Phi_\lambda(\lambda_0, \lambda)$ to be written as the product of two functions (with appropriate normalization):

$$\Phi_\lambda(\lambda_0, \lambda) = z(\lambda_0 - \lambda) \cdot \Phi_{f,\lambda}(\lambda), \quad (3.6)$$

where the slit-scattering function $z(\lambda_0 - \lambda)$ is dependent only on the difference between the wavelength setting of the monochromator and the wavelength of the flux (power) and the “spectral flux” factor $\Phi_{f,\lambda}$ is dependent only on the wavelength of the flux. The factor $\Phi_{f,\lambda}$ is the spectral radiant flux at λ_0 , $\Phi_\lambda(\lambda_0)$, and is equivalent to the responsivity factor r^f introduced in

Eq. (7.12) [29]. Both the slit-scattering function $z(\lambda_0 - \lambda)$ and the factor $\Phi_{f,\lambda}$ can be determined experimentally, although the latter requires deconvolution from the measured output flux (power) of the monochromator. The output signal V can now be expressed as:

$$V(\Delta\lambda, \lambda_0) = \int_{\Delta\lambda} s(\lambda) \cdot \tau(\lambda) \cdot z(\lambda_0 - \lambda) \cdot \Phi_{f,\lambda}(\lambda) \cdot d\lambda . \quad (3.7)$$

Equation (3.7) is the power equivalent to Eq. (7.13) [29] and is in a form that can be used for finding the spectral power responsivity of a detector. It is a measurement equation for a spectrally selective source instead of a spectrally selective detector (spectroradiometer). If the product $s \cdot \tau \cdot \Phi_{f,\lambda}$ is approximately constant (or linear) over the spectral range for which $z(\lambda_0 - \lambda)$ is significant (i.e., within $\Delta\lambda$) and z is approximately symmetrical with respect to λ_0 , Eq. (3.7) can be written:

$$V(\Delta\lambda, \lambda_0) \cong s(\lambda_0) \cdot \tau(\lambda_0) \cdot \Phi_{f,\lambda}(\lambda_0) \cdot \int_{\Delta\lambda} z(\lambda_0 - \lambda) \cdot d\lambda . \quad (3.8)$$

Equation (3.8) is the equivalent flux version of Eq. (7.18) [29]. Implicit in this derivation is the assumption that the slit-scattering function $z(\lambda_0 - \lambda)$ does not change with the wavelength setting λ_0 of the monochromator (that is, the dispersion is the same for all wavelengths) and thus $z(\lambda_0 - \lambda)$ need only be measured once. Optical aberrations, scattering, and diffraction are also assumed to be the same whether a monochromatic beam is varied in λ over the monochromator bandpass, $\Delta\lambda$, or λ_0 of the monochromator is varied over a beam of fixed wavelength λ .

Equation (3.7) is the measurement equation for an ideal monochromator. A real monochromator system has spectrally scattered light (also known as stray-light or out-of-band radiation and hereafter will be referred to as simply stray-light) due to imperfections in the monochromator (and other optics). This is light from outside the spectral region $\Delta\lambda$ which is scattered into the exit beam path and which contributes to the measured signal. Adding a stray-light term, $V_{sl}(\Delta\lambda, \lambda_0)$, to Eq. (3.8) gives:

$$V(\Delta\lambda, \lambda_0) \cong s(\lambda_0) \cdot \tau(\lambda_0) \cdot \Phi_{f,\lambda}(\lambda_0) \cdot \int_{\Delta\lambda} z(\lambda_0 - \lambda) \cdot d\lambda + V_{sl}(\Delta\lambda, \lambda_0), \quad (3.9)$$

where

$$V_{sl}(\Delta\lambda, \lambda_0) \cong \int_{\lambda \neq \Delta\lambda} s(\lambda) \cdot z(\lambda_0 - \lambda) \cdot \tau(\lambda) \cdot \Phi_{f,\lambda}(\lambda) \cdot d\lambda . \quad (3.10)$$

Equation (3.9) separates the measurement equation into two parts, the first term represents the in-band signal and the second term represents the out-of-band signal as indicated by the limits on each integral. The V_{sl} term in Eq. (3.9) is typically small for radiometric measurement systems (especially in a system using a double monochromator) and is normally ignored in the “routine” measurement equation but is included in the uncertainty estimate calculations in Sec. 7.1.2.

The integral remaining in the first term can be evaluated and combined with the “spectral flux” factor $\Phi_{f,\lambda}$ to give an expression for the power leaving the monochromator Φ'_λ :

$$\Phi'_\lambda(\lambda_0) = \Phi_{t,\lambda}(\lambda_0) \cdot \int_{\Delta\lambda} z(\lambda_0 - \lambda) \cdot d\lambda \cong \Phi_\lambda(\lambda_0, \lambda). \quad (3.11)$$

Using Eq. (3.11), the measurement equation (Eq. (3.9)) can now be written in a form that is easily applied to the situation of measuring detector spectral responsivity:

$$V(\Delta\lambda, \lambda_0) \cong s(\lambda_0) \cdot \tau(\lambda_0) \cdot \Phi'_\lambda(\lambda_0). \quad (3.12)$$

Before extending the generalized measurement equation, Eq. (3.12), to the experimental protocols used in the comparator facilities, it is important to reiterate the simplifying assumptions that were made in its development.

3.1.1 Approximations

The assumptions made in the development of the measurement equation, Eq. (3.12), are summarized and discussed below. The development of the measurement equation followed the procedure described in chapter 5 of the Self-Study Manual on Optical Radiation Measurements [28] and does not include parameters for time, polarization, or incident angle; nor does it include environmental parameters such as ambient temperature or humidity, corrections for diffraction effects (departure from geometrical (ray) optics), and nonlinear responsivity.

A key requirement to detector-based radiometry is that detector responsivities are stable over time. In general, the light from any monochromator system will be polarized and the effect of polarization on the responsivity of the detectors needs to be evaluated. However, polarization is not a problem when the detectors are measured at normal incidence to the optical axis (and the detector surfaces are isotropic). The effect of the converging beam angle on the reflectance (and transmittance) from the detector surface (and window) is small compared to the variance of repeated measurements and is typically neglected. However this is not the case when filters are used with the detectors (e.g., photometers), especially interference filters, where the transmission is a strong function of the angle of incidence. Also, the detector area must be larger than the optical beam so that all of the optical radiation is collected by the detector (i.e., the detectors are underfilled). This also requires that the detector field-of-view (FOV) be larger than the optical beam from the comparator system. The detector size and FOV of the typical 1 cm² photodiodes NIST provides meet these requirements.

Humidity can affect the power reaching the detectors by changing the transmittance of the system, but this does not affect the measurements since the optical path length is constant during the measurement. Thus, if the humidity change is small over the time of the measurement, any change in the power reaching the detectors is canceled out of the measurement. Humidity can also affect the detector itself (or its window). For example, with windowless silicon photodiodes the absorption of water by the SiO₂ surface passivation layer changes the photodiode reflectivity, which changes the detector responsivity [30]. Typically, for a windowed detector in the laboratory, an effect due to water absorption (onto the detector or window) is not observed.

The temperature variation of the laboratory is small (typically < 0.5 °C) over the measurement time; therefore, the responsivity temperature dependence is neglected over most of the spectral region. The temperature dependence can be applied as an additional uncertainty term when it is of concern, as near the band-edge of a semiconductor.

Diffraction effects can be estimated from the relationship [31, 32]:

$$\theta^d = 2.44 \cdot \frac{\lambda}{d}, \quad (3.13)$$

where θ^d (in radian) is the diffraction angle (for the first Airy disk), λ is the longest wavelength of the system, and d is the diameter of the aperture at the monochromator exit slit (the smallest aperture in the system). For the Vis/NIR SCF $\lambda \approx 2 \mu\text{m}$ and $d \approx 1 \text{ mm}$ which gives:

$$\theta_{\text{Vis/NIR}}^d = 2.44 \times \frac{2 \mu\text{m}}{1 \text{ mm}} = 4.88 \times 10^{-3} \approx 5 \text{ mrad}. \quad (3.14)$$

The Vis/NIR SCF has a focal ratio (f -number or $f/\#$) of ≈ 9 giving a beam angle of $\approx 110 \text{ mrad}$ which is over 20 times greater than the diffraction limit. For the UV SCF ($\lambda \approx 0.5 \mu\text{m}$, $d \approx 1.5 \text{ mm}$, and $f/\# \approx 5$) the diffraction effects are even smaller due to the shorter wavelengths of the light. In this case, the beam angle is ≈ 200 times greater than the diffraction limit. Thus diffraction effects can be ignored for most UV, visible, and near-IR systems of the type described in this publication. Likewise, coherence effects are negligible [33] and are ignored in the analysis of these comparator systems.

The responsivity, s , is assumed uniform throughout the area A of the incident beam on the detector. In practice, this is accomplished by reducing A (both mechanically with apertures and optically via imaging optics) so that s is uniform over A . This limits the amount of flux (power) that can be delivered to the detector but this does not hinder the responsivity measurements for typical photodiodes. Deviations from this approximation are treated as uncertainty terms.

Certain assumptions were made about the comparator system itself, [29] primarily the monochromator. Two assumptions are that the dispersion remains the same for all wavelengths and that the slit-scattering function $z(\lambda_0 - \lambda)$ does not change with the wavelength setting, λ_0 , of the monochromator. These approximations are not included in the uncertainty analysis because their combined effect was determined to be negligible. This allows $z(\lambda_0 - \lambda)$ to be measured only once for an instrument and used over the entire spectral range. Another assumption is that optical aberrations, scattering, and diffraction are the same whether the wavelength λ of a monochromatic source is varied over the monochromator bandpass $\Delta\lambda$ or whether the monochromator wavelength setting λ_0 is varied over a monochromatic source of wavelength λ . Also $z(\lambda_0 - \lambda)$ is assumed approximately symmetrical with respect to λ_0 ; this assumption has been experimentally verified for the two monochromators described in the spectral comparator facilities.

The product $s \cdot \tau \cdot \Phi_{f,\lambda}$ is assumed to be linear over the monochromator bandpass, $\Delta\lambda$. In practice, this is effected by reducing the slit widths until $s \cdot \Phi_{f,\lambda}$ is linear over $\Delta\lambda$. Reducing the bandpass also reduces the amount of optical power (flux) that can be delivered to the detector, but this is not a limitation for typical measurements. Most measurements are made using a broadband source to provide a wide range of measurement wavelengths. However, the assumption that $s \cdot \Phi_{f,\lambda}$ is linear over $\Delta\lambda$ may not be valid with some arc and discharge sources (primarily used in

the UV) that can have strong spectral variations in output intensity. Typically, the variations are small and are treated as uncertainty terms.

Stray-light is light from outside the monochromator bandpass $\Delta\lambda$ that is scattered into the beam. The amount of stray-light depends greatly on the design of the monochromator. The amount of stray-light in the transmitted flux is typically negligible for double monochromator systems (systems with two dispersing elements), but not for many single monochromator systems. The two monochromators in the comparator facilities have double dispersion elements, prism-grating or double-grating systems. Because the stray-light in the comparator systems is small in magnitude, it will not be included as a correction term in the measurement equation, but will be evaluated and treated as a term in the uncertainty budget described in Sec. 7.

Spatially-scattered light is light that is scattered outside of the beam area, A . The amount of spatially-scattered light depends on the quality and condition of the optics in the beam path. Errors caused by spatially-scattered light cancels if the test and standard detectors have the same size or are much larger than the beam area, A . It can be significant when the test detector area is small and approaches the diameter of the beam. For this reason, detectors with diameters of less than 3 mm are not accepted for calibration. This error is evaluated and corrected if the detector diameter is less than 5 mm. The uncertainty of this correction is included in the uncertainty budget in the UV and Vis/NIR SCF measurements.

3.2 Substitution Method

The substitution method transfers the responsivity (output divided by input) of a standard detector to an unknown (test) detector. This method has a number of advantages that will be discussed in general and applied specifically to photodetectors. In this section, a measurement equation will be developed for the substitution method. The general assumptions made in its development and their consequences are then discussed. Finally, the measurement equation as applied to the NIST Spectral Comparator Facilities is developed.

3.2.1 General Substitution Method

The output (signal) Y from a detector (or system) with a linear response can be written in general:

$$Y_x = s_x \cdot X_x, \quad (3.15)$$

where Y_x is the signal (e.g., in ampere) from the detector, s_x is the responsivity of the detector (e.g., in A/W), and X_x is the input to the detector (e.g., in W). Similarly, the signal from a standard detector with a known responsivity s_s is given by:

$$Y_s = s_s \cdot X_s. \quad (3.16)$$

Dividing Eq. (3.15) by Eq. (3.16) we have:

$$\frac{Y_x}{Y_s} = \frac{s_x \cdot X_x}{s_s \cdot X_s}. \quad (3.17)$$

If the input X to each system is assumed to be constant (this is the basis of the substitution method), solving for the detector responsivities s_x gives:

$$s_x = \frac{Y_x}{Y_s} s_s \quad (3.18)$$

Thus, using the substitution method, the standard detector responsivity s_s is scaled by the ratio of the outputs. In essence, the standard detector quantifies the input power X [W] to the test detector.

3.2.2 Photodetector Substitution

Photodetector responsivity measurements by detector substitution can be made using Eq. (3.18) and the following equipment: a broadband source, monochromator, focusing optics, and standard detector. A block diagram of the photodetector substitution method is shown in Figure 3.2. The radiant power (flux) Φ is the output power from the source that enters the monochromator. The spectral radiant power Φ_λ is the output power from the monochromator and τ is the transmittance of any optics (and the atmosphere) between the monochromator and the detector. The spectral radiant power received by the detectors is $\Phi_{D,\lambda} = \tau \cdot \Phi_\lambda$.

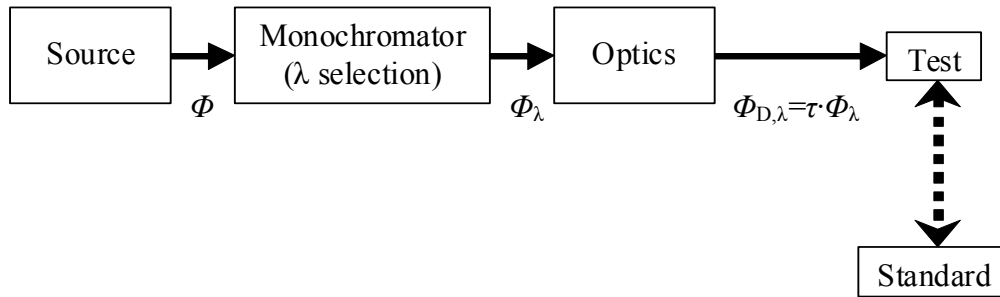


Figure 3.2. Block diagram of photodetector substitution method.

Using Eq. (3.18) assumes that the source is stable over the comparison time. This is generally true for incandescent sources (i.e., quartz-halogen (QTH) lamps), used in the VIS/NIR comparator, but less true for arc sources, used in the UV comparator.

Substitution can be done in two ways. One way is to substitute the test detector and standard detector at each wavelength and another is to repeat the wavelength scan for each detector. The former method has an advantage that the results are not affected by the drift of the source between wavelength scan, but the measurement is slower. The latter method is subject to possible drift of the source during the wavelength scan, but the measurement is faster. The latter method is employed in the NIST SCF facilities, with the addition of a monitor detector as described in the next section. The stability of the source can be the limiting factor in the signal noise of the detectors.

3.2.3 Substitution Method with Monitor

Measurement errors due to source power fluctuations are minimized by introducing a beamsplitter and monitor detector into the measurement setup. Figure 3.3 illustrates the photodetector substitution method with monitor. Here $\Phi_{D,\lambda} = \tau_{bs} \cdot \tau \cdot \Phi_\lambda$ is the power received by the detectors and $\Phi_{M,\lambda} = \rho_{bs} \cdot \tau \cdot \Phi_\lambda$ is the power received by the monitor. The transmittance and reflectance of the beam splitter are τ_{bs} and ρ_{bs} , respectively. The monitor detector and beamsplitter are assumed to be stable (constant) over the time of the measurement. Thus the monitor signal can be used to normalize the signals from the test and standard detectors. That is, the signal ratio of the test detector to monitor or standard detector to monitor will be constant regardless of the source fluctuations and the signal levels. By simultaneously measuring both the monitor detector signal and test detector or standard detector signal, source fluctuations on a time scale greater than the signal sampling rate are effectively eliminated.

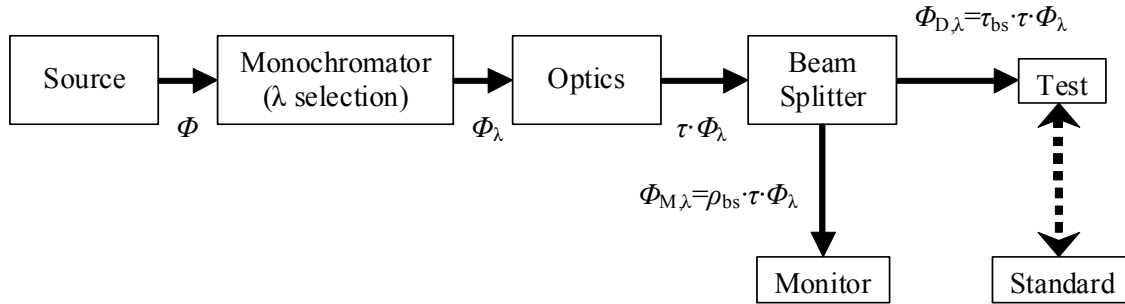


Figure 3.3. Block diagram of photodetector substitution method with monitor.

3.2.4 Measurement Equation Applied to the SCFs

The actual measurement equation for the SCFs is now developed. Dropping the λ notation and changing the sub- and superscripts for clarity from Eq. (3.12), it can easily be shown that the total signal, $V_{t,x}$, from a detector x and an amplifier is:

$$V_{t,x} = s_x \cdot G_x \cdot \tau_x \cdot \Phi_x + V_{d,x}, \quad (3.19)$$

where s_x is the detector spectral power responsivity in A/W, G_x is an explicit gain term for a transimpedance amplifier in V/A, τ_x is the transmittance of any optics (and the atmosphere) between the monochromator and the detector, Φ_x is the output power from the monochromator in W, and $V_{d,x}$ is the dark signal (sometimes called the “output offset voltage”) in V, i.e., the signal measured when no flux is incident on the detector. In practice $V_{d,x}$ is found by measuring the signal from the detector with the shutter closed at the exit slit of the monochromator. For the UV and Vis/NIR SCFs there is negligible difference between the background signal (with the source blocked before the monochromator and shutter open) and the dark/offset signal (with the shutter closed). The net signal (or just signal) V_x is the signal due to the radiant power received by the detector:

$$V_x = V_{t,x} - V_{d,x} = s_x \cdot G_x \cdot \tau_x \cdot \Phi_x. \quad (3.20)$$

This is the “routine” measurement equation for the substitution method depicted in Fig. 3.2. The measurement equation for the “substitution method with monitor” (Fig. 3.3) is written by explicitly including the transmittance τ_{bs} and reflectance ρ_{bs} of the beam splitter assembly (which also contains the reflectance of the monitor turning mirror). Implicit in this equation is the assumption that the path length from the beam splitter to the monitor is the same as the beam splitter to the working standard or test detector. Both comparator systems record simultaneous measurements taken with both the detector and monitor. The signals from the test detector x and monitor detector mx are:

$$V_x = V_{t,x} - V_{d,x} = s_x \cdot G_x \cdot \tau_{bsx} \cdot \tau_x \cdot \Phi_x, \quad (3.21)$$

and

$$V_{mx} = V_{t,mx} - V_{d,mx} = s_{mx} \cdot G_{mx} \cdot \rho_{bsx} \cdot \tau_x \cdot \Phi_x. \quad (3.22)$$

The ratio of these two signals is:

$$R_x = \frac{V_x}{V_{mx}} = \frac{s_x \cdot G_x \cdot \tau_{bsx} \cdot \tau_x \cdot \Phi_x}{s_{mx} \cdot G_{mx} \cdot \rho_{bsx} \cdot \tau_x \cdot \Phi_x}, \quad (3.23)$$

where $\tau_{bsx} \cdot \tau_x \cdot \Phi_x$ is the fraction of power (flux) received by the test detector, and $\rho_{bsx} \cdot \tau_x \cdot \Phi_x$ is the fraction of power (flux) received by the monitor.

There is a similar ratio for the two signals from the working standard detector and monitor:

$$R_x = \frac{V_s}{V_{ms}} = \frac{s_s \cdot G_s \cdot \tau_{bss} \cdot \tau_s \cdot \Phi_s}{s_{ms} \cdot G_{ms} \cdot \rho_{bss} \cdot \tau_s \cdot \Phi_s}. \quad (3.24)$$

Dividing Eq. (3.23) by Eq. (3.24) (taking the ratio of the ratios) gives:

$$\frac{R_x}{R_s} = \frac{s_x \cdot G_x \cdot \tau_{bsx} \cdot \tau_x \cdot \Phi_x}{s_{mx} \cdot G_{mx} \cdot \rho_{bsx} \cdot \tau_x \cdot \Phi_x} \cdot \frac{s_{ms} \cdot G_{ms} \cdot \rho_{bss} \cdot \tau_s \cdot \Phi_s}{s_s \cdot G_s \cdot \tau_{bss} \cdot \tau_s \cdot \Phi_s}. \quad (3.25)$$

Looking at Eq. (3.25), it is now seen that variations or drifts in the source flux or system transmittance during the time between the measurement of the test detector and the working standard detector are canceled by the monitor detector. If the beamsplitter transmittance and reflectance, monitor detector responsivity, and amplifier gain are stable (constant) over the comparison time, that is, $\tau_{bsx} = \tau_{bss}$, $\rho_{bsx} = \rho_{bss}$, $s_{mx} = s_{ms}$ and $G_{mx} = G_{ms}$, these terms cancel, leaving:

$$\frac{R_x}{R_s} = \frac{s_x \cdot G_x}{s_s \cdot G_s}. \quad (3.26)$$

Solving Eq. (3.26) for the test detector spectral responsivity s_x and substituting the signal measurements into the ratios we have:

$$s_x = \frac{R_x}{R_s} \cdot \frac{G_s}{G_x} \cdot s_s = \frac{\frac{V_x}{V_{mx}}}{\frac{V_s}{V_{ms}}} \cdot \frac{G_s}{G_x} \cdot s_s \quad (3.27)$$

This is the working form of the measurement equation. Note that it still has the general form:

$$s_x = \frac{Y_x}{Y_s} s_s \quad (3.18)$$

Depending on how the monochromator wavelength scale is calibrated, a correction term may be needed when the responsivity curves of the test and working standard detectors have different slopes. If the centroid wavelength of the bandpass is used to calibrate the monochromator wavelength scale, then there is no correction term. But if the peak wavelength of the bandpass is used, then Eq. (3.27) requires a correction term. Thus the measurement equation for spectral responsivity, s_x , (in A/W) becomes:

$$s_x = \frac{R_x}{R_s} \cdot \frac{G_s}{G_x} \cdot s_s + C_{bw} \quad (3.28)$$

where C_{bw} is a correction term due to the bandpass of the monochromator and is referred to as the bandpass error. Like the stray-light term, the bandpass error is small and can be ignored in the “routine” measurement equation. The bandpass error is described in Sec. 7.2.2 as an uncertainty term.

4. Equipment Description

In this section the components and associated electronics of the Visible to Near-Infrared Spectral Comparator Facility (Vis/NIR SCF) and Ultraviolet Spectral Comparator Facility (UV SCF) are described.

4.1 Visible to Near-Infrared Spectral Comparator Facility (Vis/NIR SCF)

The Vis/NIR SCF is a monochromator-based system that typically measures the spectral power responsivity of photodiodes in the 350 nm to 1800 nm spectral region. The Vis/NIR SCF operates from 350 nm to 1100 nm using silicon photodiodes as working standards and from 700 nm to 1800 nm using indium gallium arsenide (InGaAs) photodiodes as working standards. The spatial uniformity of a detector's power responsivity can also be measured.

The Vis/NIR SCF uses automated translation stages to position the photodetectors for measurement. The test detectors as well as the working standards are fixed onto optical mounts that rotate and tilt for accurate alignment. A variety of sources can be selected. Typically a 100 W quartz-halogen lamp is used as the source in the Vis/NIR SCF. A shutter is located just after the monochromator exit slit. A monitor detector located after the monochromator measures source fluctuations. The detectors and the exit optics are enclosed in a light tight box. A diagram of the Vis/NIR SCF is shown in Fig. 4.1. Each of the primary components is now described in greater detail.

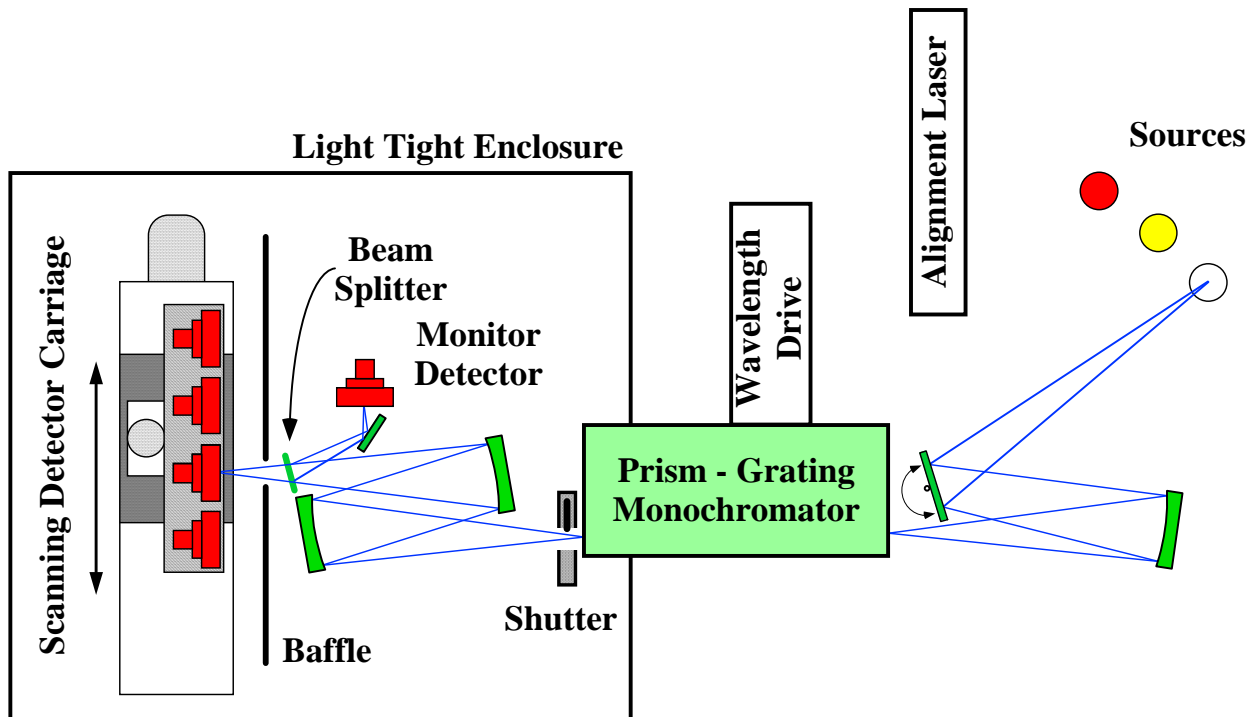


Figure 4.1. Visible to Near-Infrared Spectral Comparator Facility (Vis/NIR SCF).

4.1.1 Vis/NIR Source and Input Optics

Typically the Vis/NIR SCF uses a 100 W (12 V) quartz-halogen lamp that is constant-current controlled for stability. The lamp is used over the spectral range of 350 nm to 1800 nm. An integrating sphere with a spectral-line discharge lamp input is used as a source for calibrating the wavelength scale of the monochromator. A third source position is available for investigational use. A helium-neon (HeNe) alignment laser can be used as a source in the Vis/NIR comparator as well. The spectral output power (at the detector) of the 100 W quartz-halogen lamp with the Vis/NIR SCF monochromator is shown in Fig. 4.2.

A 46 mm x 61 mm flat mirror rotates on an automated stage for source selection. The source is imaged by a stationary 15.24 cm diameter spherical mirror onto the entrance slit of the monochromator.

Safety considerations

Quartz-halogen lamps, lasers, and arc sources are potential eye hazards. The HeNe lasers used for alignment are Laser Safety Class II. Care is taken to never look directly into any of the sources or the laser beam. Shields mounted on the sides of the optical table inhibit direct visual contact with the sources used with the comparator. Protective eyewear is worn when working in proximity to these sources.

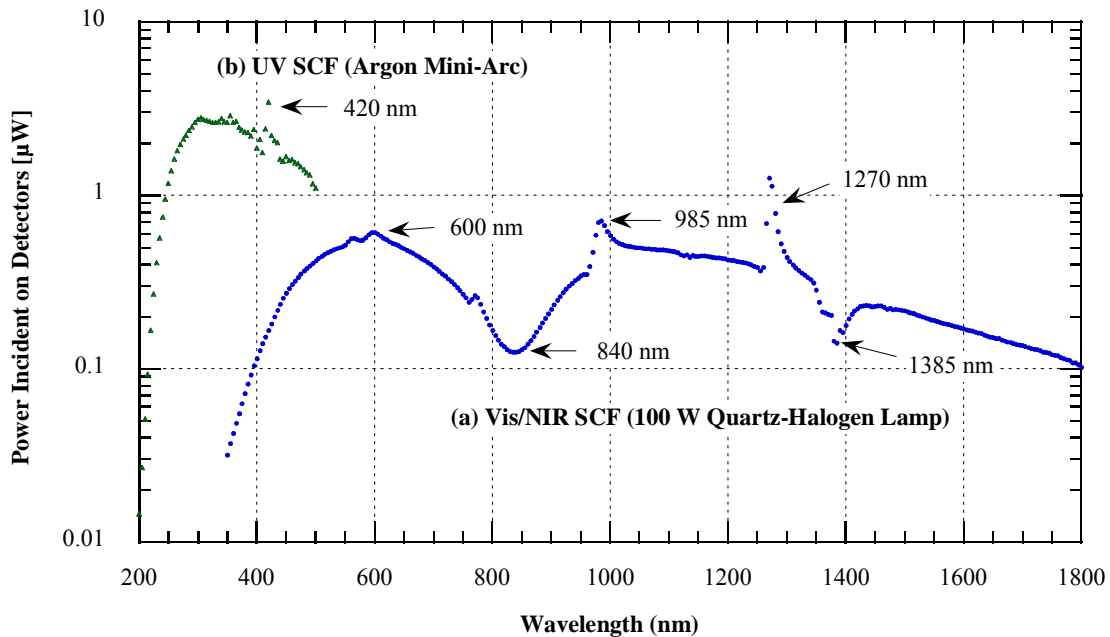


Figure 4.2. The spectral power typically incident on the detectors in the (a) Vis/NIR SCF using the 100 W quartz-halogen lamp and (b) UV SCF using the argon mini-arc as a source.

4.1.2 Vis/NIR Monochromator

The visible comparator uses a modified Applied Physics Corporation Cary-14 prism-grating monochromator. The Cary-14 employs a 30° fused silica prism in series with a 600 lines per millimeter echelette grating. The monochromator's spectral range is 186 nm to 2.65 μm, the spectral range used in the Vis/NIR SCF is 350 nm to 1800 nm. In the typical measurement configuration, the monochromator slits are set to 1.1 mm, giving an instrument FWHM bandpass of 4 nm. A circular 1.1 mm diameter aperture located just after the monochromator exit slit determines the beam size. The exit beam is $f/9$. The monochromator has a stray-light rejection of 10^{-8} . Greater than 99 % of the beam power lies within an area of 1.5 mm diameter around the optical axis.

4.1.3 Vis/NIR Shutter and Output Optics

A shutter, with a 25 mm diameter aperture, is placed after the monochromator exit slit and aperture.

Two 15.24 cm diameter spherical mirrors and two 7.62 cm diameter flat mirrors image the exit aperture of the monochromator with 1:1 magnification onto the detector. The two flat mirrors are used to optically fold the system and are not shown in Fig. 4.1. Mirrors do not produce chromatic aberrations, and the astigmatism of the spherical mirrors is corrected (to first order) by tilting the second spherical mirror perpendicular to the plane of the first spherical mirror [34].

4.1.4 Vis/NIR Translation Stages - Detector Positioning

The Vis/NIR comparator uses two orthogonal linear positioning stages to translate the test detectors and working standard detectors. The horizontal stage travel range is 400 mm with a manufacturer specified resolution of 0.1 μm and an accuracy of 0.2 μm per 100 mm. The vertical stage travel range is 50 mm with a manufacturer specified resolution of 0.1 μm and an accuracy of 0.25 μm per 25 mm.

Each detector can be manually translated along the Vis/NIR SCF optical axis for focusing. A gimbal mount allows the rotation and tilt of each detector to be adjusted perpendicular to the optical axis for alignment.

4.1.5 Vis/NIR Working Standards

The visible working standards (Vis WS) are four Hamamatsu model S1337-1010BQ silicon photodiodes with fused quartz windows. This is a p-n photodiode with a 1 cm² active area. The Hamamatsu S1337 diode is a popular diode for radiometric standards, and the linearity, uniformity, and stability of the Hamamatsu S1337 diode has been well documented [35, 36]. The Vis WS are used for measurements over the spectral range from 350 nm to 1100 nm.

For near-infrared measurements (700 nm to 1800 nm), four GPD Optoelectronics Corporation (formerly Germanium Power Devices) model GAP5000 InGaAs photodiodes mounted in temperature-controlled housings are used as working standards (IGA WS). These photodiodes have a 5 mm diameter active area.

Typically, two working standards are used for each spectral comparison measurement. The second working standard can be used as a “check” standard to verify that the measurement process is operating normally, or is “in control.”

4.1.6 Beam Splitter and Monitor Detector

Variations in the source intensity are corrected by using a beam splitter and monitor detector, as discussed in Sec. 3.2.3. The beam splitter is a 50.8 mm x 50.8 mm flat fused quartz plate. A 35 mm x 46 mm flat oval mirror is used to optically fold the beam reflected off the beam splitter to a convenient physical location for the monitor detector. Hamamatsu S1337-1010BQ silicon and EG&G Judson J16TE2-8A6-R05M-SC germanium photodiodes are used as monitor detectors in the visible and NIR spectral regions, respectively. Ideally, the monitor detector has the same spectral responsivity as the working standard used for the measurement. But for the NIR region a small stray-light uncertainty component is included because of the IGA WS and Ge monitor.

4.1.7 Alignment Lasers

Two HeNe lasers are aligned to the optical axis of the Vis/NIR comparator (defined by the positions of the monochromator entrance and exit slits). One laser is located in one of the source positions and is typically used to align the detectors. The other is located inside the enclosure and is pointed “backwards” through the comparator to align the sources. It is not shown in Fig. 4.1.

4.1.8 Enclosure

Each comparator has a light tight enclosure to eliminate the background light from the room. This is essential because the routine measurements are all dc (optically unmodulated). The enclosure is essentially a box that sits on the optical table and covers the exit portion of the monochromator, shutter and output optics, and translation stages. The test detectors, working standards, monitor detector, amplifiers, and other associated electronics are also housed inside the enclosure. Doors allow easy access to the equipment and detectors.

The enclosure also reduces the amount of dust settling on the detectors and exit optics. An exhaust fan is used to keep the temperature and humidity inside of the enclosure as close to that in the laboratory as possible. The temperature and humidity are monitored inside the enclosure and in the laboratory.

4.2 Ultraviolet Spectral Comparator (UV SCF)

The UV SCF is a monochromator-based system that measures the uniformity and spectral power responsivity of photodetectors in the 200 nm to 500 nm spectral region. The UV SCF is very similar in configuration and operation to the Vis/NIR SCF. Only the differences between the two will be described. A diagram of the UV SCF is shown in Fig. 4.3.

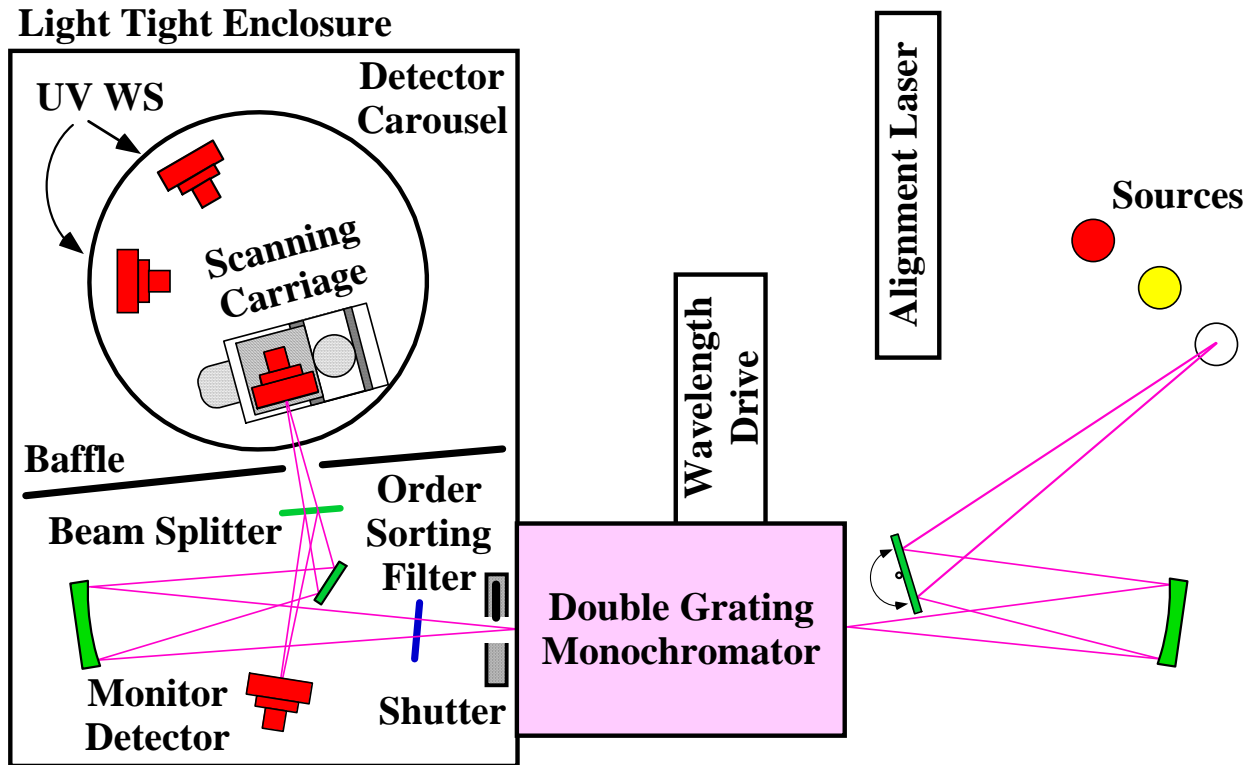


Figure 4.3. Ultraviolet Spectral Comparator Facility (UV SCF).

UV enhanced silicon photodiodes serve as the working standards for the UV SCF. A rotary stage is used in the UV SCF; currently only one test detector at a time can be measured. The test and working standard detectors are fixed onto optical mounts that rotate and tilt. Motorized translation stages position the test detector in the horizontal and vertical planes while the working standards are positioned manually.

4.2.1 UV Source and Input Optics

The UV SCF uses a NIST-designed argon mini-arc as its source over the 200 nm to 500 nm spectral range. The argon mini-arc was developed at NIST as a secondary spectral radiance standard and has been well characterized [37]. The argon mini-arc is an intense, uniform UV source, with argon gas flowing through the arc structure at ≈ 35 kPa. The arc can be operated from 30 A to 100 A, but is typically operated at ≈ 40 A (and 60 V). The arc is cooled using the normal facility 5.6 °C chilled water. The water runs through plastic, non-conducting tubing. An integrating sphere with a spectral-line discharge lamp input is used as a source for calibrating the wavelength scale of the monochromator. A third source position is available for investigational use. A helium-neon (HeNe) alignment laser can be used as a source in the UV comparator as well. The spectral radiant power at the detector on the UV SCF with the argon mini-arc source is also shown in Fig. 4.2.

A 10.16 cm diameter flat mirror on a rotary stage is used for source selection. The source is imaged by a stationary 15.24 cm diameter spherical mirror onto the entrance slit of the monochromator.

Safety considerations

UV filtering safety glasses are worn whenever the argon mini-arc source is lit. Even with safety glasses on, the argon mini-arc is never viewed directly. The HeNe alignment lasers are Laser Safety Class II. Shields mounted on the sides of the optical table inhibit direct visual contact with the sources. Since very high currents are used, extra precautions are taken when using the arc. Care is taken to avoid accidental contact with the arc electrodes and to insulate the arc from the optical table (and surroundings). Also, to avoid overheating the arc and electrical shorts, attention is paid that the cooling water is flowing before the arc is turned on and that no water leaks exist. Non-conducting plumbing is always used.

4.2.2 UV Monochromator

The UV comparator uses a Spex 1680, 1/4 m double grating monochromator with 2840 lines per millimeter gratings. The monochromator's spectral range is 180 nm to 1000 nm. The spectral range used in the detector comparator facility is 200 nm to 500 nm. In the typical measurement configuration, the entrance and exit slits are circular 1.5 mm diameter apertures with a bandpass of 4 nm. The exit beam is $f/5$. Greater than 99 % of the beam power lies within an oval area of diameters 2.0 mm and 2.5 mm around the optical axis.

4.2.3 UV Shutter and Output Optics

A shutter, with a 25 mm diameter aperture, is placed after the monochromator exit slit.

One 15.24 cm diameter spherical mirror and one 7.62 cm diameter flat mirror images the exit slit of the monochromator with 1:1 magnification. Mirrors are used to prevent chromatic aberrations.

4.2.4 UV Translation Stages - Detector Positioning

The UV comparator has optical mounts for one test detector and two working standard detectors on a rotary positioning stage. The maximum travel of the rotary stage is 360° with a manufacturer specified resolution of 0.001° and an accuracy of 0.0014° . The test detector is mounted on two automated orthogonal linear translation stages. The stages have a travel range of 50 mm with a manufacturer specified resolution of $0.1 \mu\text{m}$ and an accuracy of $0.25 \mu\text{m}$ per 25 mm. The test detector can be manually translated along the optical axis for focusing.

The working standard detectors are mounted on two manual orthogonal linear translation stages. Each detector can be manually translated along the optical axis for focusing. A gimbal mount allows the rotation and tilt of each detector to be adjusted perpendicular to the optical axis.

4.2.5 UV Working Standards

The ultraviolet working standards (UV WS) are two UDT Sensors, Inc.⁶ model UV100 silicon photodiodes with quartz windows and 1 cm^2 circular active areas. The UV100 is an inversion

⁶ UDT Sensors is now OSI Optoelectronics, 12525 Chadron Ave., Hawthorne, CA 90250, USA.

layer diode with enhanced resistance to UV radiation damage. Typically two working standards are used for each spectral comparison measurement. The second working standard can be used as a “check” standard to verify that the measurement process is operating normally, or is “in control.”

4.2.6 Beam Splitter and Monitor Detector

The beam splitter is a 50.8 mm diameter flat quartz plate. A UDT Sensors UV100 photodiode is the monitor detector.

4.2.7 Alignment Lasers

Similar to the Vis/NIR SCF, two HeNe lasers are used to align the optical path of the UV comparator. The second laser is not shown in Fig. 4.3.

4.2.8 Enclosure

The UV SCF enclosure is similar in design and construction to that of the Vis/NIR SCF.

4.3 Electronics

4.3.1 Electronics - Signal Measurement

This section describes the electronics used with the UV SCF and Vis/NIR SCF for detecting and amplifying the signals from the photodetectors. The electronics for both comparators are identical with some equipment shared between the two facilities. Only the Vis/NIR SCF will be described and the differences between the comparators will be noted.

Figure 4.4 shows a block diagram of the typical setup for measurements in the Vis/NIR SCF. The design of the electronics and control of the UV SCF is very similar to the Vis/NIR SCF. Four NIST built and characterized amplifiers are housed in one module for convenience and a separate single amplifier is used with the monitor detector. The digital voltmeters (DVMs) are computer controlled via an IEEE-488 bus. The two DVMs simultaneously measure the signals from the monitor and one of the four detectors that can be moved into the SCF beam. One DVM has a multiplexed input for selecting any of four amplifier channels or temperature monitoring inputs. (Some detectors have temperature monitoring circuitry that produces a voltage signal proportional to their temperature.)

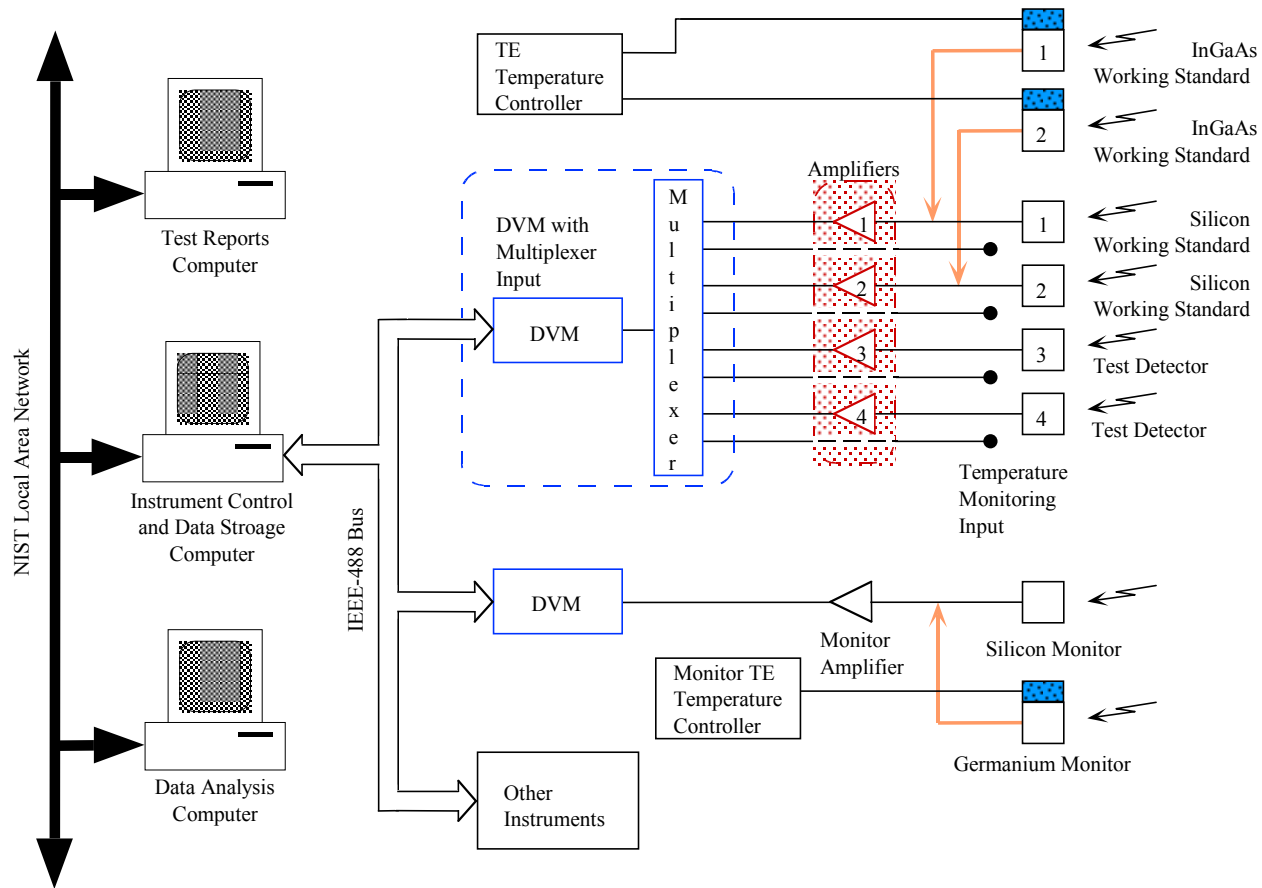


Figure 4.4. Electronic block diagram of the Vis/NIR SCF.

The amplifiers are identical in design and operate with variable gains ranging from 10^4 V/A to 10^9 V/A. References [3, 38] and several titles in the bibliography describe similar transimpedance amplifiers and their operation. The schematic for the precision transimpedance (I/V) amplifiers used in both the UV and Vis/NIR SCFs is shown in Figure 4.5.

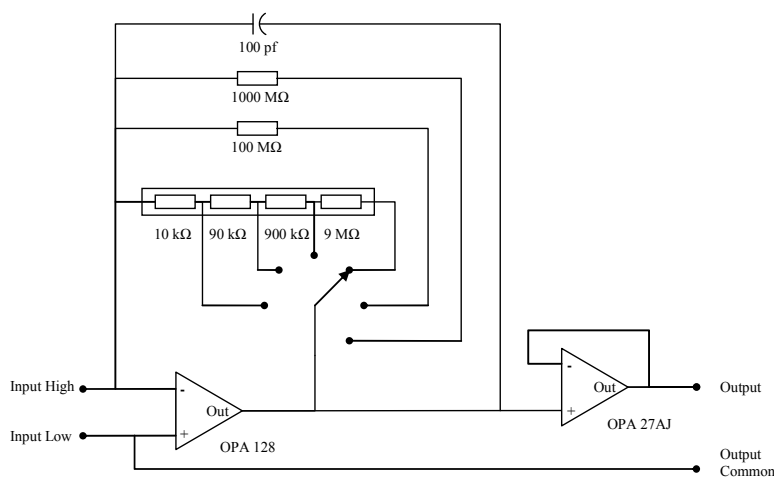


Figure 4.5. NIST SCF precision transimpedance (I/V) amplifier circuit.

The SCFs are typically operated as described above (DC mode), but with the addition of a chopper in the optical beam, AC measurements are possible for special tests. AC measurements are not discussed in this publication; see Ref. [39] for a detailed discussion of AC measurements.

4.3.2 Electronics - Auxiliary Equipment

Temperature-controlled photodiodes can be used which require thermoelectric (TE) temperature controllers shown in Fig. 4.4. The following electronics not previously mentioned are also used routinely: a 4-channel TE temperature controller for the InGaAs working standards; a stand-alone TE temperature controller for the germanium monitor; a digital I/O control unit for the optical shutter; and a laboratory environmental monitoring system. The environmental monitoring system measures the temperature and relative humidity in the laboratory and in each comparator enclosure.

5. Spectral Power Responsivity Scale Realization

This section describes the determination of the NIST spectral power responsivity scale and its traceability to a primary standard. The propagation of the scale, the operation of a cryogenic radiometer, and the calibration of the transfer standards are briefly reviewed. Then the propagation the scale from the transfer standards to the working standards is described. Scale realizations are scheduled every 12 to 18 months.

5.1 The Spectral Power Responsivity Scale Measurement Chain

The spectral radiant power responsivity measurement chain is shown in Fig. 5.1. The top of the chain is the NIST-designed reference cryogenic radiometer called the Primary Optical Watt Radiometer (POWR), which serves as the base of optical power unit. The second cryogenic radiometer, the L-1 Absolute Cryogenic Radiometer (ACR) from L-1 Standards and Technology, Inc. was verified for its low uncertainty by comparison with POWR. The L-1 ACR serves as the secondary standard to calibrate transfer standard detectors at the Spectral Irradiance and Radiance Responsivity Calibrations using Uniform Sources (SIRCUS) facility [27] in the 200 nm to 1800 nm region. The transfer detector is used to calibrate working standard detectors at the Spectral Comparator Facilities (Vis/NIR SCF and UVSCF), and then customers' detectors are routinely calibrated against the working standard detectors at the SCFs.

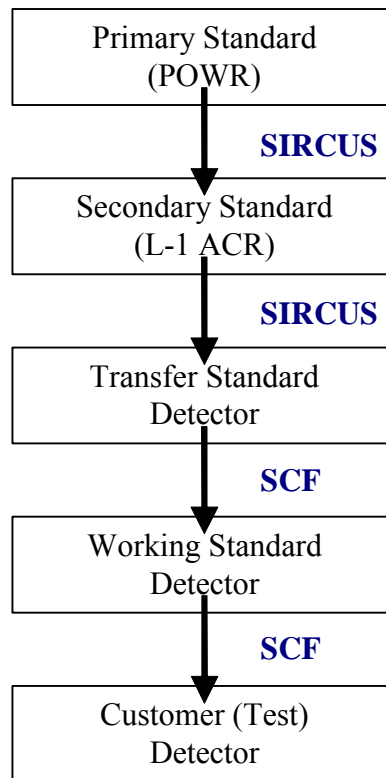


Figure 5.1. Calibration chain for the spectral power responsivity measurements.

The POWR and L-1 ACR are described in Sec. 5.2. Transfer standards (TS) are detectors designed to transfer the spectral radiant power responsivity scale from the cryogenic radiometer to working standard (WS) detectors at the SCF. Transfer standards must measure the same laser sources as the primary standard and also operate at much lower power levels in the lamp-monochromator-based SCF. Also, windowed photodiodes used as working standards at the SCF tend to have interference problems with the coherent laser emission used with cryogenic radiometers. Transfer standards are required to be stable only during the transfer measurements. Working standards, on the other hand, must maintain their responsivity scale for an extended period of time (between recalibrations) since they are used to calibrate customers' detectors throughout the year. The uncertainties in the scale realization and dissemination from the primary standard cryogenic radiometer to the working standards used in the SCF are described in Sec. **Error! Reference source not found.**

5.2 Cryogenic Radiometry

Cryogenic radiometers provide an absolute basis for optical power (flux) measurements at the lowest possible uncertainties. They are used as primary standards for optical power at many other national laboratories as well [35, 40-45]. A cryogenic radiometer is an electrical substitution radiometer (ESR) that operates by comparing the temperature rise induced by optical power absorbed in a black receiving cavity to the electrical power needed to cause the same temperature rise by resistive (ohmic) heating. Thus the measurement of optical power is determined in terms of electrical power, watt, via voltage and resistance standards maintained by NIST⁷. There are several advantages to operating at cryogenic temperatures (≈ 5 K) instead of room temperature. The heat capacity of copper is reduced by a factor of 1000, thus allowing the use of a relatively large cavity. Also the thermal radiation emitted by the cavity or absorbed from the surroundings is reduced by a factor of $\approx 10^7$, which eliminates radiative effects on the equilibrium temperature of the cavity. Finally, the cryogenic temperature allows the use of superconducting wires to the heater, thereby removing the nonequivalence of optical and electrical heating resulting from heat dissipated in the wires. Consequently, most electrical substitution radiometers, including NIST-maintained ESRs, operate at cryogenic temperatures.

The Optical Technology Division within NIST presently has two cryogenic radiometers that provide the basis for the spectral radiant power responsivity scale: the NIST-designed POWR (Figure 5.2), and the L-1 ACR [23] (Figure 5.3). The POWR is the primary U.S. national standard for the unit of optical power. It has the capability to optimize its configuration for measurements in different spectral regions and for different input laser power levels. For optimized noise performance, it can operate at temperatures as low as 1.7 K for extended periods. The L-1 ACR is also an absolute radiometer, but one whose operation is optimized for the μ W to mW power levels in the UV to NIR spectral region. In comparison with POWR, the L-1 ACR is compact and mobile, which makes it a convenient instrument to use for scale transfers. The relative combined standard uncertainty of the NIST cryogenic radiometer measurements range from 0.01 % to 0.02 % in the visible region of the spectrum [27]. The largest components of the uncertainty are those due to the systematic correction for the Brewster angle window transmittance and the nonequivalence between electrical and optical heating. An

⁷ Electrical standards are maintained in the Electronics and Electrical Engineering Laboratory at NIST.

intercomparison between POWR and the L-1 ACR showed that these two standards agreed to within 0.02 %, which is within their combined uncertainties as shown in Figure 5.4 [23].

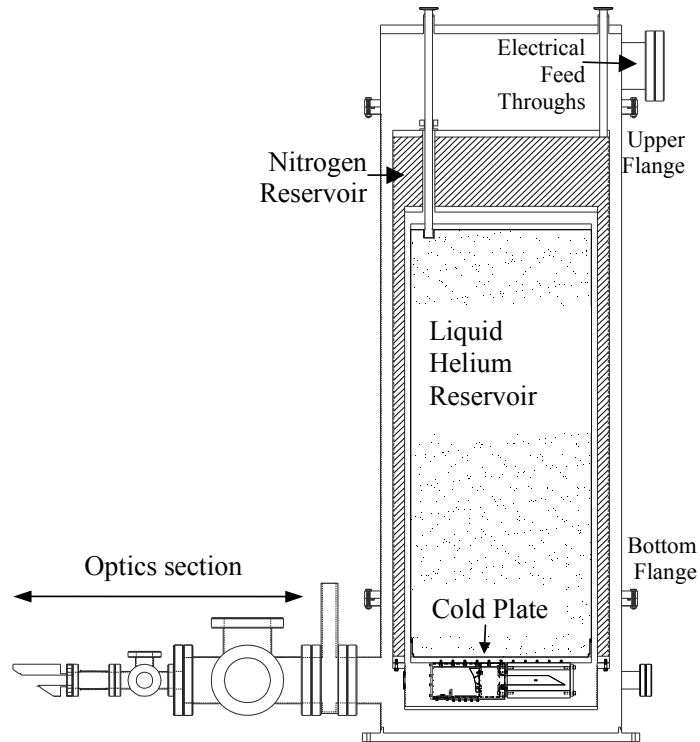


Figure 5.2. The construction of the NIST Primary Optical Watt Radiometer (POWR).

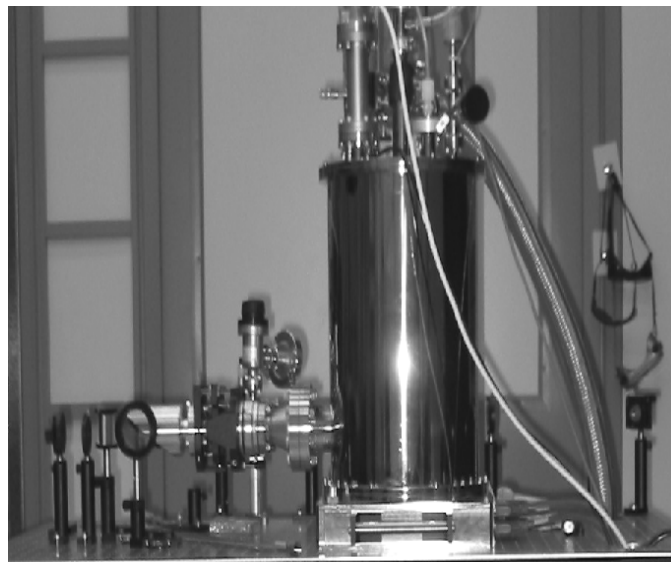


Figure 5.3. The NIST L-1 ACR used in Spectral Irradiance and Radiance Responsivity Calibrations using Uniform Sources (SIRCUS).

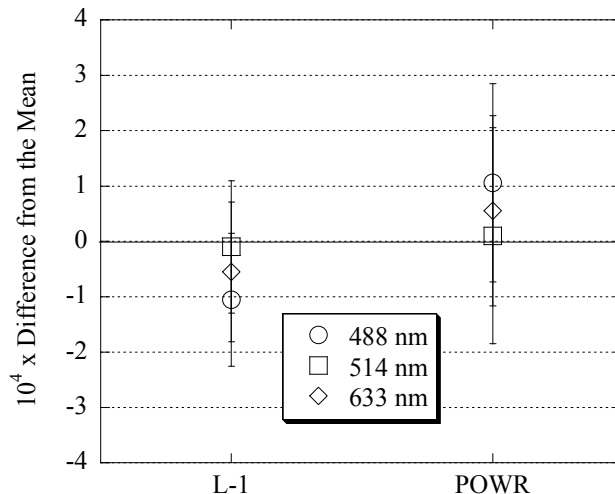


Figure 5.4. Comparison of POWR and the L-1 ACR measurements showing the agreement between the ACRs. The error bars are the measurement uncertainty.

5.3 Calibration of Transfer Standards with a Cryogenic Radiometer

The cryogenic radiometers described above use lasers as their source and a variety of transfer detectors to disseminate the spectral power responsivity scale. Historically, the scale was realized using the High Accuracy Cryogenic Radiometer (HACR) [25] at nine discrete laser lines in the visible wavelength range. A physical model was developed to interpolate the responsivity of silicon trap detectors over the spectral range from 405 nm to 920 nm [24]. Outside of this spectral range, the detector responsivity scale was based on pyroelectric detector with a spectrally flat responsivity [21]. While the pyroelectric detector had a spectrally flat responsivity, its absolute responsivity value was low. While it could extend the scale, its noise performance dramatically increased the uncertainties in the UV and the NIR spectral regions because of the low flux available on the comparator facilities (see the 1998 version of this document [46] for more information). The UV responsivity scale uncertainty was improved by calibrating the UV WS at the NIST Synchrotron Ultraviolet Radiation Facility (SURF III) with an ACR-monochromator system [47, 48]. The NIR responsivity scale uncertainty was reduced by more than a factor of two by also calibrating the pyroelectric detector with the SURF ACR-monochromator system [49].

In order to reduce the overall uncertainties in the scale, especially in the UV and NIR regions, the HACR was replaced by POWR, the newly designed cryogenic radiometer described in Sec. 5.2, and a new measurement protocol was developed with the L-1 ACR, the secondary cryogenic radiometer. The cryogenic radiometers were installed in a new laser facility called the Spectral Irradiance and Radiance Responsivity Calibrations using Uniform Sources (SIRCUS) [27]. The SIRCUS facility has tunable laser sources that cover the range from about 200 nm to over 5 μm . Installing the cryogenic radiometers in the tunable laser facility enables the spectral radiant power responsivity of the transfer detectors to be measured against the primary and secondary standard cryogenic radiometers at numerous wavelengths spanning the range from the UV to the NIR, instead of a few discrete laser lines in the visible. With access to these laser systems, the physical model is no longer used to derive the responsivity scale. Instead, a curve fit is used to interpolate between the data points.

A practical means of disseminating the optical power scale to customers is to first transfer the scale from a cryogenic radiometer in SIRCUS to working standard detectors used in the UV and Vis/NIR SCFs. This transfer of scale requires the use of a detector that can be calibrated at the lowest possible uncertainty by the cryogenic radiometer and yet operate at the flux levels available with the lamp-monochromator sources to calibrate the working standards of the UV and VIS/NIR SCF. The transfer standards are a set of three types of photodiodes that, in combination, covers the wavelength range from 200 nm to 1800 nm.

In the wavelength range from 350 nm to 950 nm, two silicon photodiode trap detectors are used. The trap detectors have excellent stability, spatial responsivity uniformity, linearity, low noise performance [17, 24, 26], and no interference problem with laser emission. Figure 5.5 shows the arrangement of the trap detectors using six windowless silicon photodiodes as the transfer standard detectors. Such a trap configuration makes its responsivity independent from surface reflectance, thus providing excellent spatial uniformity and long-term stability.

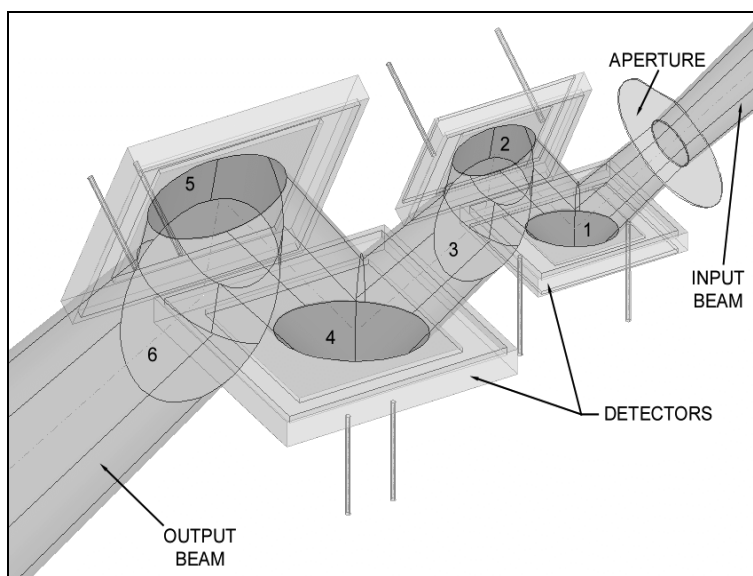


Figure 5.5. Trap detector arrangement of photodiodes maximizes the collection of the optical beam by reducing reflection losses [26].

A UV trap detector has been built at NIST, but its FOV is smaller than the $f/5$ beam from the UV SCF monochromator system. The NIR photodiodes presently available are smaller in size than those available for the visible and UV spectral regions. These NIR photodiodes in a trap detector arrangement would have a FOV smaller than the $f/9$ Vis/NIR SCF monochromator system beam.

The first step in the spectral responsivity scale determination is to transfer the spectral power responsivity scale from the cryogenic radiometer to the transfer standards. Figure 5.6 shows a diagram of the setup used to transfer the scale from the cryogenic radiometer to the transfer detectors using the substitution method. For the lowest possible measurement uncertainty, the cryogenic radiometer requires a monochromatic, collimated, intensity stabilized, laser beam. In this optical system, the combination of a laser intensity stabilizer that alters the beam transmission through a liquid crystal device and a remote beam monitor that is located

downstream on the beam path controls the laser beam intensity to better than 0.01 % over the duration of the measurement. The laser beam is then sent through the combination of a pinhole to create an Airy diffraction pattern, a variable aperture to reduce the scatter, and two spherical mirrors to collimate the beam. This creates a low scatter, collimated laser beam that can be completely collected by both the transfer standard and cryogenic radiometer. In the direct substitution method, both detectors are located in the same focal plane and translated into the laser beam path. First the cryogenic radiometer which measures the laser beam's optical power, then the transfer standard that also makes the same measurement.

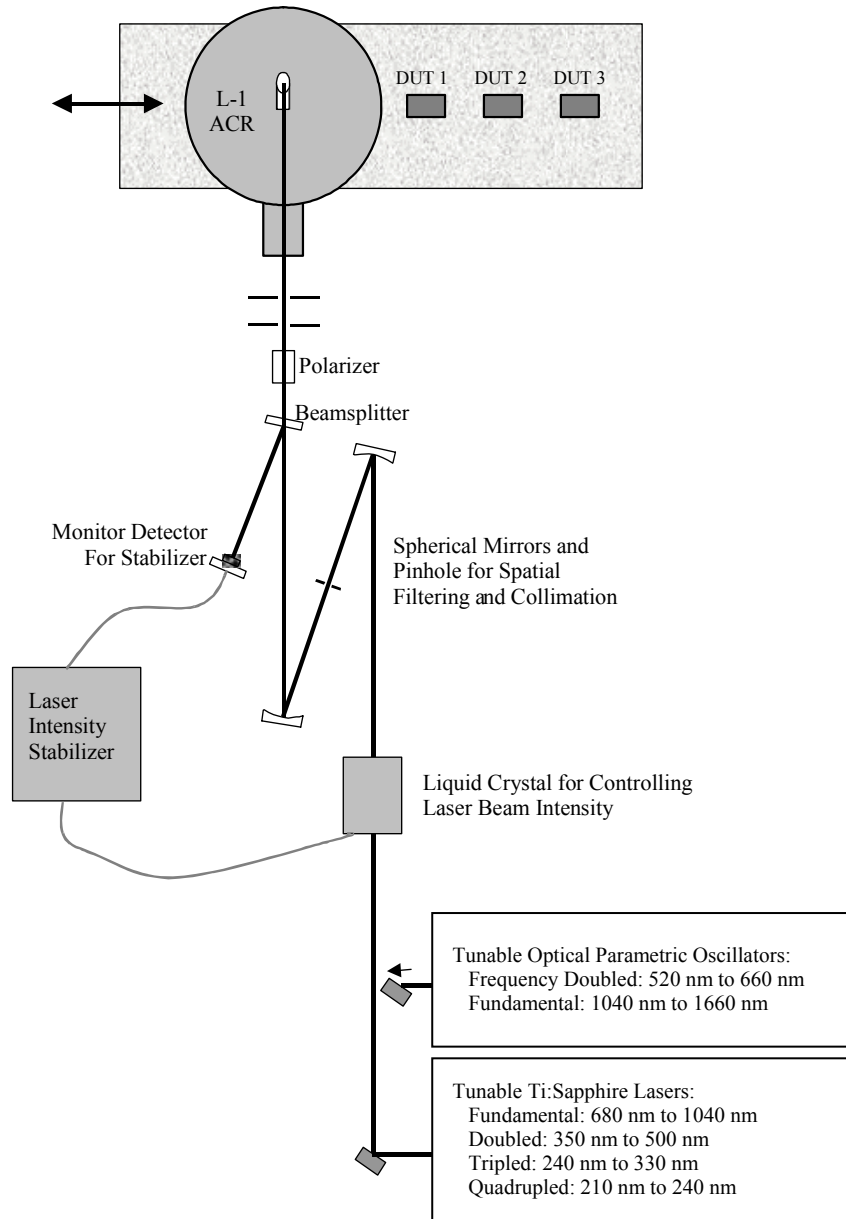


Figure 5.6. Optical configuration for the calibration of the transfer standards with the cryogenic radiometer at the SIRCUS facility.

Two silicon trap detectors (Vis Trap), two germanium photodiode transfer standards (Ge TS) that were temperature-controlled at $-30\text{ }^{\circ}\text{C}$, two indium gallium arsenide photodiode transfer standards (IGA TS), temperature-controlled to 25 ° , several UV transfer standards, and UV trap detectors have been measured by the cryogenic radiometer. The UV detectors were calibration from 210 nm to 400 nm. The Vis Trap detectors were calibrated from 325 nm to 950 nm. The Ge TS were calibrated from 850 nm to 1650 nm and the IGA TS were calibrated from 700 nm to 1800 nm. The spectral power responsivity scale realization is based on laser measurements on SIRCUS at the wavelengths shown in Figure 5.7. Because the SIRCUS calibration did not set the laser wavelengths at exact 5 nm intervals, the spectral responsivity data was interpolated using a modified cubic-spline fit to the 5 nm intervals used in the SCF measurements.

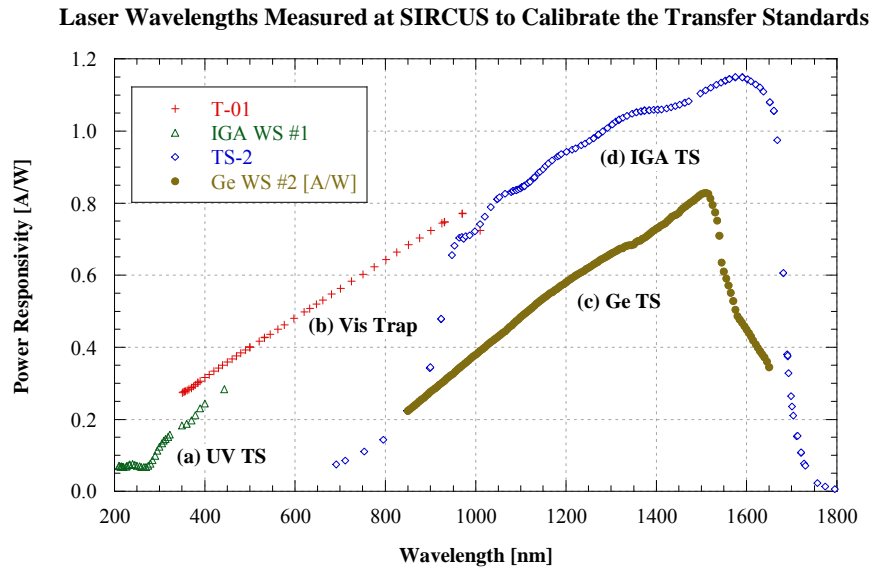


Figure 5.7. SIRCUS laser wavelengths used to calibrate the transfer standards. The data points indicate the wavelengths used for calibrating the (a) UV TS, (b) Vis Trap, (c) Ge TS, and (d) IGA TS.

5.4 Calibration of the Working Standards

Working standards are those used to calibrate customer's detectors routinely at the SCFs. Three sets of working standards are used; one set each for the UV, Visible, and NIR regions. These detectors are measured against the appropriate transfer standards at the SCF using the measurement setup and procedure described in Sec. 6.1 or on another NIST facility, such as SIRCUS. A computer program is used to determine the center of the active area for each detector. The measurements are then taken at this position. The working and transfer standards are operated unbiased (the photovoltaic or short circuit mode) and the signals are measured with calibrated transimpedance amplifiers and DVMs. The amplifier gain for both the working and transfer standards is typically set to 10^6 V/A .

The spectral responsivity is found using eq. (3.27) where $s_s = s_t$, the transfer standard responsivity determined from the cryogenic radiometer measurements. The spectral responsivity of each working standard is the weighted mean of the measurements against two transfer standards. Where the weighting constants are the inverse of a combination of the within TS and

between TS components of variance [50]. That is, the weighting includes both the statistical uncertainty of the comparison with a TS but also the variation between each TS to account for such things as drift during the measurement or (long-term) drift between the TS. The optical power used for these measurements is on the order of 1 μ W or less as shown in Figure 4.2.

5.4.1 Calibration of the Visible Si Working Standards (Vis WS)

The spectral power responsivities of the four visible working standards (Vis WS) were measured in the Vis/NIR SCF using the Vis Traps and the Ge TS. Silicon trap detectors transfer the calibration from 350 nm to 950 nm while temperature-controlled Ge TS transfer the scale to the Vis WS from 955 nm to 1100 nm. Both Vis Traps and Ge TS were measured at SIRCUS in varying step sizes against the L-1 ACR to determine the external quantum efficiencies. The external quantum efficiency data was interpolated to 5 nm intervals and used to calculate the spectral power responsivity scale for the transfer to the Vis/NIR SCF. The calibration chain for the Vis WS is shown in Figure 5.8. Basing the calibration of the Vis WS on a combination of transfer standards provides the lowest possible uncertainties over the entire wavelength range. The uncertainties for the Vis WS are described in Sec. 7.3.1.

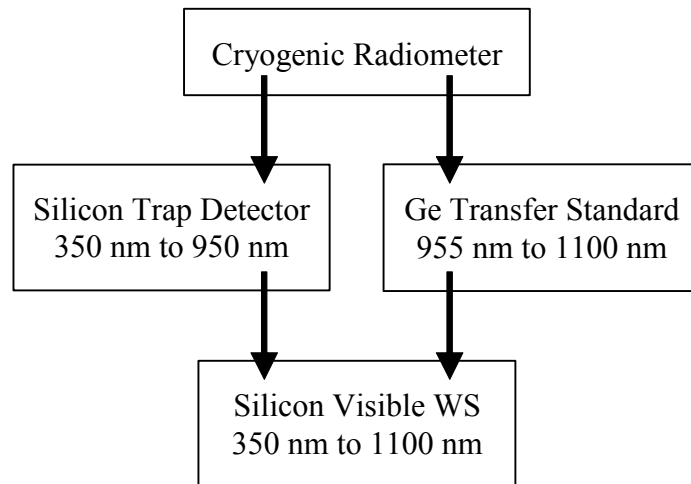


Figure 5.8. The calibration chain for the visible working standards (Vis WS).

The responsivity of Vis WS was determined by averaging 3 independent scans against each Vis Trap detector and Ge TS. That is, the WS was removed from the SCF and then realigned between each scan. The resulting data from the two sets of transfer standards were combined to create a single scale from 350 nm to 1100 nm for the Vis WS.

5.4.2 Calibration of the Ultraviolet Working Standards (UV WS)

Two UV working standards (UV WS) were calibrated from 200 nm to 400 nm by a series of measurements at the UV SCF, Vis/NIR SCF, SIRCUS, and SURF with various Si photodiode UV transfer standards and trap detectors. The UV WS were calibrated with a Vis Trap at the Vis/NIR SCF from 405 nm to 500 nm. The combination of the UV transfer standards and the Vis Trap provides the lowest uncertainties over the entire UV WS calibration range. The calibration chain for the UV working standards is shown in Figure 5.9. The uncertainties on the UV working standards are described in Sec. 7.3.3.

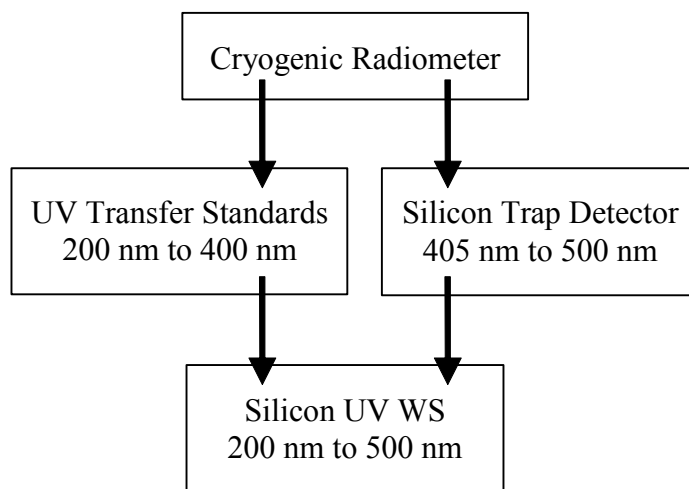


Figure 5.9. The calibration chain for the ultraviolet working standards (UV WS).

The responsivity of the UV WS was determined by an average of 3 independent scans against each UV TS and Vis Trap. As with the Vis WS, each UV WS was removed from the SCF and realigned between each scan. The resulting data from the transfer standards were combined to create a single scale from 200 nm to 500 nm for the UV WS.

5.4.3 Calibration of the Near-IR InGaAs Working Standards (IGA WS)

The IGA working standards (IGA WS) responsivities are determined on the Vis/NIR SCF using the Vis WS over the spectral region from 700 nm to 950 nm and the IGA TS from 955 nm to 1650 nm. The IGA TS were measured at the SIRCUS facility against a cryogenic radiometer in varying step sizes from 700 nm to 1800 nm to determine the external quantum efficiencies. The external quantum efficiency data was interpolated to 5 nm intervals and used to calculate the spectral power responsivity scale for the transfer to the Vis/NIR SCF. The IGA TS were not calibrated at enough wavelengths in the spectral region greater than 1650 nm to adequately interpolate the responsivity due to the steep drop in the IGA responsivity in this spectral region. The previous calibration of the IGA WS was used between 1655 nm and 1800 nm (as described below). This combination of the Vis WS and the InGaAs TS provided the lowest uncertainties over the entire IGA working standards responsivity range. Figure 5.10 shows the NIR measurement chain and the measurement uncertainties are described in Sec. 7.3.2.

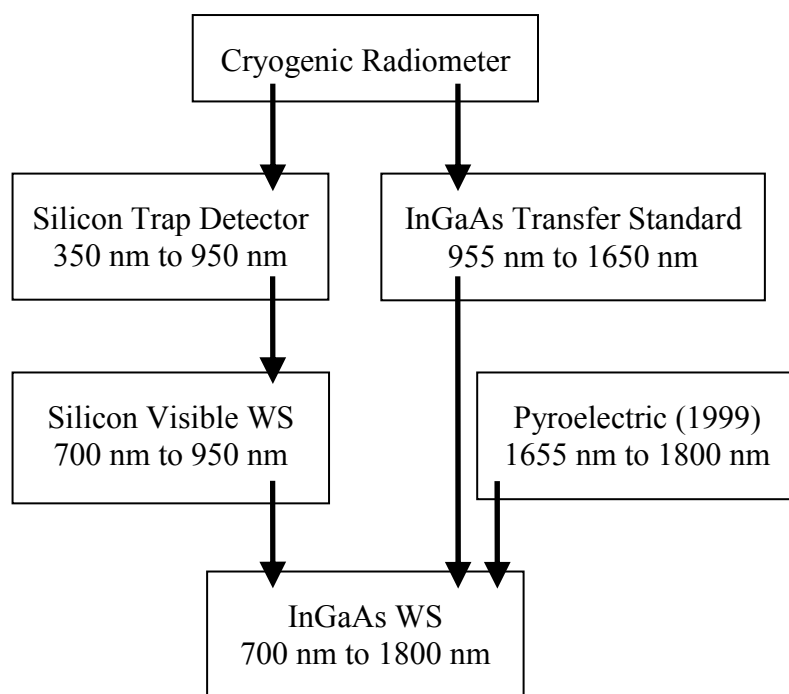


Figure 5.10. The calibration chain for the InGaAs working standards (IGA WS).

The scale transfer of the IGA WS was determined by averaging 3 independent scans against the Vis WS and the IGA TS. Each IGA WS was removed from the SCF and realigned between each scan. The resulting data from the two sets of standards were combined to create a single scale from 700 nm to 1650 nm for the IGA WS

Until 1999, a slightly different calibration method was used. The scale in the 1650 nm to 1800 nm spectral region is still based on this method at the time of this publication. The IGA WS responsivities were determined at the Vis/NIR SCF using a Vis Trap over the spectral region

from 700 nm to 920 nm and a pyroelectric detector from 925 nm to 1800 nm. This calibration occurred before the POWR cryogenic radiometer was operational. The previous primary cryogenic radiometer, HACR, was used to calibrate the Vis Trap. The relative responsivity of the pyroelectric detector was measured from 700 nm to 1800 nm with the SURF ACR-monochromator system [49]. The relative responsivity of the IGA WS was measured with the pyroelectric detector from 700 nm to 1800 nm on the Vis/NIR SCF. The IGA WS relative responsivity was scaled to the calibrated power responsivity from 700 nm to 920 nm. This combination gave the lowest transfer uncertainty. Figure 5.11 shows the 1999 NIR measurement chain.

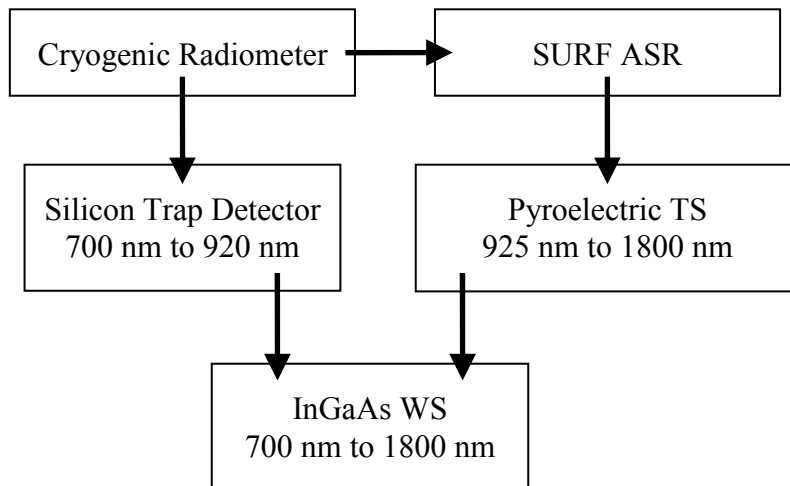


Figure 5.11. The 1999 calibration chain for the InGaAs working standards (IGA WS).

The scale transfer of the IGA WS was determined by averaging 3 independent scans against each Vis Trap and the pyroelectric detector. Each IGA WS was removed from the SCF and realigned between each scan. The resulting data from the two sets of transfer standards were combined to create a single scale from 700 nm to 1800 nm for the IGA WS.

6. Calibration Procedures and Computer Automation

6.1 Spectral Radiant Power Responsivity

This section describes the spectral radiant power responsivity measurement procedures for both the UV SCF and Vis/NIR SCF. These correspond to Service ID numbers 39071C through 39078C. The primary operational difference between the two SCFs is that the UV SCF can accommodate one test detector per responsivity measurement run while the Vis/NIR SCF can measure two test detectors. The responsivity spatial uniformity for new photodiodes, which is included in 39071C, 39073C, and 39077C, is also measured as described in Sec. 6.2.

6.1.1 Calibration Procedures

New photodiodes are visually inspected for defects and placed in the specially designed mounting fixtures described in Sec. 9.4. Each photodiode has a serial number engraved on the mount. The photodiode dynamic impedance (shunt resistance) is measured with an HP 4145A I-V plotter to confirm the manufacturer's specification. [Note: The shunt resistance of the photodiode needs to be about 1000 times greater than the input impedance of the transimpedance amplifier for it not to deviate from linear operation [26, 39]. For the transimpedance amplifier circuit typically used with the SCFs, the open-loop gain of the op-amp is 10^6 and an amplifier gain (determined by the feedback resistor) of 10^6 is used, thus giving an input impedance of $G_{\text{amp}}/G_{\text{ol}} = 1 \Omega$. Thus the photodiode shunt resistance must be greater than $10 \text{ k}\Omega$ for a non-linearity in the current-to-voltage conversion of less than 0.01 %.] If needed, the diode window is cleaned⁸ with lens tissue and spectral-grade acetone before any optical measurements are made. Methanol can be used immediately after acetone when cleaning optics to get rid of any acetone residue or a mixture of methanol/acetone is sometimes used [51]. Ethanol has also been used by others to clean photodiodes and optical windows [30].

The spectral responsivity is determined by substitution with two working standards using the "substitution method with monitor" described in Sec. 3.2.3. The two working standards are selected from a randomly generated weekly schedule. The test detector(s) and working standard detectors are aligned perpendicular to the optical axis by using the He-Ne laser as the monochromator source and retroreflecting the He-Ne beam back onto itself. The appropriate broadband source used for the measurement is chosen and the detector positioned at the focal plane of the SCF exit optics. A computer program automatically centers the active area of each detector to the optical axis.

The typical comparison measurement consists of scanning the monochromator through the desired spectral range at wavelength intervals of 5 nm for each detector. The test detector(s) and Vis WS are operated unbiased (the photovoltaic or short-circuit mode) and the signals are measured with calibrated transimpedance amplifiers and DVMs. Figure 4.2 shows that the optical power used for these measurements is typically less than $1 \mu\text{W}$. The test-to-monitor (Eq. (3.23)) and working standard-to-monitor (Eq. (3.24)) ratio data are stored on the computer for later analysis to determine the spectral responsivity. The standard deviation of the test (or

⁸ Cleaning a photodiode can change its responsivity.

working standard) and monitor detector ratios is less than either individual signal standard deviation. This is the result of simultaneously sampling both the test (or working standard) and monitor detector in a beam with small fluctuations in power level. Examples of the typical signals from a Hamamatsu S1337 and the monitor photodiode are shown in Figure 6.1. Also shown are the signal ratios and the relative standard deviations of each signal and ratio. Figure 6.1 shows the ratio relative standard deviation is lower than either individual signal standard deviation.

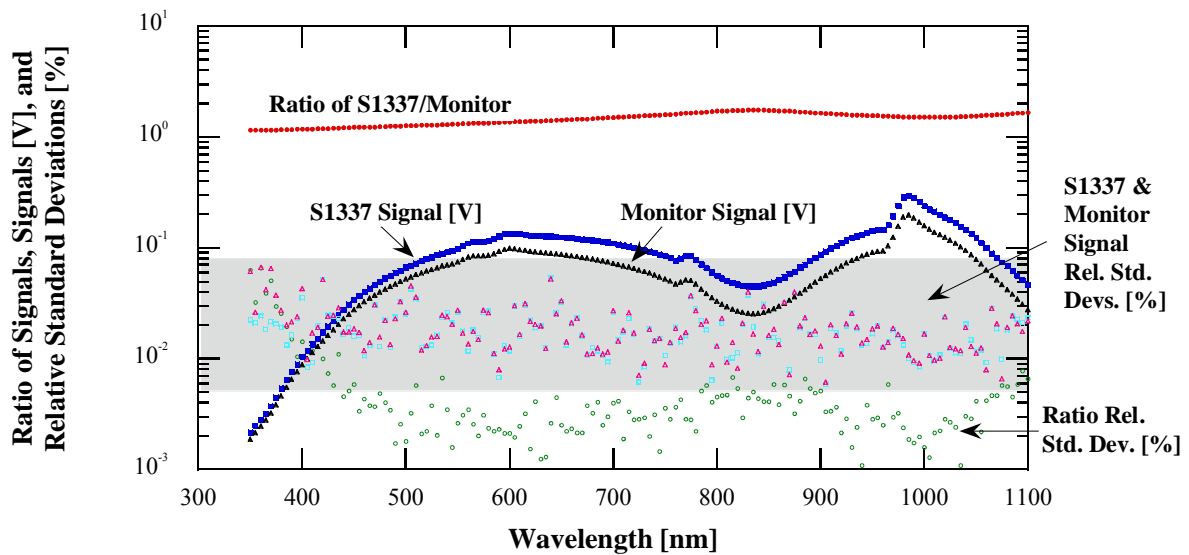


Figure 6.1. Typical signals from Hamamatsu S1337 and monitor photodiodes.

In Figure 6.1 all curves are the means of 10 samples. The relative standard deviations of the S1337 and monitor signals are shown respectively as open squares and triangles in the shaded area. The relative standard deviations of the ratios are shown as open circles and for measurements above 400 nm are lower than the individual signal standard deviations. Note: The S1337 and monitor signal standard deviation curves are nearly indistinguishable because the source noise rather than detector noise dominates the measurement.

The laboratory environment (temperature and humidity) is monitored and recorded at the start of each scan. This data is not used to correct the measurement results. The temperature of detectors that have temperature sensors built into their housings can also be recorded. The average temperature during the measurements is reported.

The spectral responsivity is determined by using Eq. (3.27) for each test and working standard detector spectral scan combination. The reported spectral responsivity of the test detector is the weighted mean [50] of all the scans with both working standard detectors. Examples of typical photodiode spectral responsivities are shown in Figure 6.2.

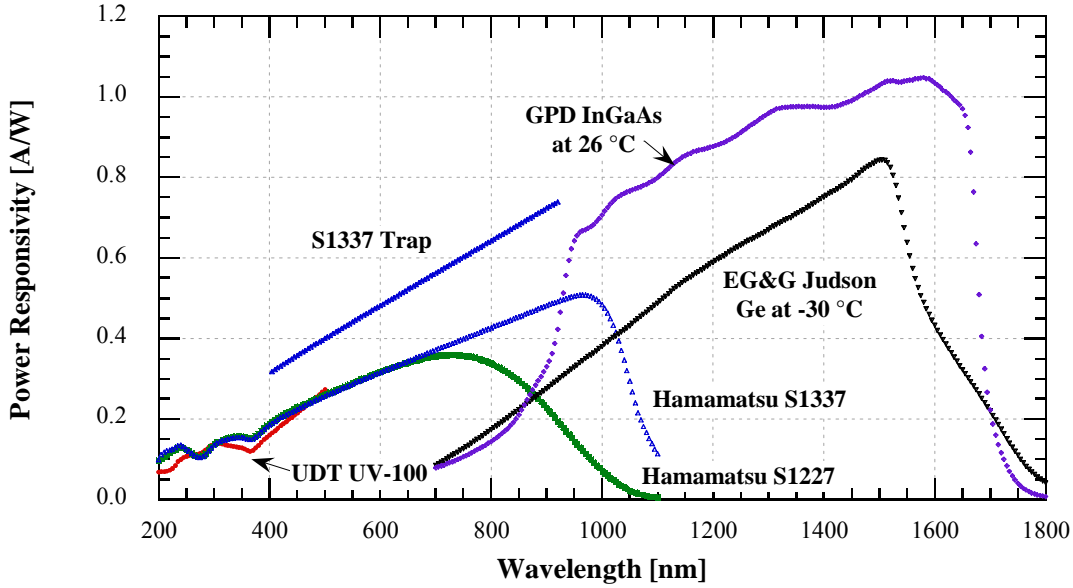


Figure 6.2. Spectral responsivities of typical Si, InGaAs, and Ge photodiodes.

6.1.2 Quantum Efficiency

The quantum efficiency is the photon-to-electron conversion efficiency of a photoelectric detector. The quantum efficiency of a detector is often required for particular applications. There is a simple calculation to convert spectral responsivity [A/W] to external quantum efficiency. The external quantum efficiency, η_{ext} , is given by [13, 24]:

$$\eta_{\text{ext}}(\lambda) = \frac{i(\lambda) \cdot h \cdot c}{\Phi(\lambda) \cdot n \cdot e \cdot \lambda}, \quad (6.1)$$

where i is the photocurrent (output current minus the dark output), h is Planck's constant, c is the velocity of light, Φ is the input radiant flux (power), n is the index of refraction of air, e is the elementary electronic charge, and λ is the spectral wavelength (in air). Substituting for the constants h , c , n , and e gives:

$$\eta_{\text{ext}}(\lambda) = 1239.48 \times \frac{i(\lambda)}{\Phi(\lambda) \cdot \lambda} = 1239.48 \times \frac{s(\lambda)}{\lambda}, \quad (6.2)$$

where $s(\lambda) = i(\lambda)/\Phi(\lambda)$ is the spectral responsivity [A/W], and for convenience, λ is in nm. Examples of typical photodiode EQEs are shown in Figure 6.3.

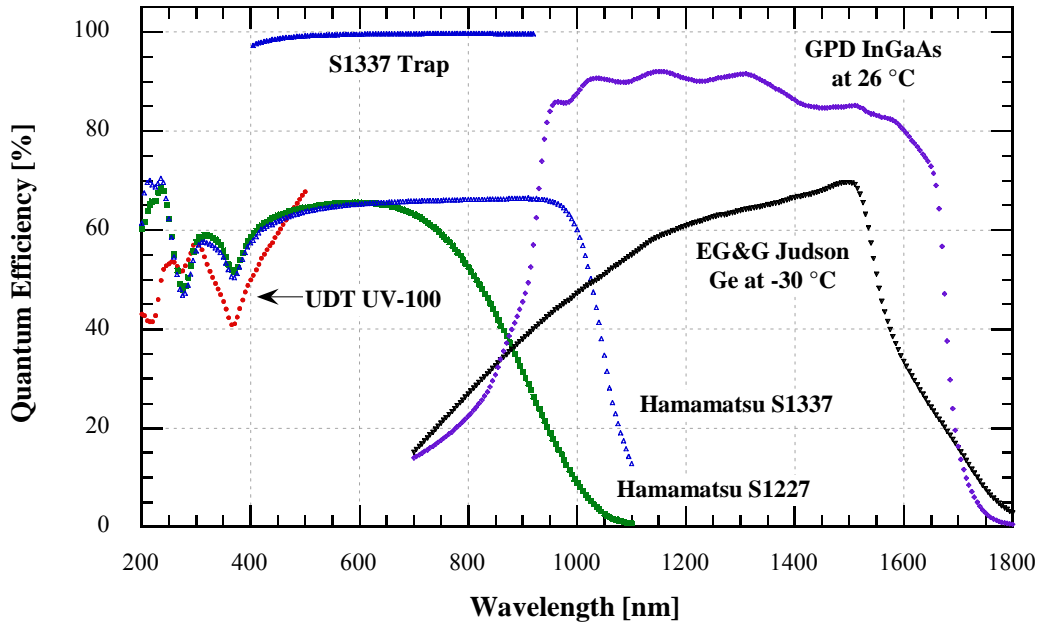


Figure 6.3. Quantum efficiencies of typical Si, InGaAs, and Ge photodiodes.

6.2 Spatial Uniformity

This section describes the procedures used in NIST Service ID numbers 39071C, 39073C, 39077C, and 39081S to determine the responsivity spatial uniformity of detectors. The spatial uniformity measurement procedures are the same for both the UV SCF and Vis/NIR SCF. The major difference between the two is the beam size. The UV SCF beam diameter is 1.5 mm and the Vis/NIR SCF beam diameter is 1.1 mm as described in sections 4.1 and 4.2. Also, only one detector can be measured at a time in the UV SCF while all four detector positions can be used in the Vis/NIR SCF for spatial uniformity measurements since no working standard detector is needed.

The spatial uniformity is measured for all photodiodes issued from NIST, at 350 nm for the OSI Optoelectronics UV-100 photodiodes (39071C), at 500 nm for the Hamamatsu S2281 photodiodes (for 39073C and 39077C). UV-100 photodiodes are not issued if the responsivity nonuniformity (i.e., slope) is greater than 1 % over the active area or greater than 0.5 % within the center 50 % of the active area or if a discontinuity (a peak or valley) in the responsivity greater than 0.5 % is found within the center 90 % of the active area. Hamamatsu S2281 photodiodes are not issued if the nonuniformity is greater than 0.5 % over the active area or greater than 0.25 % within the center 50 % of the active area or if a discontinuity greater than 0.25 % is found within the center 90 % of the active area.

In the early 1990's, it was found that many silicon photodiodes have a significant change in the uniformity as a function of wavelength, particularly as the wavelength approached the bandgap (1100 nm). Nonuniformity is due to inhomogeneity in the photodiode material - typically inhomogeneity in surface recombination centers at shorter wavelengths [52, 53] and bulk recombination centers at longer wavelengths [54]. The nonuniformity near the bandgap has also been related to the nonuniformity of the bonding material's reflectance [55]. Because the

semiconductor is almost transparent near the bandgap, changes in the spatial reflectivity of the bonding material affect the amount of light reflected and therefore the responsivity of the photodiode.

Since 1993, the uniformity of the S1337-1010BQ and the S2281 diodes are also measured at 1000 nm [56]. Photodiodes are not issued if the nonuniformity is greater than 1 % over the active area or greater than 0.5 % within the center 50 % of the active area. Also, if a discontinuity greater than 0.5 % is found within the center 90 % of the active area.

S1337-1010BQ and S2281 photodiodes with a significant change in uniformity between 500 nm and 1000 nm are seen less frequently in recently manufactured diodes. Diodes issued by NIST prior to the discovery of this effect in 1993 were not measured at 1000 nm. When these diodes are resubmitted for measurement (39074S), the uniformity is checked at 1000 nm; and the customer is notified if a significant nonuniformity is found.

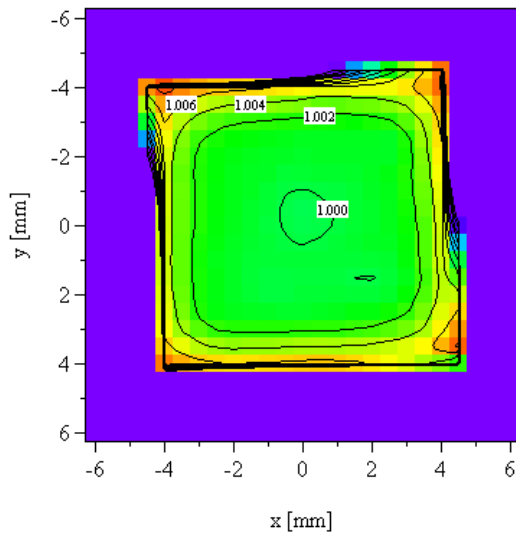
6.2.1 Measurement Method and Calibration Procedure

The detectors are aligned as described in Sec. 6.1.1. The typical measurement consists of setting the monochromator to the desired wavelength and scanning a 12 mm x 12 mm area in 0.5 mm steps, for a 1 cm² test detector. The test detector is operated unbiased (the photovoltaic or short-circuit mode); and the signal is measured with a calibrated transimpedance amplifier and a DVM. The typical amplifier gain for the test detector is 10⁶ V/A. Figure 4.2 shows the optical power for these measurements is typically less than 1 μW. The test to monitor (Eq. (3.23)) ratio data is stored on the computer for later analysis.

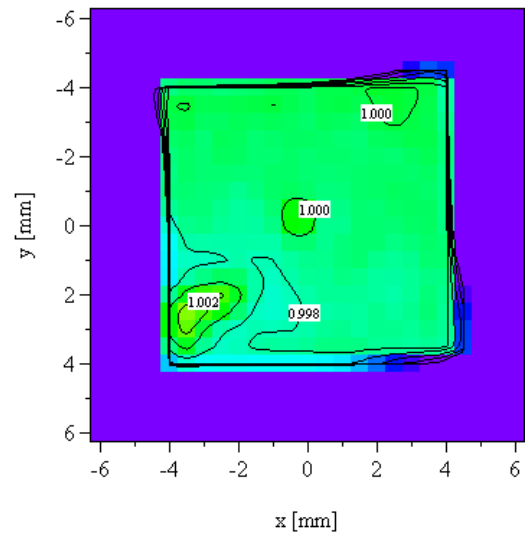
The scans are always in the same horizontal direction; and the vertical direction is reversed in a “raster” scan, starting in the upper left corner moving to the lower right corner of the photodiode. The scan is large enough for the beam to move completely off of the active area (or onto an aperture). Scanning horizontally in only one direction puts the stage drive against the same side of the drive screw. For the vertical, gravity keeps the stage always against the same side of the screw. This reduces hysteresis in the movement of the stages.

The laboratory environment (temperature and humidity) is monitored and recorded at the beginning and end of each scan. This data is not used to correct the measurement results. The temperature detectors that have temperature sensors built into their housings can also be recorded. The average temperature during the measurements is reported.

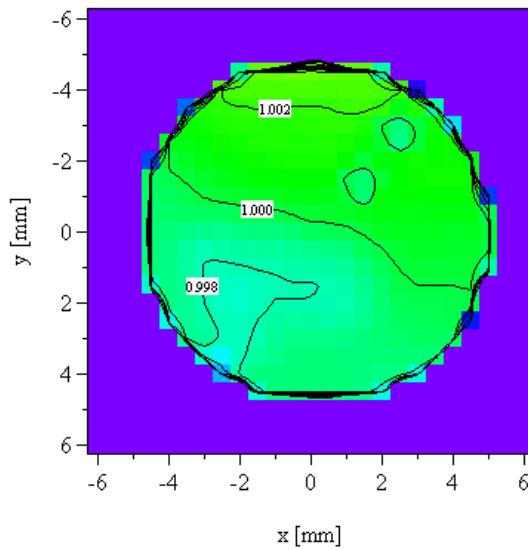
The test to monitor detector ratios are normalized to the mean of the center ratios. The reported spatial uniformity figure is constructed from these normalized ratios. Figure 6.4 shows the spatial uniformities of the central portion of typical Hamamatsu S1337-1010BQ and S2281 photodiodes at 500 nm and 1000 nm. Similar spatial uniformity scans are shown in Figure 6.5a for UV-100 at 350 nm and Figure 6.5b, c, and d for Judson EG&G thermoelectrically cooled Ge photodiodes at 1000 nm, 1500 nm, and 1600 nm, respectively.



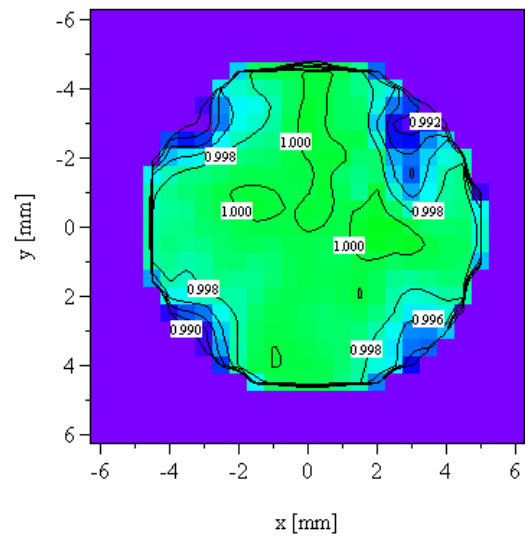
(a) Hamamatsu S1337 at 500 nm.



(b) Hamamatsu S1337 at 1000 nm.

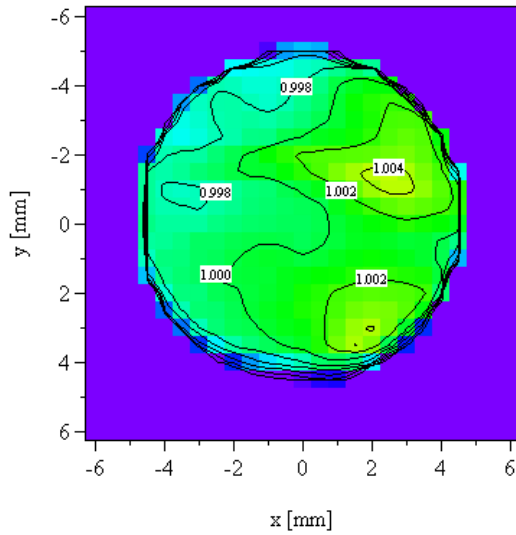


(c) Hamamatsu S2281 at 500 nm.

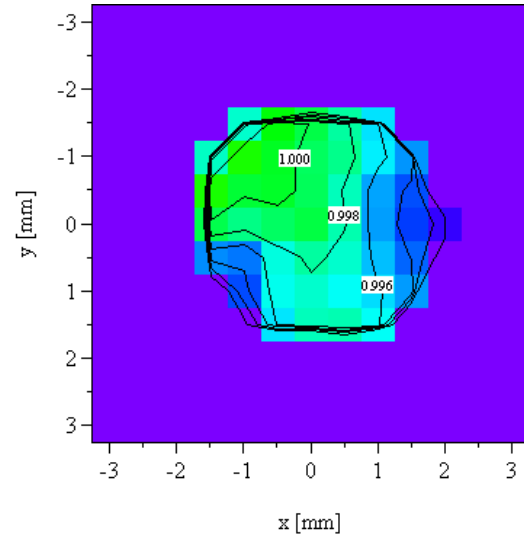


(d) Hamamatsu S2281 at 1000 nm.

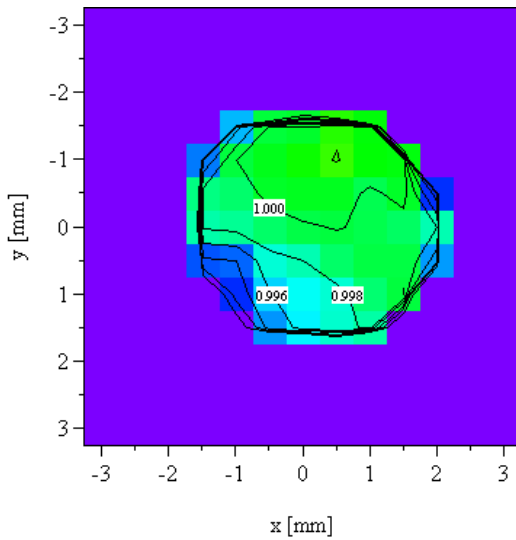
Figure 6.4. Spatial uniformities of typical Hamamatsu S1337 and S2281 photodiodes. The responsivities are normalized to the center values.



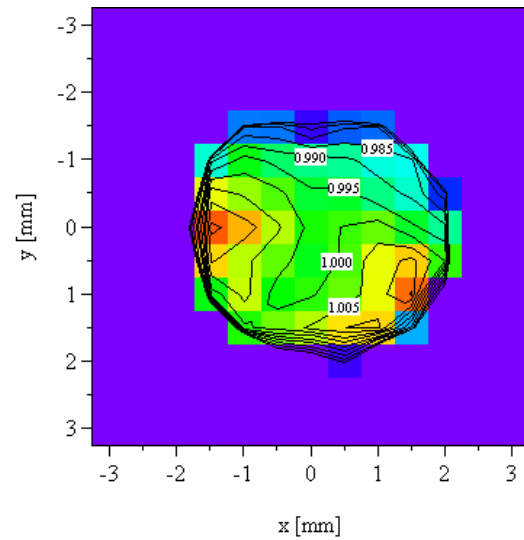
(a) OSI Optoelectronics UV-100 at 350 nm.



(b) EG&G Judson TE Ge at 1000 nm.



(c) EG&G Judson TE Ge at 1500 nm.



(d) EG&G Judson TE Ge at 1600 nm.

Figure 6.5. Spatial uniformities of typical OSI Optoelectronics UV-100 and EG&G Judson Ge photodiodes. The responsivities are normalized to the center values.

6.2.2 Limitations

The size of the active area to be measured has to be significantly larger than the beam size to avoid the edges of the active area or aperture in front of the detector. Also the spatial shape of the optical beam is assumed constant during the measurement.

6.3 Computer Automation

This section describes the computer automation of the UV and Vis/NIR comparator facilities. The automated equipment and computer software used for typical measurements are briefly described. The operation of the spectral comparator facilities would not be practical without a high degree of computer automation.

6.3.1 Computer Automated Equipment

A block diagram of the computer controlled equipment for the Vis/NIR SCF is shown in Figure 6.6. All of the equipment is controlled by one computer via an IEEE-488 (GPIB) bus. This computer stores all of the data and the analyzed responsivity files. A local area network (LAN) connects this computer with other computers which are used for data analysis, writing test reports, and calibration related file backups; allowing the SCF control computer to be dedicated to taking measurements. Daily backups of the data files are made to an external hard drive connected to the SCF control computer.

Several key components of the SCFs are controlled by commercial servo motor controllers: the horizontal and vertical (x,y) translation stages, source section, and the rotary stage in the UV SCF. The wavelength drive of the Cary-14 monochromator used with the Vis/NIR SCF was modified and is also driven by a computer controlled servo motor with an absolute encoder mounted on the wavelength drive shaft.

All of the DVMs, lock-in amplifiers, and multiplexers are computer controlled. A digital I/O module addressed over the IEEE-488 bus signals the shutter controllers to open or close. A commercial laboratory environmental monitor records the laboratory and enclosure temperature and humidity. Some test (customer) detectors have temperature monitoring circuitry that produces a voltage signal or resistance proportional to their temperature. These signals can also be multiplexed via computer control to the DVM. The WS temperature controllers are also computer controlled via the IEEE 488 bus.

The UV SCF equipment and computer control is very similar to the Vis/NIR. The only differences are in the monochromator wavelength control and the translation of the detectors into the optical beam. The UV monochromator wavelength drive did not require any modification to be computer controlled and as mentioned, the UV SCF uses a rotary stage to move the detectors and only one detector has automated horizontal and vertical (x,y) translation stages.

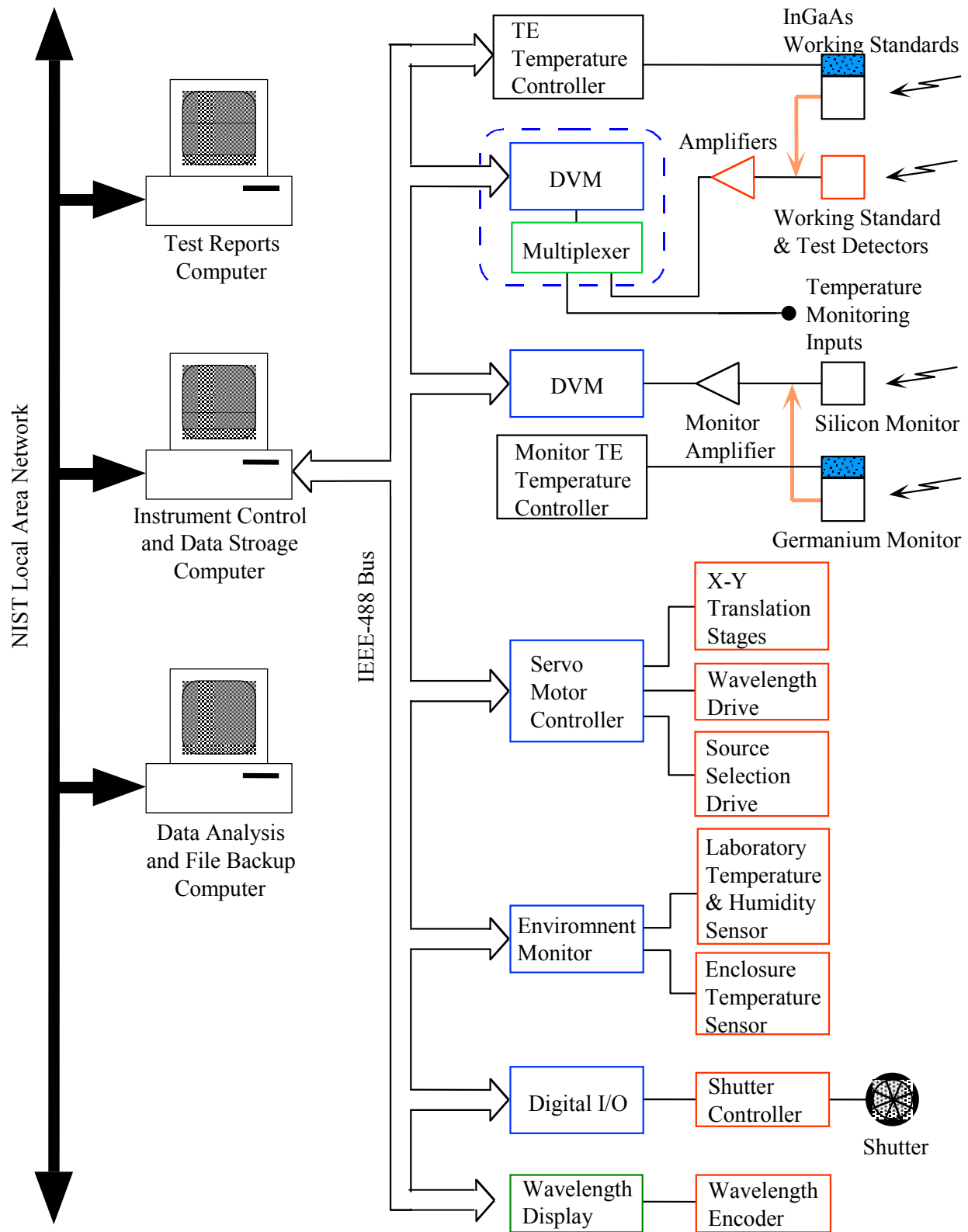


Figure 6.6. Vis/NIR SCF computer control block diagram.

6.3.2 Computer Calibration Programs

SCF Setup Program

This program performs three functions: initialize the SCF instruments, align the test and working standard (WS) detectors, and verify the signal levels from the detectors before starting measurements. The operator uses this program interactively, via the front panel controls and a joystick to control the translation stages, to align new detectors in the SCF. This program updates a file that contains the detector names and translation stage (x,y) positions used by other computer programs.

Spectral Power Scanning Program

This program takes data from one to four detectors (test and working standard detectors), stores the data on hard disk, and prints the results. The analysis program can be set to automatically run when the measurements finish. The operator sets several detector parameters such as the time constant, amplifier gain, whether to use a detector (position), and whether the detector is a working standard. Other operator inputs are the spectral range start and stop wavelengths, spectral step size, number of samples at each wavelength, number of (repeat) scans for the measurement, and which SCF source to use. The operator can also input specific comments about the measurement.

After the parameters have been entered, the program positions the first detector into the beam and starts taking data. The program determines the test (measurement) number and creates unique filenames for each detector using this number and the detector's name entered in the SCF setup program. The program updates the computer display with the current scan number, the detector name and position for the current measurement, filename, and the file pathname. The program also graphs the test detector to monitor ratio (Eq. (3.23)), the working standard detector to monitor ratio (Eq. (3.24)), and the percent standard deviation of the ratios. The program saves the "raw" ratio data files on the hard disk after each detector spectral scan. After completion of the measurement, records are printed of the operator inputs and graphs of the detector to monitor ratios and the percent standard deviation of the ratios.

Spectral Power Responsivity Calculation Program

This program calculates the spectral power responsivity for the test detector. The results are stored on the hard disk and the responsivity and relative measurement uncertainty data are printed as graphs, along with the detector filenames, and control settings. The inputs to the program are the test and working standard detector "raw" ratio data filenames, working standard reference (calibration) data filename, and the selection of the transimpedance amplifier used with the test detector.

The gain range and detector position in the SCF are extracted from the data files for the test and working standard detectors. This is used to select the corrected (calibrated) gain factor for the appropriate NIST amplifier. For detectors with internal amplifiers the gain range is multiplied by the customer supplied amplifier gain correction factor to determine the corrected gain factor, or a factor of 1.0 is used if no amplifier gain correction is supplied. Next, the program reads and formats the ratio data files and the working standard reference data file. The program determines

the responsivity for a test detector by using Eq. (3.27) for each spectral scan combination of test detector and working standard. Then, if more than one spectral scan was taken, a weighted mean is calculated. Where the weighting constants are the inverse of a combination of the within TS and between TS components of variance. The uncertainty for the weighted average is also calculated as the inverse of the square root of the sum of the weights [50].

Spatial Scanning Program

This program spatially scans the SCF beam across the active area of the detector by using the x,y translation stages to translate the detector. The data is stored on hard disk, and the measurement results are printed when the program finishes execution. One detector in the UV SCF and up to four detectors in the Vis/NIR SCF can be measured at one time. The measurements can be programmed to repeat at different wavelengths.

The program inputs are the scan wavelength, number of samples at each data point, detector parameters such as the time constant and amplifier gain, whether to use a detector (position), and operator comments. Also input are the spatial scan horizontal (x) and vertical (y) dimensions and step sizes. The program determines the test number and creates a unique test filename with the test number, detector name, and wavelength.

The program moves the detector to the first x and y position and takes the detector-to-monitor signal ratio measurement (Eq. (3.23)). The program scans the detector from top to bottom and left to right. That is, the x,y movement is from the top left to the bottom right (or top right depending on the number of columns measured). The program displays a *quasi* three dimensional graph of the signal ratios.

7. Uncertainty Evaluation

The uncertainty evaluation for the detector spectral power responsivity measurements is explained in this section. First the uncertainty is evaluated for the measurement equation developed in Sec. 3. In addition to the uncertainty terms that come directly from the measurement equation there are terms due to the wavelength uncertainty of the monochromator, long-term stability of the working standards, and the assumptions and approximations made during the development of the measurement equation. Second, the uncertainty for each group of working standards and the transfer to customer detectors is given in detail. The uncertainty analysis follows the method outlined in Refs. [7, 8, 57]. A general discussion of the sources of error in radiometry can be found in Refs. [58, 59]. A detailed explanation of the evaluation and expression of measurement uncertainty in radiometry is given in Refs. [60, 61].

Note: The uncertainty evaluation described in this section was prepared before the publication of Ref. [61] and thus differs somewhat from the analysis described there. In the future, the uncertainty evaluation will follow Ref. [61].

7.1 Uncertainty Calculation from the Measurement Equation

In general, a measurement result y can be expressed as a functional relationship f of N input quantities x_i given by,

$$y = f(x_1, x_2, \dots, x_N). \quad (7.1)$$

If the input quantities are not correlated, the combined standard uncertainty $u_c(y)$ is given by the law of propagation of uncertainty as the following sum,

$$u_c(y) = \sqrt{\sum_{i=1}^N \left(\frac{\partial f}{\partial x_i} \cdot u(x_i) \right)^2}, \quad (7.2)$$

where the partial derivatives $\partial f/\partial x_i$ are the sensitivity coefficients and $u(x_i)$ are the standard uncertainties of each input x_i . This method is also called the root-sum-of-squares or “RSS” method.

When the functional relationship involves products and quotients, as the measurement equation described in this document, the relative combined standard uncertainty $u_c(y)/y$ is more convenient, and is given by

$$u_{c,rel}(y) \equiv \frac{u_c(y)}{y} = \sqrt{\sum_{i=1}^N \left(\frac{1}{y} \cdot \frac{\partial f}{\partial x_i} \cdot u(x_i) \right)^2}, \quad (7.3)$$

where $(1/y) \cdot (\partial f/\partial x_i)$ is the relative sensitivity coefficient. The expanded uncertainty U is obtained by multiplying $u_c(y)$ by a coverage factor k ,

$$U = k \cdot u_c(y), \quad (7.4)$$

where k is chosen on the basis of the level of confidence desired. Replacing $u_c(y)$ with the relative combined standard uncertainty $u_{c,rel}(y)$ gives the relative expanded uncertainty $U_{rel} \equiv U/y$. The coverage factor $k = 2$ is used in this document following the NIST policy [9] so that the interval defined by U has a level of confidence of approximately 95 %.

The uncertainty $u_0(s_x)$ in the test detector spectral responsivity, calculated from the simplified measurement equation (Eq. (3.27)), is considered. The calculation is made by using the propagation of standard uncertainty relationship in Eq. (7.2). The measurement equation for spectral responsivity, $s_x(\lambda)$, is:

$$s_x(\lambda) = \frac{R_x(\lambda)}{R_s(\lambda)} \cdot \frac{G_s}{G_x} \cdot s_s(\lambda). \quad (7.5)$$

The responsivity uncertainty of the test detector at a single wavelength $u_0(s_x)$ is:

$$u_0(s_x) = \left[\left(\frac{\partial s_x}{\partial R_x} \cdot u(R_x) \right)^2 + \left(\frac{\partial s_x}{\partial R_s} \cdot u(R_s) \right)^2 + \left(\frac{\partial s_x}{\partial G_s} \cdot u(G_s) \right)^2 + \left(\frac{\partial s_x}{\partial G_x} \cdot u(G_x) \right)^2 + \left(\frac{\partial s_x}{\partial s_s} \cdot u(s_s) \right)^2 \right]^{\frac{1}{2}} \quad (7.6)$$

The relative uncertainty $u_0(s_x)/s_x$ is:

$$\frac{u_0(s_x)}{s_x} = \sqrt{\left(\frac{u(R_x)}{R_x} \right)^2 + \left(\frac{u(R_s)}{R_s} \right)^2 + \left(\frac{u(G_s)}{G_s} \right)^2 + \left(\frac{u(G_x)}{G_x} \right)^2 + \left(\frac{u(s_s)}{s_s} \right)^2} \quad (7.7)$$

or

$$u_{0,rel}(s_x) = \sqrt{u_{rel}^2(R_x) + u_{rel}^2(R_s) + u_{rel}^2(G_s) + u_{rel}^2(G_x) + u_{rel}^2(s_s)}$$

where $u(R_x)$ is the standard deviation of the mean of i ratios of the test detector and the monitor, $u(R_s)$ is the standard deviation of the mean of i ratios of the standard detector and the monitor, $u(G_s)$ is the standard detector amplifier gain uncertainty, $u(G_x)$ is the test detector amplifier gain uncertainty, $u(s_s)$ is the standard detector uncertainty, and i is the number of ratio measurements taken. The quantities $u(R_x)$ and $u(R_s)$ are measurement noise.

The standard detector uncertainty, $u(s_s)$, is determined previously by the absolute cryogenic radiometer transfer measurements. The amplifier gains, G_s and G_x , are calibrated using a precision current source and DVM. The amplifier gain uncertainties, $u(G_s)$ and $u(G_x)$, are the RSS of the uncertainties from the precision current source and DVM.

The first two terms contribute uncertainty due to the measurement statistics (Type A uncertainties). The remaining terms are Type B uncertainties. If more than one scan is taken for

a measurement, then a weighted mean, is calculated. Where the weighting constants are the inverse of a combination of the within scan and between scan components of variance. The uncertainty for the weighted average is also calculated as the inverse of the square root of the sum of the weights [50]. The uncertainty for the weighted mean is an indication of the measurement repeatability. Repeated scans are used when the test detector exhibits short-term drift.

Note that Eq. (3.27) is simplified with assumptions that several measurement conditions are ideal. In real world detector measurements, additional uncertainty components from the characteristics of the detector being measured and the measurement facility (discussed in the next section) should be considered. Extending Eq. (7.7) and assuming that these additional uncertainty contributions, $u_{1,rel}(s_x)$, $u_{2,rel}(s_x)$, $u_{3,rel}(s_x)$, ... are not correlated, the relative combined standard uncertainty, $u_{c,rel}(s_x)$, of the test detector spectral responsivity is given by:

$$u_{c,rel}(s_x) = \sqrt{u_{0,rel}^2(s_x) + u_{1,rel}^2(s_x) + u_{2,rel}^2(s_x) + \dots + u_{n,rel}^2(s_x)}. \quad (7.8)$$

7.2 Uncertainty Components in Test Detector Calibration

The uncertainty components not discussed in the previous section include 1) the wavelength scale uncertainty in the monochromator, 2) effect of the monochromator bandpass, 3) ambient temperature effects on the detectors, 4) long-term stability of working standards, 5) measurement reproducibility, 6) uncertainty in the DVMs' calibration, 7) spectral stray-light and 8) other factors not considered significant. All the uncertainty components, including those discussed in Sec. 7.1 based on the measurement equation, are listed in Table 7.1.

Table 7.1 Uncertainty components in photodetector calibration

Symbol	Type	Component of uncertainty
$u_{rel}(S_s)$	B	Uncertainty of the working standard detector
$u_{rel}(R_x)$	A	Noise in the test-to-monitor ratio
$u_{rel}(R_s)$	A	Noise in the standard-to-monitor ratio
$u_{rel}(G_x)$	B	Amplifier gain for test detector
$u_{rel}(G_s)$	B	Amplifier gain for standard detector
$u_{1,rel}(s_x)$	B	Wavelength scale uncertainty of monochromator
$u_{2,rel}(s_x)$	B	Effect of bandpass of monochromator
$u_{3,rel}(s_x)$	B	Ambient temperature of detectors
$u_{4,rel}(s_x)$	B	Long-term stability of the working standards
$u_{5,rel}(s_x)$	A	Measurement reproducibility
$u_{6,rel}(s_x)$	B	Calibration of DVMs used to measure R_x and R_s
$u_{7,rel}(s_x)$	B	Spectral stray-light effect
$u_{8,rel}(s_x)$	A	Other components (spatial nonuniformity of responsivity, etc.)

The first five components were discussed in Sec. 7.1. Each of the components $u_{1,rel}(s_x)$ to $u_{8,rel}(s_x)$ is discussed below and is evaluated in sections 7.3 and 7.4.

7.2.1 Wavelength Uncertainty of the Monochromator

The wavelength scale of both SCF monochromators is calibrated annually by using several laser and spectral-line discharge lamp lines, and a correction curve is fitted. There are residual errors (typically less than 0.1 nm) after the wavelength scale is corrected. Random shifts in the wavelength scale due to the scanning mechanism and drift of the scale over time are negligible compared to the residual scale errors.

The uncertainty in the measured spectral responsivity due to an uncertainty component is called an uncertainty contribution. The uncertainty contribution due to wavelength uncertainty is proportional to the slope of the ratio of the test to monitor and standard to monitor signal ratios, $dr_x/d\lambda$, where $r(\lambda) = R_x(\lambda)/R_s(\lambda)$ and $dr_x/d\lambda$ is the sensitivity coefficient. The relative uncertainty contribution $u_{1,\text{rel}}(s_x)$ is calculated as the product of the sensitivity coefficient and the standard uncertainty $u(\lambda)$ of the wavelength,

$$u_{1,\text{rel}}(r_x(\lambda_i)) = \frac{\{r_x(\lambda_{i+1}) - r_x(\lambda_i)\}}{r_x(\lambda_i)} \cdot \frac{1}{\Delta\lambda} \cdot u(\lambda), \quad (7.9)$$

where $r_x(\lambda_i)$ is the signal ratio at the i th wavelength point, $r_x(\lambda_{i+1})$ is at the next measurement point, separated by scanning interval $\Delta\lambda$.

The wavelength errors tend to cancel out if the test detector and the standard detector are the same type, having nearly identical relative spectral responsivity curves ($R_x(\lambda) \approx R_s(\lambda)$). Thus, this uncertainty is normally insignificant for typical photodiode measurements, except in wavelength regions where responsivity curve sharply rises or drops near the bandgap. This error can also be significant for filtered detectors, radiometers, and photometers, which tend to have steep slopes in the responsivity curve and/or sharp cut-on and cut-off regions.

Also, it should be noted that wavelength errors also occur if the bandpass of the monochromator is asymmetric and if the wavelength calibration is done using the peak of the bandpass. The SCFs do not have this error, because the monochromators' bandpasses have been verified as symmetric and the centroid wavelength is used for wavelength calibration.

7.2.2 Effect of Bandpass

The bandpass of the monochromator can cause errors when the spectral responsivity curve is not linear within the full-bandwidth of the bandpass, and can cause significant errors where spectral responsivity curves change rapidly, e.g., near rising or falling parts of the curve, or at the peak or valley of the curve. The measured spectral responsivity is a convolution of the true spectral responsivity and the normalized bandpass function. At each wavelength point, the measured responsivity $s_{\text{meas}}(\lambda_0)$ is calculated as a product of the true spectral responsivity $s(\lambda)$ and the normalized bandpass function $b(\lambda_0 - \lambda)$, thus,

$$s_{\text{meas}}(\lambda_0) = \int_{\lambda} s(\lambda) \cdot b(\lambda_0 - \lambda) \cdot d\lambda \quad \text{with} \quad \int_{\lambda} b(\lambda) = 1. \quad (7.10)$$

To estimate this error without knowing the true responsivity $s(\lambda)$, the measured responsivity data is used as $s(\lambda)$ for an approximation. The spectral responsivity data is first interpolated to a 1 nm

interval, and the $b(\lambda)$ function (normally a triangular function) is also calculated at 1 nm intervals and normalized so that the sum of all $b(\lambda)$ values is equal to 1, then a sum-product calculation is performed as given in Eq. (7.10). The error due to the bandpass can be evaluated by looking at the difference between $s_{\text{meas}}(\lambda)$ and $s(\lambda)$.

$$\varepsilon_{\text{B,rel}}(\lambda) = \frac{s_{\text{meas}}(\lambda) - s(\lambda)}{s(\lambda)} \quad (7.11)$$

In substitution measurements, this error also tends to cancel out if the test detector and standard detector have similar spectral responsivity curves. In this case, the relative error for the test detector $\varepsilon_{\text{B,rel,test}}(\lambda)$ and for the working standard detector $\varepsilon_{\text{B,rel,std}}(\lambda)$ can be calculated, and the substitution error $\varepsilon_{\text{B,sub}}(\lambda)$ in the measured test detector is given by:

$$\varepsilon_{\text{B,sub}}(\lambda) = \varepsilon_{\text{B,rel,test}}(\lambda) - \varepsilon_{\text{B,rel,std}}(\lambda). \quad (7.12)$$

An example of a calculation of Eq. (7.12) for a UV photodiode for a triangular 4 nm bandpass function is shown in Figure 7.1.

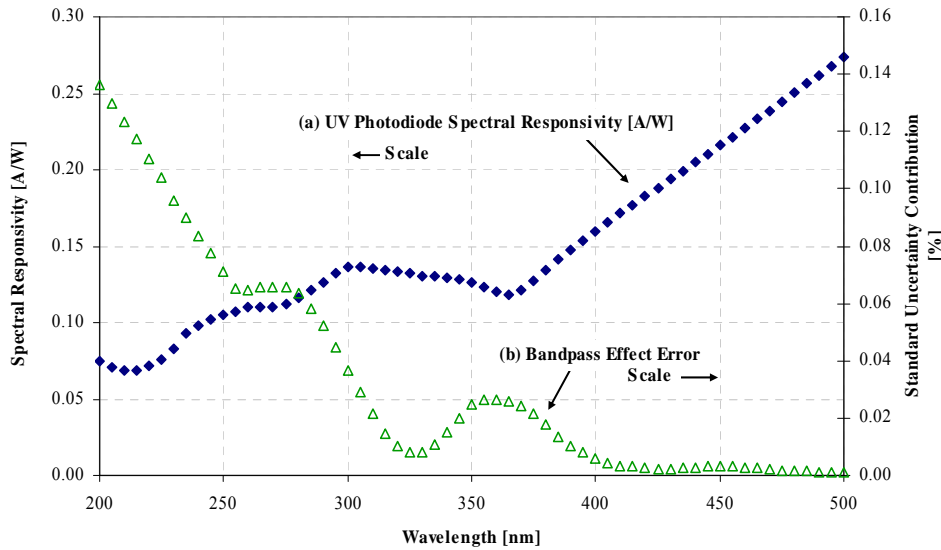


Figure 7.1. Error due to effect of bandpass for UV photodiode. The figure shows the (a) UV photodiode spectral responsivity [A/W] and (b) the bandpass effect error standard uncertainty contribution [%].

If a correction is not made for the bandpass error, the estimated error is converted to a standard uncertainty using a rectangular distribution, thus,

$$u_{2,\text{rel}}(s_x) = \varepsilon_{\text{B,sub}}(\lambda) / \sqrt{3}. \quad (7.13)$$

7.2.3 Ambient Temperature

The responsivity temperature coefficient is typically small for most detectors, but can be significant depending on the type of detector and wavelength region, especially for wavelengths near the bandgap of a semiconductor photodiode. The ambient temperature inside the SCF enclosures is recorded and the average value during a calibration is reported in the NIST calibration report. The temperature variation in the enclosures is small during the measurements (normally less than 0.5 °C). The temperature sensors have a small uncertainty, thus, altogether, ± 0.5 °C combined standard uncertainty is typically reported for the ambient temperature. **Since it is not possible to know in advance what the ambient temperature will be when the customer uses a detector, a temperature coefficient uncertainty component is not included in the customer detector uncertainty estimates.**

The effect of ambient temperature changes for the UV WS and monitor is negligible in the 200 nm to 500 nm spectral region where calibrations are performed. The IGA WS and Ge monitor are thermoelectrically temperature controlled, and thus their temperature does not change. **Thus, the temperature effects are negligible for the UV and IGA WS and are not listed in the uncertainty budgets.**

For the Vis WS and monitor detector the ambient temperature effect is negligible for most of the spectral range. In the NIR spectral region (> 960 nm for the Hamamatsu S1337 and S2281) the temperature effect can be a significant uncertainty component. For the Vis WS, the change in temperature is estimated to be a maximum of 1 °C from the time the Vis WS was calibrated to the time (possibly months later) when a customer detector is calibrated.

7.2.4 Long-term Stability

The working standards are calibrated on a 12 to 18 month schedule, and the long-term stability of their responsivities between recalibrations is critical for reliable calibration results. The working standard long-term stability is evaluated by the change in spectral responsivity between each calibration. Stability data needs to be accumulated over several calibrations to obtain an accurate estimate of the stability.

For the Vis WS and monitor detector the temperature effect is less than the long-term uncertainty for most of the spectral range. In the NIR spectral region (> 960 nm for the Hamamatsu S1337 and S2281) the temperature effect may be larger than the stated long-term uncertainty. However, mounting the silicon working standards in recently acquired temperature-controlled fixtures is expected to reduce the temperature effect significantly, and should reduce the uncertainty component for long-term stability in the NIR spectral region.

The long-term changes in the UV WS and the temperature controlled IGA WS are not affected significantly by temperature variations. **The long-term uncertainty component is not included in the customer detector uncertainty estimates.** The customer should evaluate and include the long-term uncertainty of their detector in their measurement uncertainty analysis.

7.2.5 Measurement Reproducibility

There is also a statistical uncertainty term (Type A) reflecting the reproducibility of the measurements (e.g., setting up the measurement again the next day). The uncertainty due to reproducibility includes day-to-day temperature and alignment variations.

New detectors types (models) that have never been measured before by NIST are calibrated three times with the detectors being re-mounted and aligned for each measurement. This produces three independent measurements and the reproducibility component is the relative standard deviation of the three scans.

7.2.6 DVM Uncertainty

The values R_x and R_s are the ratios of signals which were taken simultaneously by two DVMs. One DVM is used for both test detector and standard detector and the second DVM is used for the monitor, thus systematic errors normally cancel out unless the test detector and standard detector use different DVM ranges for the same wavelengths (i.e., very different responsivities). Similarly, if the dark signal (shutter closed) and total signal (shutter open) use the same DVM range then the systematic errors cancel when the (net) signal is calculated.

The stability of the two DVMs over the measurement time (typically 1 h) is of concern. The 24 h “Percent of Reading” manufacturer specification is used in lieu of a stability specification to calculate the uncertainty. **The DVM uncertainty is typically found to be negligible (<0.01 %) compared to other components, and is not listed in the subsequent uncertainty budget.**

7.2.7 Spectral Stray-light

In principle, stray-light in a double monochromator as used in the SCFs is normally negligible. To verify this, the stray-light error was estimated by using a simple model of a slit-scattering function of the double monochromator:

$$z(\lambda_0 - \lambda) = \begin{cases} 1 & \text{for } (\lambda_0 - \Delta\lambda/2) \leq \lambda \leq (\lambda_0 + \Delta\lambda/2) \\ 10^{-7} & \text{otherwise} \end{cases} \quad (7.14)$$

The $\Delta\lambda$ is the in-band (bandpass) region of the monochromator and is set to 4 nm for the SCFs. The value of 10^{-7} is based on measurements taken with a portable tunable laser system where the laser was tuned over the in-band region at several wavelength settings of the monochromators. The measurements for the Vis/NIR SCF monochromator were very similar to measurements taken on an identical model monochromator [62]. These values are typical for a double monochromator. From Eq. (3.7), the in-band signal $V_{IB}(\lambda_0)$ of the detector at wavelength λ_0 is given by:

$$V_{IB}(\lambda_0) = \int_{\Delta\lambda} S_x(\lambda) \cdot \Phi_{\lambda,rel}(\lambda) \cdot \tau(\lambda) \cdot z(\lambda_0 - \lambda) \cdot d\lambda, \quad (7.15)$$

where $\Phi_{\lambda,rel}(\lambda)$ is the relative spectral radiant flux entering the entrance slit of the monochromator, and $\tau(\lambda)$ is the spectral transmittance of the monochromator system. For simplicity, $\tau(\lambda)$ is assumed to be constant.

Similarly, from Eq. (3.10), the stray-light signal $V_{SL}(\lambda_0)$ of the detector is given by:

$$V_{SL}(\lambda_0) = \int_{\lambda \neq \lambda_0} S_x(\lambda) \cdot \Phi_{\lambda,rel}(\lambda) \cdot \tau(\lambda) \cdot z(\lambda_0 - \lambda) \cdot d\lambda. \quad (7.16)$$

The spectral integration is done over the entire region where the spectral responsivity is not zero (to the extent the data is available). The relative error due to stray-light is then estimated by:

$$\varepsilon_{SL}(\lambda_0) = \frac{V_{SL}}{V_{IB}}. \quad (7.17)$$

This error also tends to be cancelled out if the test detector and standard detector have similar responsivity curves. The value from Eq. (7.17) gives the worst case. This error was calculated for each type of working standard detector used with the SCFs and the spectrum of the quartz-halogen lamp or the argon mini-arc. The error due to stray-light was found to be negligible in all cases at any wavelength. **Because the errors were found to be negligible, this component is not listed in the subsequent uncertainty budgets.**

7.2.8 Other Components

Several other factors that could contribute uncertainty components were mentioned in Sec. 3.1.1 and are discussed here. Stable detector responsivities are fundamental for detector-based radiometry. Detector responsivity stability has been the subject of several past and present studies [63-72]; and, for this application, short-term instability has not been observed. Long-term stability has already been discussed. Effects of polarization have been studied and found to be negligible for the typical situation, where the detectors are measured at normal incidence to the optical axis (and the detector surfaces are isotropic). The effect of the converging beam angle on the reflectance (and transmittance) from the detector surface (and window) is small compared to the variance of repeated measurements and is typically neglected. Water condensation (onto the detector or window) and the effects of water absorption have not been observed and are neglected. As mentioned earlier, diffraction and coherence effects are negligible for these comparator systems.

The responsivity spatial uniformity is typically measured but not explicitly used in the uncertainty analysis. Since the same beam size and geometry is used for both the calibration of the WS detectors and the customer's detectors and the automatic alignment is very reproducible, the spatial non-uniformity effects are negligible. No estimate for the uncertainty component is given for different beam sizes or geometries. These could significantly add to the estimated uncertainty given in this publication.

Similarly, the monochromator beam profile and shape have been measured, but are not explicitly used in the uncertainty analysis, because they have negligible effect on the measurement.

Spatially (or geometrically) scattered light is light scattered out of the nominal monochromator beam and is thought to be primarily due to imperfections in the optics. The spatially scattered light cancels when the test and standard detectors are the same size or are large enough to collect all of the radiation from the monochromator over an area of uniform responsivity. This is the typical measurement condition and thus the spatially scattered light is normally neglected. But,

occasionally, test detectors having a different size of the sensitive area are measured, in which case, the error due to the scattered light is considered. As mentioned in Sec. 3.2.4, the background signal voltage from the detector amplifier has been measured (beam blocked and shutter open) and found to be negligibly different than the signal with the shutter closed.

The reflected beam from the test detector(s) and working standard detectors travels “backwards” along the optical axis and is assumed to be scattered inside the monochromator. Any of the reflected beam that returns to the detector is considered part of the geometrically scattered light discussed above. The reflected beam from the monitor is not returned along the same path and is diffusely scattered inside the enclosure on the other side of the baffle from the test detector and working standard detectors. It contributes to the background radiation previously mentioned.

Effects of detector nonlinearity have been discussed in the literature [3, 36, 38, 54, 73-79]. The detector linearity has been measured for the Hamamatsu S1337-1010BQ and the OSI Optoelectronics UV-100 silicon photodiodes and is discussed in Sec. 9. At the power levels used for routine measurements, nonlinearity is not a consideration.

The frequency response of the detector and amplifier is important to consider when comparing absolute measurements between chopped (optically modulated or ac) and dc measurements. Chopped measurements are not part of the typical calibration and are not considered here. Information on uncertainties with chopped radiation measurements can be found in Ref. [39].

7.3 Transfer from Cryogenic Radiometer to Working Standards

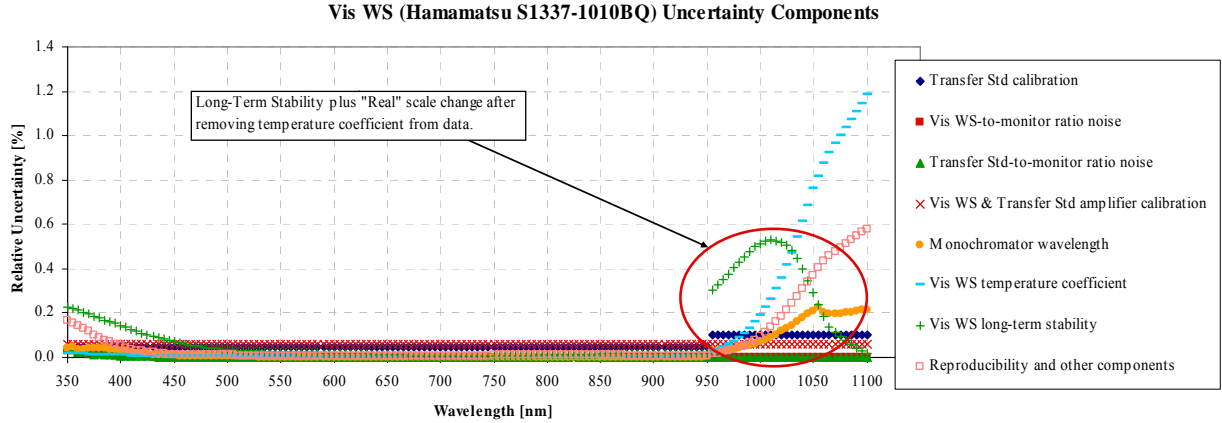
In this section a detailed listing of the uncertainty components for each type of working standard is provided along with a description of how each component was obtained. The data was calculated at 5 nm intervals as shown in the figures; and abbreviated numerical tables are provided. The amplifier calibration uncertainties are all identical because identical amplifiers are used and they are calibrated using the same equipment and procedure. Wavelength calibration, bandpass effects, ambient temperature effects, long-term ambient stability, reproducibility, DVM uncertainty, stray-light uncertainty components were calculated as described in Sec. 7.2 using typical data. All uncertainty components were considered independent and combined by RSS to get the relative combined standard uncertainty shown.

7.3.1 Visible Silicon Working Standards (Vis WS) Uncertainty

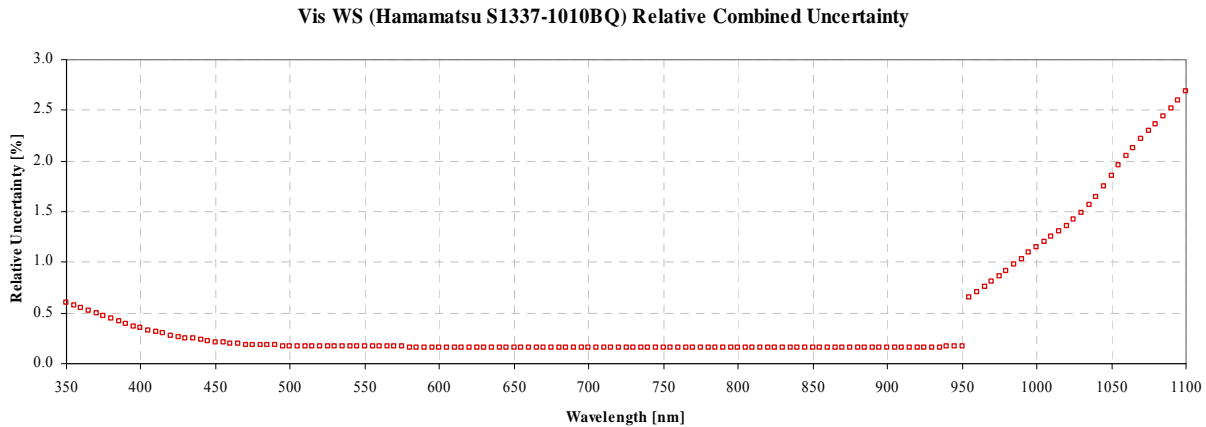
Table 7.2 lists the uncertainty components for the two transfer calibrations used for the Vis WS. The Vis Trap and Ge TS uncertainties are from the L-1 ACR transfer [23]. The bandpass effect is negligible (<0.01 %). The amplifier uncertainty components (0.04 %) for the WS and TS are combined by RSS for a value of 0.06 % in the table. As mentioned in Sec. 7.2.3, the change in ambient temperature is estimated to be a maximum of 1 °C. The long-term stability is estimated by using the typical data for a Vis WS over a one year period. All the components are shown at 5 nm intervals in Figure 7.2a. The components were combined by RSS to get the relative combined standard uncertainty listed in Table 7.2 and shown at 5 nm intervals in Figure 7.2b.

Table 7.2. Visible working standard uncertainty (transfer from Vis Trap and Ge TS)

Wavelength [nm]	Uncertainty contribution from each component of uncertainty [%]								Relative combined standard uncertainty [%]
	Transfer Std calibration	Vis WS-to- monitor ratio noise	Transfer Std-to- monitor ratio noise	Vis WS & Transfer Std amplifier calibration	Monochro- mator wavelength	Vis WS temperature coefficient	Vis WS long-term stability	Reproducib- ility and other components	
	Type B	Type A	Type A	Type B	Type B	Type B	Type B	Type A	
350	0.05	0.03	0.04	0.06	0.04	0.02	0.23	0.17	0.30
375	0.05	0.01	0.01	0.06	0.04	0.01	0.19	0.10	0.23
400	0.05	0.00	0.01	0.06	0.03	0.01	0.14	0.05	0.17
425	0.05	0.00	0.01	0.06	0.02	0.01	0.10	0.03	0.13
450	0.05	0.00	0.00	0.06	0.01	0.01	0.07	0.01	0.11
475	0.05	0.00	0.00	0.06	0.01	0.00	0.05	0.01	0.09
500	0.05	0.00	0.00	0.06	0.00	0.00	0.04	0.01	0.09
525	0.05	0.00	0.00	0.06	0.00	0.00	0.03	0.01	0.08
550	0.05	0.00	0.00	0.06	0.00	0.00	0.02	0.01	0.08
575	0.05	0.00	0.00	0.06	0.00	0.00	0.02	0.01	0.08
600	0.05	0.00	0.00	0.06	0.00	0.00	0.02	0.01	0.08
625	0.05	0.00	0.00	0.06	0.00	0.00	0.02	0.01	0.08
650	0.05	0.00	0.00	0.06	0.00	0.00	0.01	0.01	0.08
675	0.05	0.00	0.00	0.06	0.00	0.00	0.01	0.01	0.08
700	0.05	0.00	0.00	0.06	0.00	0.00	0.01	0.01	0.08
725	0.05	0.00	0.00	0.06	0.00	0.00	0.00	0.01	0.08
750	0.05	0.00	0.00	0.06	0.00	0.00	0.01	0.01	0.08
775	0.05	0.00	0.00	0.06	0.00	0.00	0.01	0.01	0.08
800	0.05	0.00	0.00	0.06	0.00	0.00	0.01	0.01	0.08
825	0.05	0.00	0.00	0.06	0.00	0.00	0.01	0.01	0.08
850	0.05	0.00	0.00	0.06	0.00	0.00	0.01	0.01	0.08
875	0.05	0.00	0.00	0.06	0.00	0.00	0.02	0.01	0.08
900	0.05	0.00	0.00	0.06	0.00	0.00	0.02	0.01	0.08
925	0.05	0.00	0.00	0.06	0.00	0.01	0.02	0.01	0.08
950	0.05	0.00	0.00	0.06	0.00	0.02	0.02	0.01	0.08
975	0.10	0.00	0.00	0.06	0.04	0.07	0.40	0.04	0.43
1000	0.10	0.00	0.00	0.06	0.07	0.19	0.52	0.09	0.57
1025	0.10	0.00	0.00	0.06	0.13	0.42	0.50	0.21	0.71
1050	0.10	0.00	0.00	0.06	0.21	0.76	0.29	0.37	0.93
1075	0.10	0.00	0.00	0.06	0.20	1.0	0.10	0.49	1.1
1100	0.10	0.00	0.00	0.06	0.22	1.2	0.02	0.58	1.3



(a)



(b)

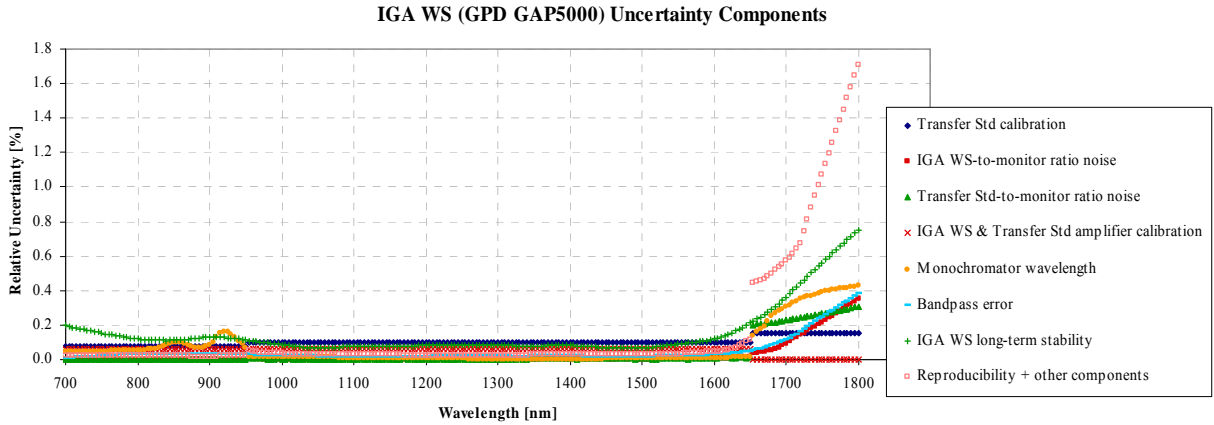
Figure 7.2. Visible WS uncertainty: (a) Vis WS uncertainty components at 5 nm intervals, (b) Vis WS relative combined standard uncertainty. The discontinuity in the curve at 950 nm is the result of calibrations with different standards.

7.3.2 Near-Infrared InGaAs Working Standards (IGA WS) Uncertainty

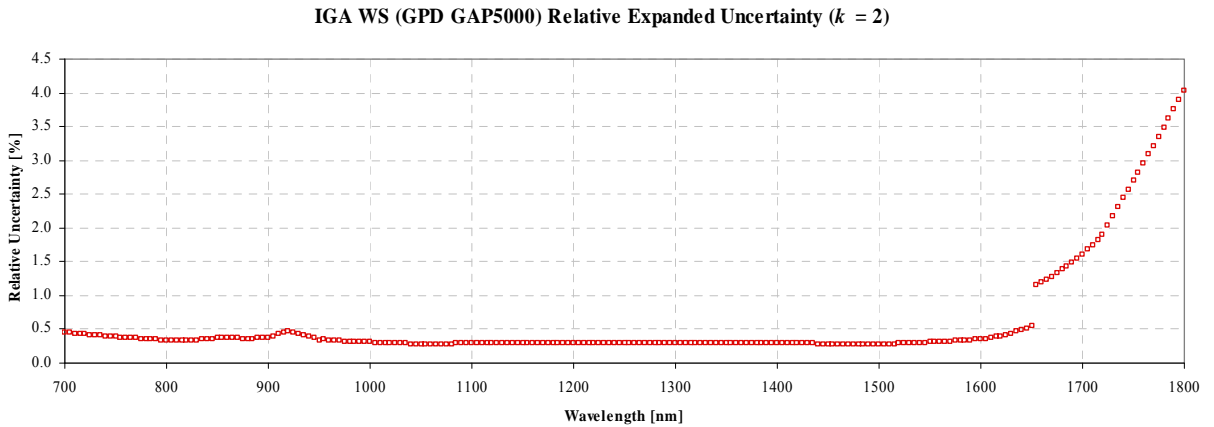
Table 7.3 lists the power responsivity transfer measurement uncertainty components using the Vis WS and IGA TS. The amplifier uncertainty components (0.04 %) for the WS and TS are combined by RSS for a value of 0.06 % in the table from 700 nm to 1650 nm for the measurements with the Vis WS and IGA TS. The amplifier uncertainty component is not included for the relative measurements with the pyroelectric detector in 1999 from 1650 nm to 1800 nm. The long-term stability is the typical data for the IGA WS over one year. The measurement uncertainty components are shown in 5 nm intervals in Figure 7.3a. The relative combined standard uncertainty was determined by the RSS of all the components and is listed in Table 7.3. Figure 7.3b shows the relative combined standard uncertainty at 5 nm intervals.

Table 7.3. Near-Infrared InGaAs working standard uncertainty (transfer from Vis WS, IGA TS, and pyroelectric detector)

Wavelength [nm]	Uncertainty contribution from each component of uncertainty [%]								Relative combined standard uncertainty [%]
	Transfer Std calibration	IGA WS-to- monitor ratio noise	Transfer Std-to- monitor ratio noise	IGA WS & Transfer Std amplifier calibration	Monochro- mator wavelength	Bandpass error	IGA WS long-term stability	Reproducib- ility and other components	
	Type B	Type A	Type A	Type B	Type B	Type B	Type B	Type A	
700	0.08	0.00	0.00	0.06	0.04	0.01	0.20	0.02	0.23
725	0.08	0.00	0.00	0.06	0.04	0.01	0.19	0.02	0.21
750	0.08	0.00	0.00	0.06	0.05	0.01	0.19	0.02	0.19
775	0.08	0.00	0.00	0.06	0.05	0.01	0.18	0.02	0.18
800	0.08	0.00	0.00	0.06	0.05	0.01	0.18	0.02	0.17
825	0.08	0.00	0.00	0.06	0.06	0.01	0.17	0.02	0.17
850	0.08	0.00	0.00	0.06	0.10	0.02	0.17	0.02	0.18
875	0.08	0.00	0.00	0.06	0.08	0.02	0.17	0.02	0.18
900	0.08	0.00	0.00	0.06	0.08	0.02	0.16	0.02	0.19
925	0.08	0.00	0.00	0.06	0.16	0.02	0.16	0.02	0.23
950	0.08	0.00	0.00	0.06	0.07	0.02	0.15	0.02	0.17
975	0.10	0.00	0.01	0.06	0.01	0.02	0.15	0.04	0.16
1000	0.10	0.00	0.00	0.06	0.01	0.02	0.15	0.03	0.15
1025	0.10	0.00	0.00	0.06	0.01	0.03	0.14	0.03	0.14
1050	0.10	0.00	0.00	0.06	0.01	0.03	0.14	0.03	0.14
1075	0.10	0.00	0.00	0.06	0.01	0.03	0.13	0.03	0.14
1100	0.10	0.00	0.00	0.06	0.01	0.03	0.13	0.03	0.14
1125	0.10	0.00	0.00	0.06	0.01	0.03	0.13	0.03	0.14
1150	0.10	0.00	0.00	0.06	0.01	0.03	0.13	0.03	0.14
1175	0.10	0.00	0.00	0.06	0.01	0.03	0.12	0.03	0.14
1200	0.10	0.00	0.00	0.06	0.01	0.03	0.12	0.02	0.15
1225	0.10	0.00	0.00	0.06	0.00	0.03	0.12	0.02	0.15
1250	0.10	0.00	0.00	0.06	0.00	0.03	0.11	0.02	0.15
1275	0.10	0.00	0.00	0.06	0.00	0.03	0.11	0.02	0.15
1300	0.10	0.00	0.00	0.06	0.00	0.03	0.12	0.02	0.15
1325	0.10	0.01	0.00	0.06	0.00	0.03	0.13	0.02	0.14
1350	0.10	0.00	0.00	0.06	0.00	0.03	0.12	0.03	0.14
1375	0.10	0.01	0.01	0.06	0.00	0.03	0.11	0.03	0.15
1400	0.10	0.01	0.01	0.06	0.00	0.02	0.10	0.03	0.15
1425	0.10	0.00	0.00	0.06	0.00	0.02	0.08	0.03	0.14
1450	0.10	0.01	0.01	0.06	0.00	0.02	0.07	0.03	0.14
1475	0.10	0.01	0.01	0.06	0.00	0.02	0.07	0.03	0.14
1500	0.10	0.00	0.01	0.06	0.01	0.02	0.07	0.03	0.14
1525	0.10	0.01	0.00	0.06	0.01	0.01	0.08	0.03	0.14
1550	0.10	0.01	0.01	0.06	0.01	0.01	0.08	0.03	0.15
1575	0.10	0.01	0.01	0.06	0.01	0.01	0.08	0.04	0.16
1600	0.10	0.01	0.01	0.06	0.01	0.02	0.08	0.05	0.18
1625	0.10	0.01	0.01	0.06	0.01	0.02	0.08	0.06	0.21
1650	0.10	0.02	0.01	0.06	0.01	0.02	0.08	0.12	0.27
1675	0.15	0.05	0.21	---	0.22	0.02	0.08	0.49	0.66
1700	0.15	0.09	0.23	---	0.31	0.02	0.08	0.57	0.80
1725	0.15	0.16	0.25	---	0.36	0.02	0.08	0.74	1.0
1750	0.15	0.22	0.27	---	0.39	0.02	0.08	1.1	1.3
1775	0.15	0.28	0.29	---	0.41	0.02	0.08	1.4	1.7
1800	0.15	0.35	0.31	---	0.43	0.02	0.08	1.7	2.0



(a)



(b)

Figure 7.3. Near-Infrared IGA WS uncertainty: (a) IGA WS uncertainty components at 5 nm intervals, (b) IGA WS relative combined standard uncertainty.

7.3.3 Ultraviolet Silicon Working Standards (UV WS) Uncertainty

The power responsivity transfer measurement uncertainty components for the UV WS which are traceable to the L-1 ACR are listed in Table 7.4. The amplifier uncertainty components (0.04 %) for the WS and TS are combined by RSS for a value of 0.06 % in the table. The long-term stability is the typical data for a UV WS over a one year period and is a significant component in the uncertainty. As with the Vis WS and IGA WS, the measurement uncertainty components are shown in 5 nm intervals in Figure 7.4a. The relative combined standard uncertainty listed in Table 7.4 was determined by the RSS of each component. Figure 7.4b shows the relative combined standard uncertainty at 5 nm intervals.

Table 7.4. UV working standard uncertainty (transfer from UV TS and Vis Trap)

Wavelength [nm]	Uncertainty contribution from each component of uncertainty [%]									Relative combined standard uncertainty [%]
	Transfer Std calibration	UV-100 WS-to- monitor ratio noise	Transfer Std-to- monitor ratio noise	UV-100 WS & Transfer Std amplifier calibration		Monochro- mator wavelength	Bandpass error	UV100 WS long-term stability	Reproduc- ibility and other components	
	Type B	Type A	Type A	Type B	Type B	Type B	Type B	Type B	Type A	
200	1.3	0.67	0.66	0.06	0.00	0.14	0.70	0.27	1.7	
220	0.05	0.06	0.06	0.06	0.10	0.11	0.62	0.27	0.70	
240	0.05	0.01	0.02	0.06	0.08	0.08	0.53	0.33	0.64	
260	0.05	0.01	0.01	0.06	0.04	0.06	0.42	0.29	0.52	
280	0.05	0.02	0.01	0.06	0.02	0.06	0.21	0.20	0.31	
300	0.05	0.01	0.01	0.06	0.03	0.04	0.13	0.20	0.26	
320	0.05	0.01	0.01	0.06	0.04	0.01	0.21	0.11	0.26	
340	0.05	0.01	0.01	0.06	0.05	0.02	0.26	0.12	0.30	
360	0.05	0.01	0.01	0.06	0.06	0.03	0.27	0.15	0.33	
380	0.05	0.01	0.01	0.06	0.06	0.02	0.25	0.25	0.37	
400	0.05	0.01	0.01	0.06	0.04	0.01	0.21	0.19	0.30	
420	0.05	0.00	0.01	0.06	0.03	0.00	0.15	0.05	0.18	
440	0.05	0.01	0.00	0.06	0.03	0.00	0.08	0.03	0.12	
460	0.05	0.01	0.01	0.06	0.03	0.00	0.05	0.02	0.10	
480	0.05	0.01	0.00	0.06	0.02	0.00	0.06	0.02	0.10	
500	0.05	0.01	0.01	0.06	0.02	0.00	0.06	0.01	0.10	

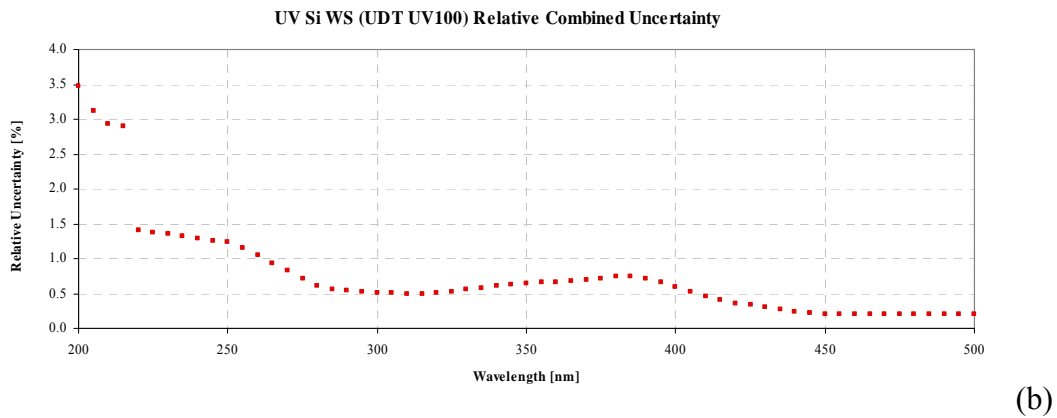
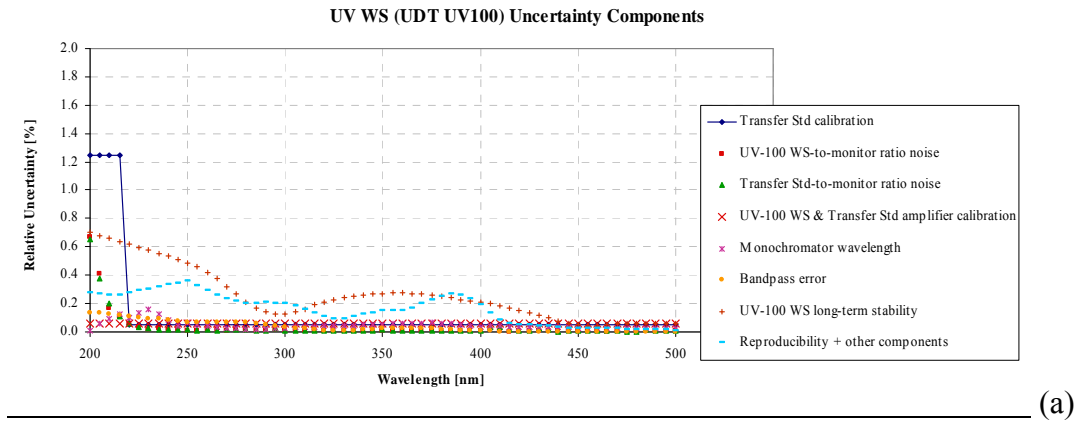


Figure 7.4. Ultraviolet WS uncertainty: (a) UV WS uncertainty components at 5 nm intervals, (b) UV WS relative combined standard uncertainty.

7.4 Transfer from Working Standards to Customer Detectors

This section details the uncertainty components when transferring the spectral power responsivity scale from the working standards to customer detectors. The tables and figures are calculated for specific photodiode models and would, in general, be different for other detectors. These tables and figures serve as a starting point to estimate the minimum uncertainty value possible from this measurement service using the current configuration.

The uncertainty in the spectral responsivity transferred to a customer's detector is determined similarly to the working standards using Eq. (7.8). Since, in general, it is not possible to know the details of how a customer's detector is used; NIST policy [9, 57] is to not include estimates of the uncertainties introduced by transporting the detector or its use by the customer. These additional uncertainties include long-term stability, differences in stray-light, beam geometry, and laboratory environmental conditions.

The stray-light is negligible and effects due to wavelength calibration uncertainty are minimized when the working standard and test detector have the same response curve. In the case of a germanium photodiode calibrated with the IGA WS, stray-light and bandpass are almost completely negligible except near the ends of the responsivity spectral range where their responsivities greatly differ.

The uncertainties were calculated at 5 nm intervals as shown in the figures. Abbreviated numerical uncertainty tables are provided. The amplifier calibration uncertainties are all identical because the amplifiers are identical units and are calibrated using the same equipment and procedure. Wavelength calibration, bandpass effects, ambient temperature effects, long-term ambient stability, reproducibility, DVM uncertainty, stray-light uncertainty components were calculated as described in Sec. 7.2 using typical data. All uncertainty components were considered independent and were combined by RSS to get the relative combined standard uncertainty shown.

The relative combined standard uncertainty as described in the previous section for the three types of SCF WS is listed in Table 7.5 at 50 nm intervals and shown in Figure 7.5 at 5 nm intervals. NIST policy is to report to customers the uncertainty using an expansion factor of $k=2$. The example expanded uncertainties are listed in Table 2.2 at 50 nm intervals and shown at 5 nm intervals in Figure 2.1. The uncertainty components are described and shown for example customer detectors in the following sections.

Table 7.5 Relative combined standard uncertainties for NIST spectral power responsivity working standards for the UV, visible, and NIR spectral regions.

Wavelength [nm]	Relative combined standard uncertainty [%]		
	UV (UV WS)	Visible (Vis WS)	NIR (IGA WS)
200	1.7		
250	0.62		
300	0.26		
350	0.32	0.30	
400	0.30	0.17	
450	0.10	0.11	
500	0.10	0.09	
550		0.08	
600		0.08	
650		0.08	
700		0.08	0.23
750		0.08	0.19
800		0.08	0.17
850		0.08	0.18
900		0.08	0.19
950		0.08	0.17
1000		0.57	0.15
1050		0.93	0.14
1100		1.3	0.14
1150			0.14
1200			0.15
1250			0.15
1300			0.15
1350			0.14
1400			0.15
1450			0.14
1500			0.14
1550			0.15
1600			0.18
1650			0.27
1700			0.80
1750			1.3
1800			2.0

UV SCF and Vis/NIR SCF WS Relative Combined Uncertainties

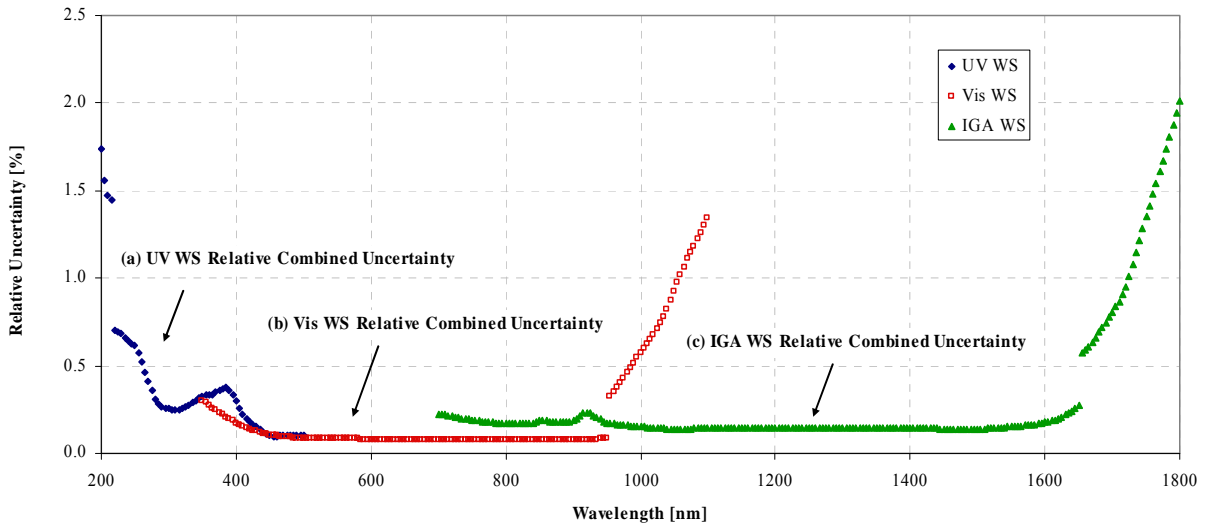


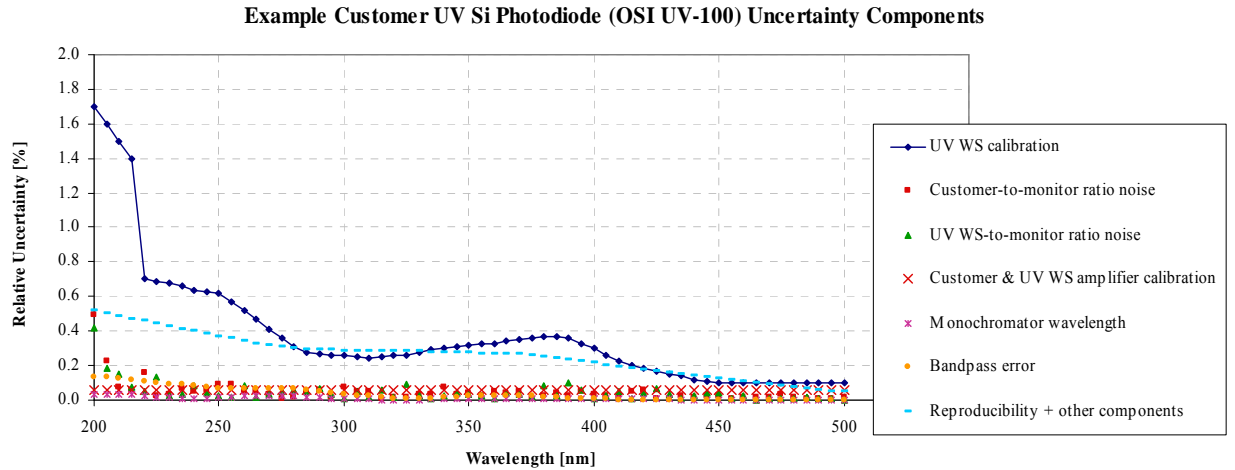
Figure 7.5. Relative combined standard uncertainties for NIST spectral power responsivity working standards (a) UV WS, (b) Vis WS, and (c) IGA WS.

7.4.1 UV Silicon Customer Detector Example Uncertainty

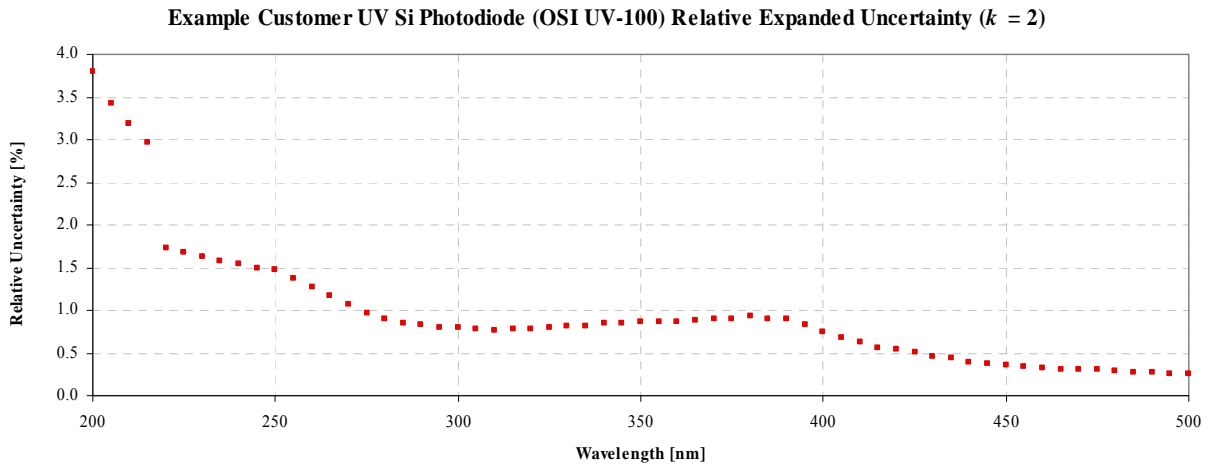
Table 7.6 lists the example uncertainty components for the calibration of a customer’s UV silicon photodiode using the UV WS. The UV WS calibration uncertainty is the relative combined standard uncertainty from Table 7.4. The amplifier uncertainty components (0.04 %) for the customer and WS are combined by RSS for a value of 0.06 % in the table. Uncertainty components for the temperature coefficient and long-term stability are not included in the uncertainty for transfer calibrations to customer photodiodes. The example relative combined standard uncertainty was determined by the RSS of the components. The measurement uncertainty components are shown in 5 nm intervals in Figure 7.6a. Table 7.6 lists the relative expanded standard uncertainty ($k = 2$) and Figure 7.6b shows the relative expanded standard uncertainty ($k = 2$) at 5 nm intervals.

Table 7.6. Example uncertainty for customer OSI Optoelectronics UV-100 silicon photodiode

Wavelength [nm]	Uncertainty contribution from each component of uncertainty [%]							Relative combined standard uncertainty [%]	Relative expanded uncertainty ($k = 2$) [%]	
	UV WS calibration	Customer- to-monitor ratio noise	UV WS-to- monitor ratio noise	Customer & UV WS amplifier calibration		Monochro- mator wavelength	Bandpass error			Reproducibility + other components
	Type B	Type A	Type A	Type B	Type B	Type B	Type A			
200	1.7	0.49	0.42	0.06	0.04	0.14	0.52	1.9	3.8	
220	0.70	0.16	0.05	0.06	0.03	0.11	0.46	0.86	1.7	
240	0.64	0.05	0.08	0.06	0.01	0.08	0.40	0.77	1.5	
260	0.52	0.05	0.08	0.06	0.02	0.06	0.34	0.64	1.3	
280	0.31	0.02	0.06	0.06	0.02	0.06	0.30	0.45	0.90	
300	0.26	0.08	0.01	0.06	0.01	0.04	0.29	0.40	0.80	
320	0.26	0.01	0.02	0.06	0.00	0.01	0.29	0.39	0.78	
340	0.30	0.08	0.03	0.06	0.01	0.02	0.28	0.42	0.84	
360	0.33	0.05	0.01	0.06	0.01	0.03	0.27	0.43	0.86	
380	0.37	0.03	0.09	0.06	0.01	0.02	0.25	0.46	0.92	
400	0.30	0.03	0.01	0.06	0.01	0.01	0.21	0.37	0.74	
420	0.18	0.05	0.04	0.06	0.01	0.00	0.18	0.27	0.54	
440	0.12	0.02	0.03	0.06	0.00	0.00	0.14	0.20	0.40	
460	0.10	0.02	0.03	0.06	0.00	0.00	0.11	0.16	0.32	
480	0.10	0.01	0.01	0.06	0.00	0.00	0.08	0.14	0.28	
500	0.10	0.02	0.00	0.06	0.00	0.00	0.05	0.13	0.26	



(a)



(b)

Figure 7.6. Example customer UV Si photodiode uncertainty: (a) Example uncertainty components at 5 nm intervals for transfer to a customer’s OSI Optoelectronics UV-100 silicon photodiode, (b) Example relative expanded uncertainty ($k = 2$).

7.4.2 Visible Silicon Customer Detector Example Uncertainty

Table 7.7 lists the uncertainty components for the calibration of a customer’s Hamamatsu S1337-1010BQ or S2281 visible silicon photodiode using the Vis WS. The Vis WS calibration uncertainty is the relative combined standard uncertainty from Table 7.1. The amplifier uncertainty components (0.04 %) for the customer and WS are combined by RSS for a value of 0.06 % in the table. The bandpass uncertainty component is negligible, but included for comparison to the UV and NIR customer photodiode uncertainty tables. Uncertainty components for the temperature coefficient and long-term stability are not included in the uncertainty for transfer calibrations to customer photodiodes. The example relative combined

standard uncertainty was determined by the RSS of the components and is listed in Table 7.7. Figure 7.7a shows the measurement uncertainty components in 5 nm intervals. Figure 7.7b shows the relative expanded standard uncertainty ($k = 2$) at 5 nm intervals.

Table 7.7. Example uncertainty for customer Hamamatsu S1337-1010BQ or S2281 silicon photodiode

Wavelength [nm]	Uncertainty contribution from each component of uncertainty [%]							Relative combined standard uncertainty [%]	Relative expanded uncertainty ($k = 2$) [%]
	Vis WS calibration	Customer- to-monitor ratio noise	Vis WS-to- monitor ratio noise	Customer & Vis WS amplifier calibration	Monochro- mator wavelength	Bandpass error	Reproducibility + other components		
	Type B	Type A	Type A	Type B	Type B	Type B	Type A		
350	0.30	0.03	0.04	0.06	0.00	0.02	0.17	0.36	0.72
375	0.23	0.01	0.01	0.06	0.00	0.01	0.10	0.26	0.52
400	0.17	0.00	0.01	0.06	0.00	0.01	0.05	0.19	0.38
425	0.13	0.00	0.00	0.06	0.00	0.00	0.03	0.15	0.30
450	0.11	0.00	0.00	0.06	0.00	0.00	0.01	0.12	0.24
475	0.09	0.00	0.00	0.06	0.00	0.00	0.01	0.11	0.22
500	0.09	0.00	0.00	0.06	0.00	0.00	0.01	0.11	0.22
525	0.08	0.00	0.00	0.06	0.00	0.00	0.01	0.10	0.20
550	0.08	0.00	0.00	0.06	0.00	0.00	0.01	0.10	0.20
575	0.08	0.00	0.00	0.06	0.00	0.00	0.01	0.10	0.20
600	0.08	0.00	0.00	0.06	0.00	0.00	0.01	0.10	0.20
625	0.08	0.00	0.00	0.06	0.00	0.00	0.01	0.10	0.20
650	0.08	0.00	0.00	0.06	0.00	0.00	0.01	0.10	0.20
675	0.08	0.00	0.00	0.06	0.00	0.00	0.01	0.10	0.20
700	0.08	0.00	0.00	0.06	0.00	0.00	0.01	0.10	0.20
725	0.08	0.00	0.00	0.06	0.00	0.00	0.01	0.10	0.20
750	0.08	0.00	0.00	0.06	0.00	0.00	0.01	0.10	0.20
775	0.08	0.00	0.00	0.06	0.00	0.00	0.01	0.10	0.20
800	0.08	0.00	0.00	0.06	0.00	0.00	0.01	0.10	0.20
825	0.08	0.00	0.00	0.06	0.00	0.00	0.01	0.10	0.20
850	0.08	0.00	0.00	0.06	0.00	0.00	0.01	0.10	0.20
875	0.08	0.00	0.00	0.06	0.00	0.00	0.01	0.10	0.20
900	0.08	0.00	0.00	0.06	0.00	0.00	0.01	0.10	0.20
925	0.08	0.00	0.00	0.06	0.00	0.00	0.01	0.10	0.20
950	0.08	0.00	0.00	0.06	0.00	0.00	0.01	0.10	0.20
975	0.43	0.00	0.00	0.06	0.00	0.01	0.04	0.44	0.88
1000	0.57	0.00	0.00	0.06	0.01	0.01	0.09	0.58	1.2
1025	0.71	0.00	0.00	0.06	0.02	0.02	0.21	0.74	1.5
1050	0.93	0.00	0.00	0.06	0.02	0.02	0.37	1.0	2.0
1075	1.1	0.00	0.00	0.06	0.01	0.02	0.49	1.3	2.6
1100	1.3	0.00	0.00	0.06	0.00	0.03	0.58	1.5	3.0

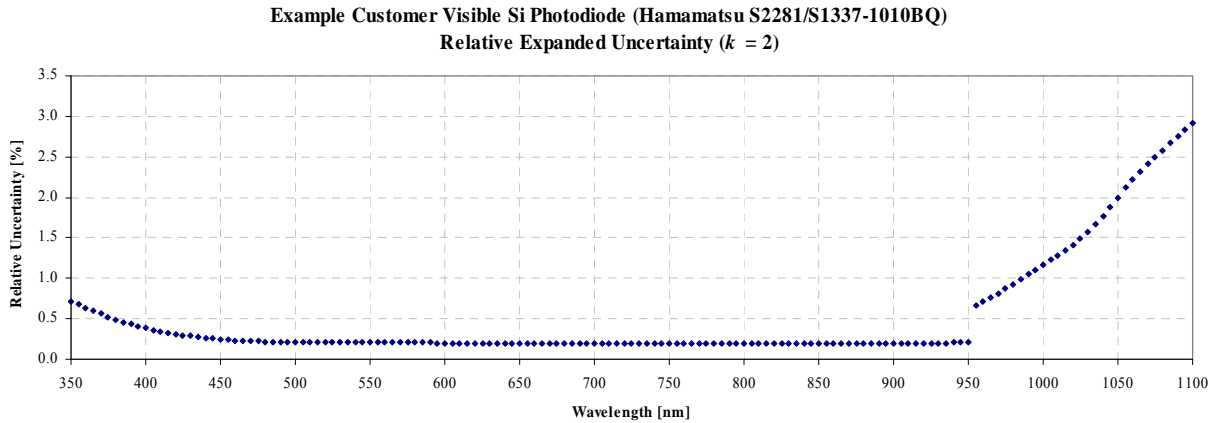
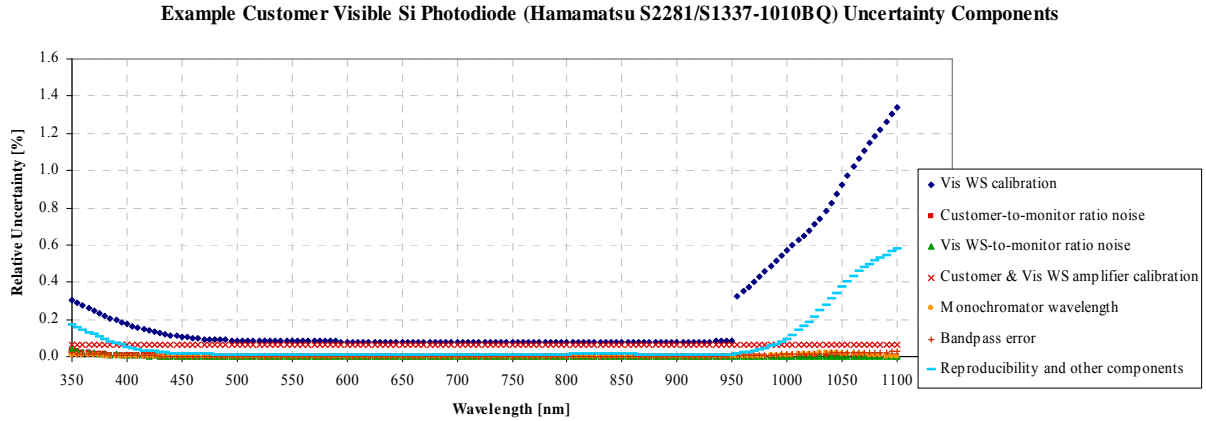


Figure 7.7. Example customer Hamamatsu 1337-1010BQ or S2281 Si photodiode uncertainty: (a) Example uncertainty components at 5 nm intervals, (b) Example relative expanded uncertainty ($k = 2$). The discontinuity in the curve at 950 nm is the result of Vis WS calibration with different standards.

7.4.3 Near-Infrared Customer Detector Example Uncertainties

The calibration uncertainties for example customer indium gallium arsenide (InGaAs) and germanium (Ge) photodiodes are presented in Table 7.8 and Table 7.9 respectively. Several of the data columns are detector-dependent, thus these tables are presented as examples of typical uncertainties for these types of photodiodes. The reported uncertainty does not include several components – such as responsivity uniformity, polarization sensitivity, linearity, temperature coefficient, and long-term stability – that are unknown for customer’s photodetectors and radiometers in general.

7.4.3.1 InGaAs Detector Example Uncertainty

Table 7.8 lists the uncertainty components for the calibration of a customer’s InGaAs photodiode using the IGA WS. The IGA WS calibration uncertainty is the relative combined standard uncertainty from Table 7.3. The amplifier uncertainty components (0.04 %) for the customer

and WS are combined by RSS for a value of 0.06 % in the table. The bandpass uncertainty component is negligible, but included for comparison to the other customer uncertainty tables. Uncertainty components for the temperature coefficient and long-term stability are not included in the uncertainty for transfer calibrations to customer photodiodes. The example relative combined standard uncertainty was determined by the RSS of the components and is listed in Table 7.8. The measurement uncertainty components are shown in 5 nm intervals in Figure 7.8a. Figure 7.8b shows the relative expanded uncertainty ($k = 2$) at 5 nm intervals.

The example relative expanded uncertainty ($k = 2$) presented in Table 7.8 is for a GPD Optoelectronics GPD5000 InGaAs photodiode. Several of the uncertainty components are detector-dependent in Table 7.8, thus this table is presented as an example representing typical uncertainties for this type of photodiode. The uncertainty is analyzed for each type of customer-supplied InGaAs photodiode.

Table 7.8. Example uncertainty for customer InGaAs photodiode

Wavelength [nm]	Uncertainty contribution from each component of uncertainty [%]							Relative combined standard uncertainty [%]	Relative expanded uncertainty ($k = 2$) [%]
	IGA WS calibration	Customer- to-monitor ratio noise	IGA WS-to- monitor ratio noise	Customer & IGA WS amplifier calibration	Monochro- mator wavelength	Bandpass error	Reproducibility + other components		
	Type B	Type A	Type A	Type B	Type B	Type B	Type A		
700	0.23	0.02	0.02	0.06	0.01	0.00	0.08	0.25	0.50
725	0.21	0.02	0.02	0.06	0.01	0.01	0.10	0.24	0.48
750	0.19	0.02	0.02	0.06	0.01	0.01	0.12	0.24	0.48
775	0.18	0.02	0.03	0.06	0.01	0.01	0.14	0.24	0.48
800	0.17	0.02	0.03	0.06	0.00	0.01	0.16	0.24	0.48
825	0.17	0.02	0.03	0.06	0.00	0.01	0.17	0.25	0.50
850	0.18	0.02	0.03	0.06	0.01	0.01	0.19	0.28	0.56
875	0.18	0.02	0.02	0.06	0.01	0.01	0.22	0.29	0.58
900	0.19	0.01	0.02	0.06	0.01	0.01	0.24	0.31	0.62
925	0.23	0.01	0.01	0.06	0.01	0.01	0.26	0.35	0.70
950	0.17	0.01	0.01	0.06	0.01	0.01	0.28	0.33	0.66
975	0.16	0.00	0.01	0.06	0.01	0.01	0.29	0.34	0.68
1000	0.15	0.00	0.00	0.06	0.01	0.01	0.29	0.33	0.66
1025	0.14	0.00	0.00	0.06	0.01	0.01	0.28	0.32	0.64
1050	0.14	0.00	0.00	0.06	0.01	0.01	0.28	0.32	0.64
1075	0.14	0.00	0.00	0.06	0.01	0.01	0.27	0.31	0.62
1100	0.14	0.00	0.00	0.06	0.01	0.01	0.27	0.31	0.62
1125	0.14	0.00	0.00	0.06	0.01	0.01	0.27	0.31	0.62
1150	0.14	0.00	0.00	0.06	0.01	0.01	0.28	0.32	0.6
1175	0.14	0.00	0.00	0.06	0.01	0.01	0.28	0.32	0.6
1200	0.15	0.00	0.00	0.06	0.00	0.01	0.27	0.31	0.6
1225	0.15	0.00	0.00	0.06	0.00	0.01	0.26	0.31	0.6
1250	0.15	0.00	0.00	0.06	0.00	0.01	0.24	0.29	0.6
1275	0.15	0.00	0.00	0.06	0.00	0.01	0.22	0.27	0.5
1300	0.15	0.00	0.00	0.06	0.00	0.01	0.20	0.26	0.52
1325	0.14	0.00	0.00	0.06	0.00	0.01	0.19	0.24	0.48
1350	0.14	0.00	0.00	0.06	0.00	0.01	0.18	0.24	0.48
1375	0.15	0.00	0.01	0.06	0.00	0.01	0.18	0.24	0.48
1400	0.15	0.00	0.01	0.06	0.00	0.02	0.18	0.24	0.48
1425	0.14	0.00	0.00	0.06	0.00	0.01	0.17	0.23	0.5
1450	0.14	0.00	0.00	0.06	0.00	0.01	0.16	0.22	0.44
1475	0.14	0.00	0.00	0.06	0.00	0.01	0.15	0.22	0.44
1500	0.14	0.01	0.00	0.06	0.00	0.01	0.15	0.21	0.42
1525	0.14	0.01	0.01	0.06	0.00	0.01	0.14	0.21	0.42
1550	0.15	0.01	0.01	0.06	0.00	0.02	0.13	0.21	0.42
1575	0.16	0.01	0.01	0.06	0.00	0.02	0.13	0.22	0.44
1600	0.18	0.01	0.01	0.06	0.00	0.03	0.16	0.25	0.5
1625	0.21	0.01	0.01	0.06	0.00	0.05	0.22	0.31	0.6
1650	0.27	0.02	0.01	0.06	0.02	0.08	0.30	0.42	0.8
1675	0.66	0.02	0.02	0.06	0.08	0.10	0.40	0.78	1.6
1700	0.80	0.03	0.02	0.06	0.04	0.11	0.52	1.0	1.9
1725	1.0	0.04	0.04	0.06	0.04	0.10	0.64	1.2	2.4
1750	1.3	0.06	0.05	0.06	0.04	0.09	0.76	1.6	3.2
1775	1.7	0.08	0.07	0.06	0.01	0.07	0.88	1.9	3.8
1800	2.0	0.11	0.08	0.06	0.01	0.05	1.0	2.3	4.6

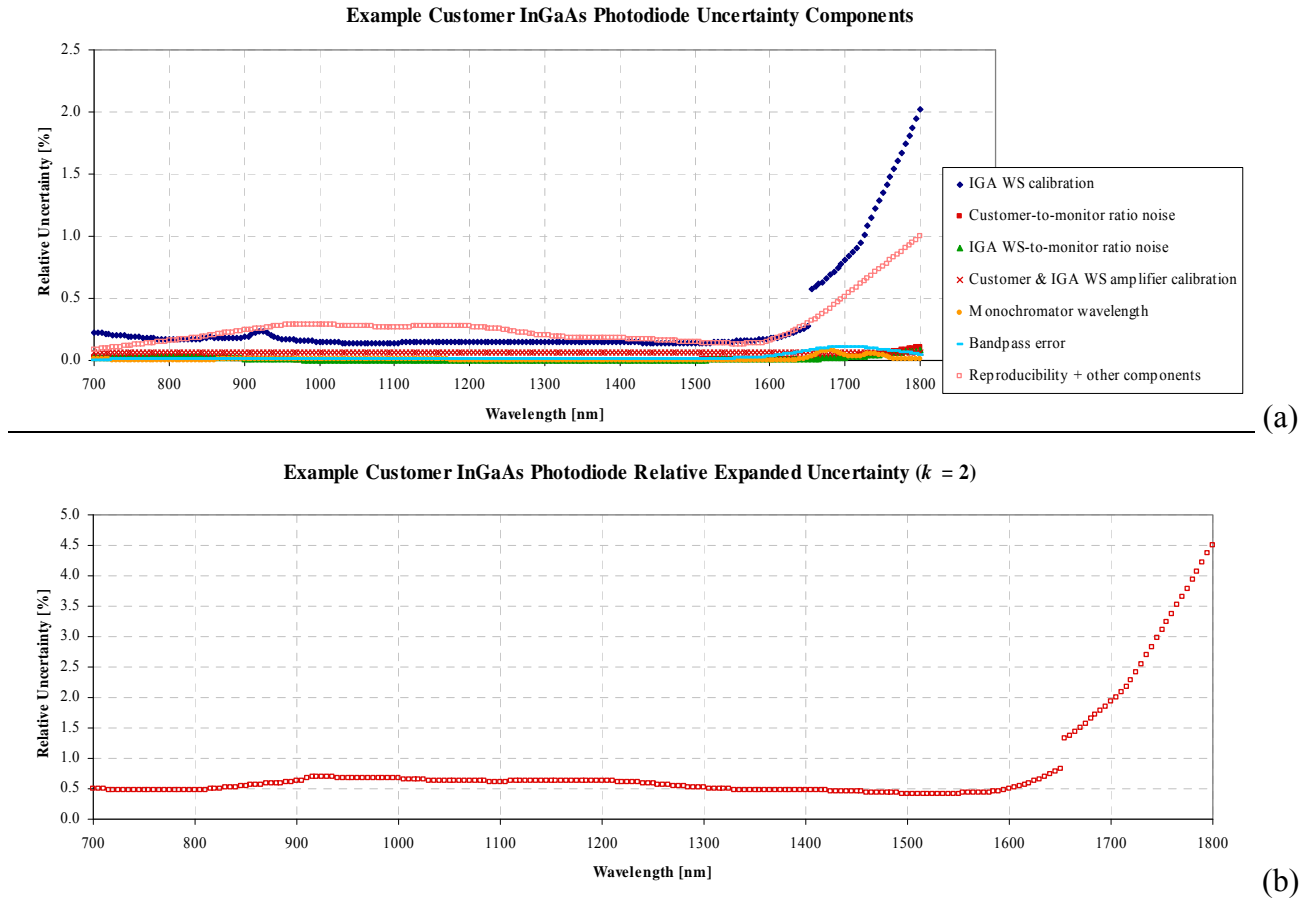


Figure 7.8. Example customer InGaAs photodiode uncertainty: (a) Example uncertainty components at 5 nm intervals, (b) Example relative expanded uncertainty ($k = 2$).

7.4.3.2 Ge Detector Example Uncertainty

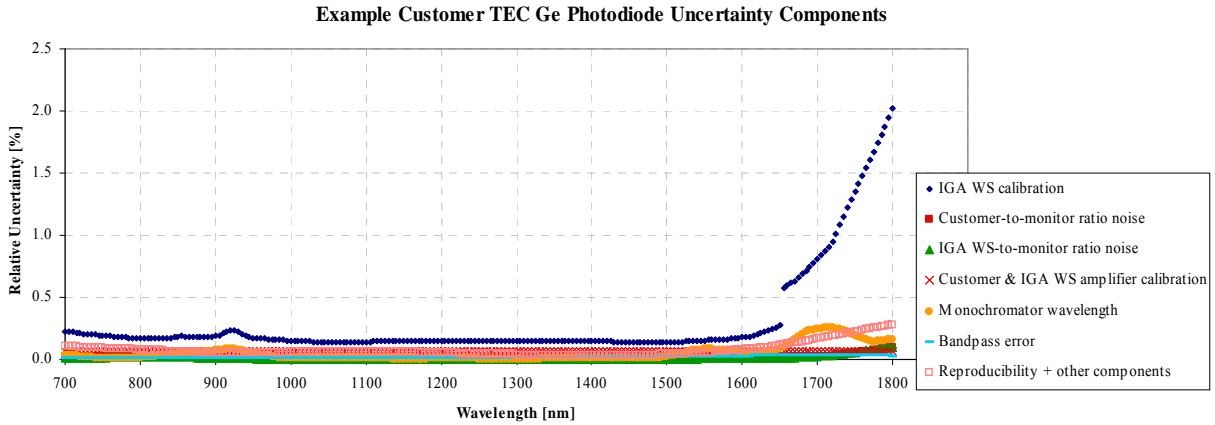
Table 7.9 lists the uncertainty components for the calibration of a customer’s thermoelectrically cooled Ge photodiode using the IGA WS. The IGA WS uncertainty is the relative combined standard uncertainty from Table 7.3. The amplifier uncertainty components (0.04 %) for the customer and WS are combined by RSS for a value of 0.06 % in the table. The bandpass uncertainty component is negligible, but included for comparison to the other customer uncertainty tables. Uncertainty components for the temperature coefficient and long-term stability are not included in the uncertainty for transfer calibrations to customer photodiodes. The example relative combined standard uncertainty was determined by the RSS of the components and is listed in Table 7.9. Figure 7.9a shows the measurement uncertainty components at 5 nm intervals. Figure 7.9b shows the relative expanded uncertainty ($k = 2$) at 5 nm intervals.

The example relative expanded uncertainty ($k = 2$) presented in Table 7.9 is for a Judson EG&G J16TE2-8A6-R05M-SC Ge photodiode. As with the InGaAs transfer uncertainty in Table 7.8 several of the uncertainty components are detector-dependent, thus this table is

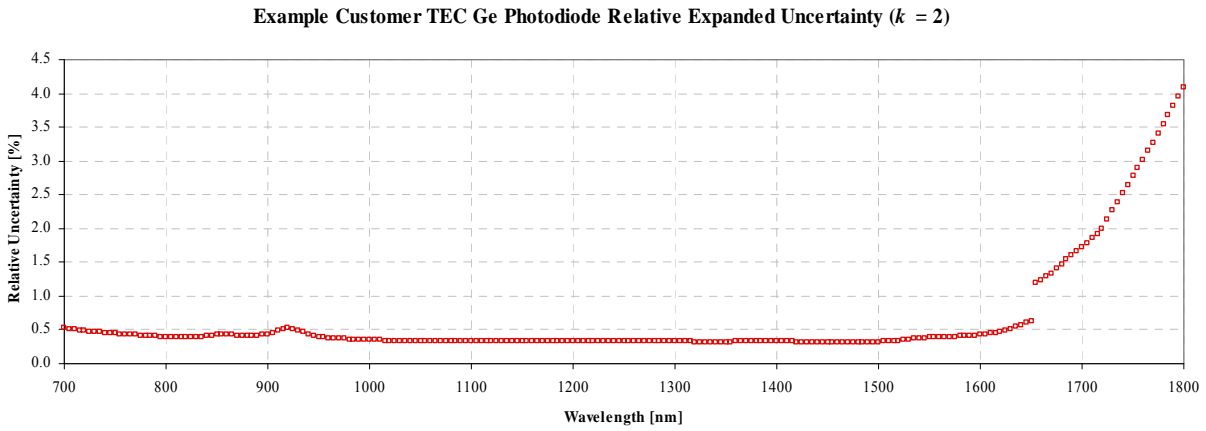
presented as an example representing typical uncertainties for this type of photodiode. The uncertainty is analyzed for each type of customer-supplied photodiode.

Table 7.9. Example uncertainty for customer TE cooled Ge photodiode

Wavelength [nm]	Uncertainty contribution from each component of uncertainty [%]							Relative combined standard uncertainty [%]	Relative expanded uncertainty ($k = 2$) [%]
	IGA WS calibration	Customer- to-monitor ratio noise	IGA WS-to- monitor ratio noise	Customer & IGA WS amplifier calibration	Monochro- mator wavelength	Bandpass error	Reproducibility + other components		
	Type B	Type A	Type A	Type B	Type B	Type B	Type A		
700	0.23	0.02	0.01	0.06	0.04	0.01	0.11	0.26	0.52
725	0.21	0.02	0.01	0.06	0.02	0.01	0.10	0.24	0.48
750	0.19	0.02	0.02	0.06	0.01	0.01	0.09	0.22	0.44
775	0.18	0.02	0.02	0.06	0.01	0.01	0.08	0.21	0.42
800	0.17	0.02	0.02	0.06	0.01	0.01	0.08	0.20	0.40
825	0.17	0.02	0.02	0.06	0.03	0.01	0.07	0.20	0.40
850	0.18	0.02	0.02	0.06	0.05	0.01	0.06	0.21	0.42
875	0.18	0.02	0.02	0.06	0.05	0.01	0.06	0.21	0.42
900	0.19	0.01	0.01	0.06	0.07	0.01	0.05	0.22	0.44
925	0.23	0.01	0.01	0.06	0.08	0.01	0.05	0.26	0.52
950	0.17	0.01	0.01	0.06	0.05	0.01	0.05	0.19	0.38
975	0.16	0.00	0.00	0.06	0.02	0.01	0.05	0.18	0.36
1000	0.15	0.00	0.00	0.06	0.01	0.01	0.06	0.17	0.34
1025	0.14	0.00	0.00	0.06	0.01	0.01	0.06	0.17	0.34
1050	0.14	0.00	0.00	0.06	0.01	0.01	0.07	0.17	0.34
1075	0.14	0.00	0.00	0.06	0.02	0.01	0.07	0.17	0.34
1100	0.14	0.00	0.00	0.06	0.01	0.01	0.07	0.17	0.34
1125	0.14	0.00	0.00	0.06	0.01	0.01	0.07	0.17	0.34
1150	0.14	0.00	0.00	0.06	0.00	0.01	0.06	0.17	0.34
1175	0.14	0.00	0.00	0.06	0.00	0.01	0.06	0.17	0.34
1200	0.15	0.00	0.00	0.06	0.01	0.01	0.05	0.17	0.34
1225	0.15	0.00	0.00	0.06	0.01	0.01	0.05	0.17	0.3
1250	0.15	0.00	0.00	0.06	0.01	0.01	0.04	0.17	0.34
1275	0.15	0.00	0.00	0.06	0.00	0.01	0.04	0.16	0.32
1300	0.15	0.00	0.00	0.06	0.00	0.01	0.04	0.16	0.32
1325	0.14	0.00	0.00	0.06	0.00	0.01	0.03	0.16	0.32
1350	0.14	0.00	0.00	0.06	0.01	0.01	0.03	0.16	0.32
1375	0.15	0.00	0.00	0.06	0.01	0.02	0.03	0.16	0.32
1400	0.15	0.00	0.00	0.06	0.01	0.02	0.03	0.16	0.32
1425	0.14	0.00	0.00	0.06	0.01	0.02	0.03	0.16	0.32
1450	0.14	0.00	0.00	0.06	0.01	0.02	0.03	0.16	0.32
1475	0.14	0.00	0.00	0.06	0.01	0.02	0.03	0.16	0.32
1500	0.14	0.00	0.00	0.06	0.02	0.02	0.04	0.16	0.32
1525	0.14	0.00	0.00	0.06	0.06	0.02	0.05	0.17	0.34
1550	0.15	0.01	0.01	0.06	0.08	0.02	0.05	0.19	0.38
1575	0.16	0.01	0.01	0.06	0.07	0.02	0.06	0.20	0.40
1600	0.18	0.01	0.01	0.06	0.06	0.03	0.08	0.21	0.42
1625	0.21	0.01	0.01	0.06	0.06	0.03	0.09	0.24	0.5
1650	0.27	0.01	0.01	0.06	0.09	0.03	0.11	0.32	0.6
1675	0.66	0.02	0.02	0.06	0.19	0.03	0.14	0.70	1.4
1700	0.80	0.02	0.02	0.06	0.24	0.03	0.17	0.86	1.7
1725	1.0	0.03	0.04	0.06	0.25	0.03	0.19	1.1	2.2
1750	1.3	0.05	0.06	0.06	0.19	0.03	0.22	1.4	2.8
1775	1.7	0.07	0.08	0.06	0.14	0.03	0.25	1.7	3.4
1800	2.0	0.10	0.10	0.06	0.16	0.03	0.28	2.0	4.0



(a)



(b)

Figure 7.9. Example customer TE cooled Ge photodiode uncertainty: (a) Example uncertainty components at 5 nm intervals, (b) Example relative expanded uncertainty ($k = 2$).

7.4.4 Filtered Detector Example Uncertainty (Photometer)

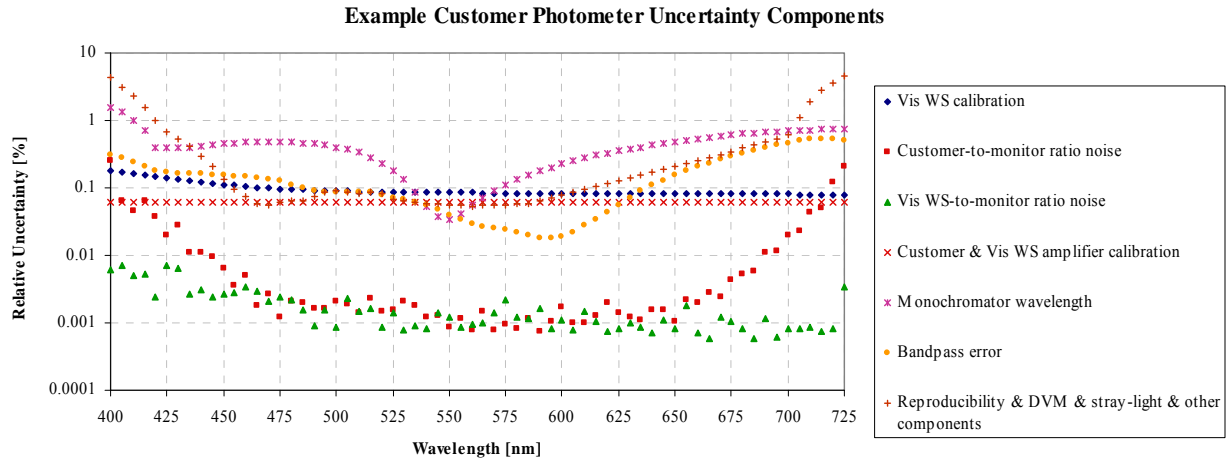
Special tests of filtered detectors (such as photometers) can be made under service ID number 39080S. It should be noted that the relative uncertainty due to the reproducibility will increase due to the decrease in signal in the “wings” of the response. As mentioned in Sec. 7.2.1, when the slope of the responsivity curve is steep, the uncertainty due to wavelength calibration increases. Also the uncertainty due to stray-light and bandwidth can increase by orders of magnitude relative to the uncertainties within the bandpass of the filtered detector.

Table 7.10 lists the uncertainty components for the calibration of a customer’s photometer using the Vis WS. The Vis WS calibration uncertainty is the relative combined standard uncertainty from Table 7.2. The amplifier uncertainty components (0.04 %) for the customer and WS are combined by RSS for a value of 0.06 % in the table. The bandpass uncertainty component is not negligible for a detector with sharp changes in responsivity like a photometer. Also, the DVM and stray-light uncertainty components are significant for this measurement and are combined by RSS with the reproducibility. Uncertainty components for the temperature coefficient and long-term stability are not included in the uncertainty for transfer calibrations to customer detectors. The example relative expanded uncertainty ($k = 2$) was determined by the RSS of the components and is listed in Table 7.10. The measurement uncertainty components are shown in 5 nm intervals in Figure 7.10a. Figure 7.10b shows the relative expanded uncertainty ($k = 2$) at 5 nm intervals.

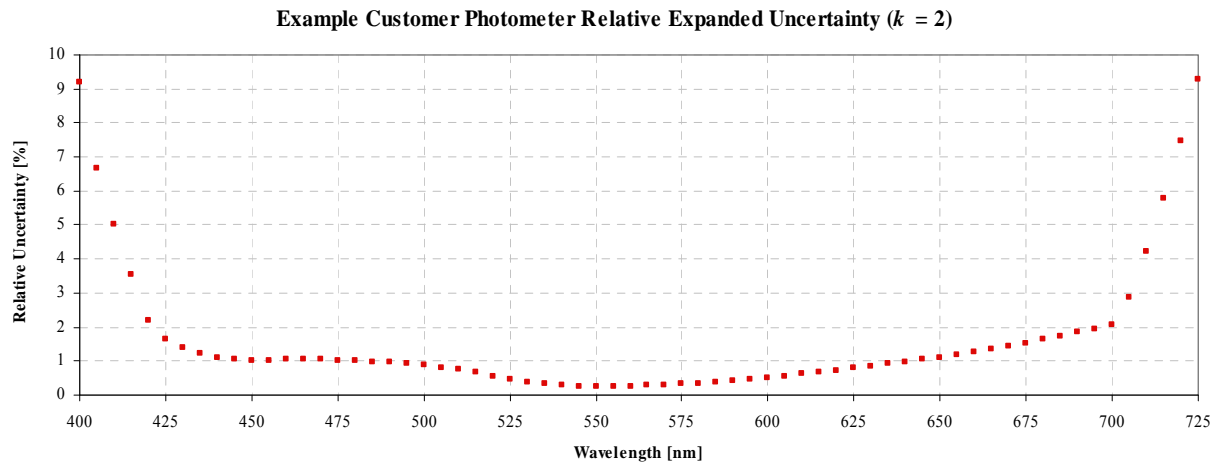
Because several of the uncertainty components are photometer dependent, Table 7.10 is presented as an example illustrating typical uncertainties for a customer’s photometer. The uncertainty is analyzed for each type of customer-supplied photometer.

Table 7.10. Example uncertainty for customer photometer

Uncertainty contribution from each component of uncertainty [%]									
Wavelength [nm]	Vis WS calibration	Customer- to-monitor ratio noise	Vis WS-to- monitor ratio noise	Customer & Vis WS amplifier calibration	Monochro- mator wavelength	Bandpass error	Reproducibility, DVM, stray-light, and other components	Relative combined standard uncertainty	Relative expanded uncertainty ($k = 2$)
	Type B	Type A	Type A	Type B	Type B	Type B	Type A	[%]	[%]
400	0.18	0.26	0.01	0.06	1.6	0.31	4.3	4.6	9.2
425	0.14	0.02	0.01	0.06	0.39	0.17	0.68	0.82	1.6
450	0.11	0.01	0.00	0.06	0.45	0.15	0.14	0.51	1.0
475	0.10	0.00	0.00	0.06	0.48	0.13	0.06	0.51	1.0
500	0.09	0.00	0.00	0.06	0.40	0.09	0.09	0.44	0.88
525	0.09	0.00	0.00	0.06	0.18	0.07	0.07	0.23	0.46
550	0.08	0.00	0.00	0.06	0.03	0.04	0.06	0.13	0.26
575	0.08	0.00	0.00	0.06	0.11	0.02	0.06	0.16	0.32
600	0.08	0.00	0.00	0.06	0.22	0.02	0.08	0.26	0.52
625	0.08	0.00	0.00	0.06	0.35	0.06	0.13	0.39	0.78
650	0.08	0.00	0.00	0.06	0.48	0.15	0.21	0.55	1.1
675	0.08	0.00	0.00	0.06	0.60	0.30	0.35	0.76	1.5
700	0.08	0.02	0.00	0.06	0.70	0.46	0.60	1.0	2.0
725	0.08	0.21	0.00	0.06	0.74	0.51	4.5	4.6	9.2



(a)



(b)

Figure 7.10. Example customer photometer uncertainty: (a) Example uncertainty components at 5 nm intervals, (b) Example relative expanded uncertainty ($k = 2$).

7.5 Spatial Uniformity Measurement Uncertainty

The uncertainty components for the responsivity spatial uniformity measurement of a typical Si photodiode are listed in Table 7.11. Measurement repeatability, i.e., short-term drift, is the relative standard deviation of three measurements in the center of the active area of the detector during the spatial scanning measurements. The measurement noise is the average standard deviation of the mean of the three measurements. The relative combined standard uncertainty is the RSS of the measurement repeatability, noise, and the one-day DVM uncertainty specification.

The measurement repeatability uncertainty depends on the SNR of the detector and noise due to the amplifier and DVM. The measurement noise varies spectrally, primarily due to the change in monochromator flux magnitude with wavelength. Note that the variation in responsivity over the measured area is typically much larger than this uncertainty value.

The reported uncertainty is not an indication of the uniformity measurement reproducibility. It does not consider other components which contribute to the reproducibility uncertainty, such as, the ability to reproduce the same irradiance geometry and detector alignment. Uniformity reproducibility results have been reported [56] for a Hamamatsu S1337-1010BQ with a standard deviation of 0.033 % at 500 nm and 0.25 % at 1000 nm.

The intended primary use of the reported uniformity results is qualitative. The reported uniformity indicates if any large discontinuities are present in the responsivity uniformity that can lead to larger than expected uncertainties in responsivity measurements. Quantitative application of the reported uniformity results requires examination of the irradiance geometry and equipment involved.

Table 7.11. Photodetector spatial uniformity measurement repeatability uncertainty

Wavelength [nm]	Uncertainty contribution from each component of uncertainty [%]			Relative combined standard uncertainty [%]
	Repeatability	Measurement noise	DVM	
	Type B	Type A	Type A	
500	0.0020	0.0012	0.0007	0.0025
1000	0.0056	0.0033	0.0007	0.0065

8. Quality System

The spectroradiometric detector measurements described in this publication are part of the NIST Optical Technology Division calibration services and are in compliance with the NIST Quality System for Measurement Services [8, 80] based on the ISO/IEC 17025:2005 [1, 81]. Although quality procedures have always been in place, they varied from calibration service to calibration service within the Division. The quality control procedures were typically limited to the technical aspects of the measurements, such as the yearly calibration of voltmeters, the use of multiple working standards, and their routine rotation.

In 1993 the Optical Technology Division began developing a calibration quality system based on ANSI/NCSL Z540-1-1994 (the predecessor of ISO/IEC 17025) [82-84]. The outcome was to unify all the calibration services offered by the Division with standard formats and similar procedures. Balancing functionality and bureaucracy was a concern from the start. Efforts were directed toward developing a useful and practical quality system. Excessively sophisticated and complex procedures are avoided, along with redundant documentation. Tools such as checklists, forms, and flowcharts are used where applicable.

8.1 Control Charts

Control charts are a standard statistical tool used for tracking a process over time [85]. For calibrations, the working standards are randomly chosen each week allowing all of the working standards to be compared to each other over time. The responsivity of a given working standard detector can then be tracked over time using control charts. In practice, only a few wavelengths (e.g., every 100 nm) need to be plotted on a control chart for each working standard. An example control chart for a visible working standard at 600 nm is shown in Fig. 8.1. The center line is the mean responsivity during a period when the measurement process is stable (i.e., “in control”). The upper control limit (UCL) and lower control limit (LCL) are respectively plus and minus three times the standard deviation of the responsivity reproducibility measurements. This should include almost all of the expected random measurement fluctuations. Figure 8.1 shows a trend in the responsivity measurements that does not appear to be due to random fluctuations but is still within the control limits. This demonstrates the value of control charts.

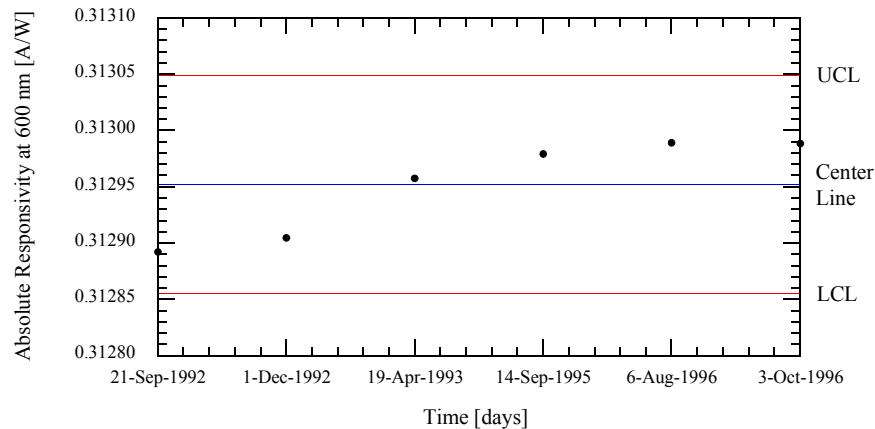


Figure 8.1. Control chart example for a NIST Visible Working Standard (Vis WS).

8.2 Interlaboratory Comparisons

NIST has historically been involved with many interlaboratory comparisons of spectral power responsivity. In 1993 NIST participated in an international intercomparison carried out by the Bureau International des Poids et Mesures (BIPM) over the 250 nm to 1000 nm wavelength region [36, 86]. There have also several bilateral intercomparisons, such as a NIR bilateral intercomparison between NRC (Canada) and NIST in 2001 [87].

The International Committee of Weights and Measures (Comite' International des Poids et Mesures, CIPM), under the authority given to it in the Metre Convention, crafted a Mutual Recognition Arrangement (MRA). In 1999, the CIPM MRA was signed by the directors of the national metrology institutes (NMIs) of thirty-eight Member States of the Metre Convention (including NIST, the U.S. NMI) and representatives of two international organizations. Sixty-seven other institutes have now signed the MRA⁹. The MRA objectives are to establish the degree of equivalence of national measurements standards maintained by NMIs; to provide for the mutual recognition of calibration and measurement certificates issued by NMIs; and to thereby provide governments and other parties with a secure technical foundation for wider agreements related to international trade, commerce and regulatory affairs.

Under the MRA, the metrological equivalence of national measurement standards are to be determined by a set of key comparisons chosen and organized by the Consultative Committees of the CIPM working closely with Regional Metrology Organizations (RMOs).

At the annual meeting in 1997 of the Consultative Committee for Photometry and Radiometry (CCPR), several Key Comparisons were identified in the field of optical radiation metrology, one of which, K2, was spectral (power) responsivity. The Key Comparison of Spectral Responsivity was divided into three separate comparisons covering different spectral regions:

⁹ More information about the MRA can be found at the BIPM website <http://www.bipm.org/en/cipm-mra/>.

K2.a (900 nm to 1600 nm), K2.b (300 nm to 1000 nm), and K2.c (200 nm to 400 nm). These intercomparisons and NIST's participation are described in the following sections.

8.2.1 CCPR K2.a (NIR) 900 nm to 1650 nm

The Key Comparison K2.a which covered the spectral range from 900 nm to 1600 nm was piloted by NIST. InGaAs photodiodes were used as the intercomparison artifacts. All of the measurements are complete, but the final results have not been published [88] at the time of this document's publication.

8.2.2 CCPR K2.b (Visible) 400 nm to 950 nm

The Key Comparison CCPR-K2.b (300 nm to 1000 nm) was piloted by the BIPM. A total of 17 NMIs participated in this comparison. Four silicon detectors (single element and trap type) were measured by each participant and by the pilot laboratory (BIPM). Figure 8.2 summarizes the results.

The following graph is given to provide more information on the transfer detectors (they are not graphs of equivalence): they show the relative differences from the KCRV (base line) when either traps or single diodes are used as transfer detectors. The uncertainty bars (coverage factor $k=2$) correspond to NIST's uncertainty combined with the uncertainty of the transfer. They do not include the uncertainty of the reference.

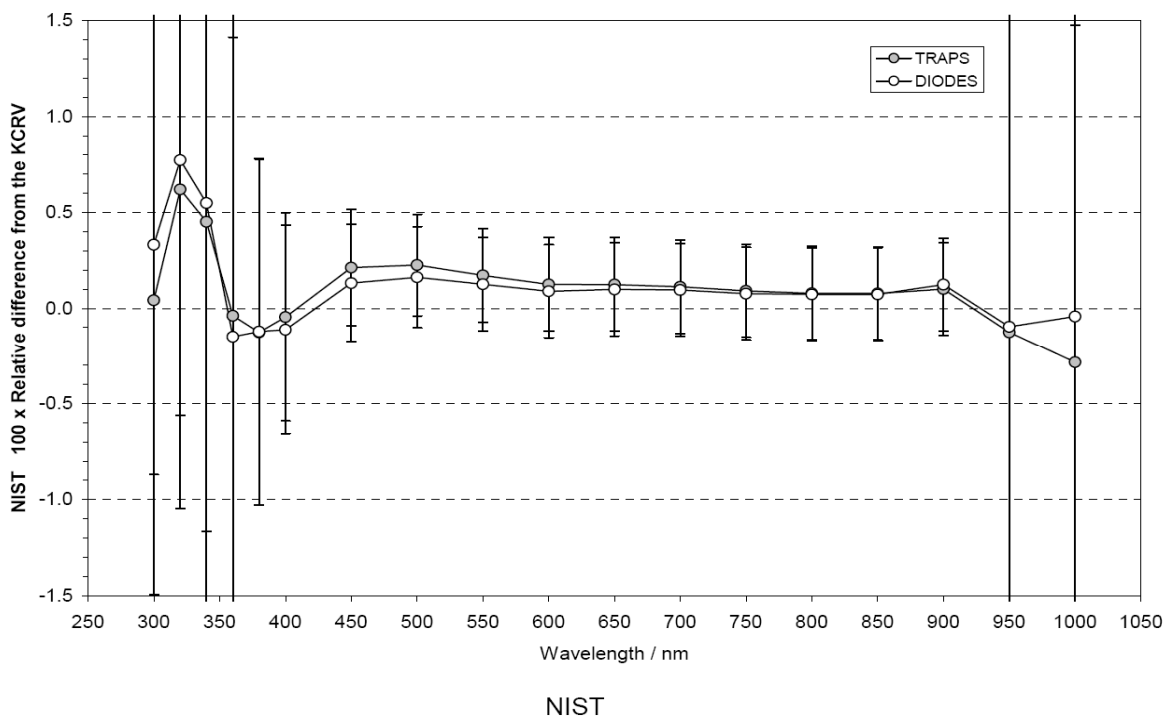


Figure 8.2. NIST difference from KCRV in CCPR K2.b (Visible) Key Comparison (NIST measured in Dec. 2000.).

8.2.3 CCPR K2.c (UV) 200 nm to 450 nm

The third spectral responsivity Key Comparison (K2.c) started in December 2003 and covers the spectral region of 200 nm to 400 nm. This comparison is still in progress and no results are available at the time of the publication [88] of this document.

8.3 Changes in the Spectral Power Responsivity Scale

8.3.1 UV Scale (200 nm to 500 nm)

The most recent realization of NIST's spectral radiant power responsivity scale in the 200 nm to 500 nm spectral region (UV SCF) was 2005. The changes in the UV WS assigned values from the previous realization in 2001 are shown in Figure 8.3. The difference between the two realizations includes changes in both the realized scale and in the responsivities of the UV WS. Some of the changes seen are larger than the 2005 expanded uncertainty ($k = 2$). Because of these changes, new UV photodiodes were investigated to replace the current UV WS. The photodiodes chosen as new UV WS are the International Radiation Devices (IRD) model UVG-100 photodiodes¹⁰. These diodes have a 10 mm x 10 mm active area. The characterization and calibration of a group of four UVG-100 diodes is continuing at this time. It is expected that they will replace the current UV WS in 2008.

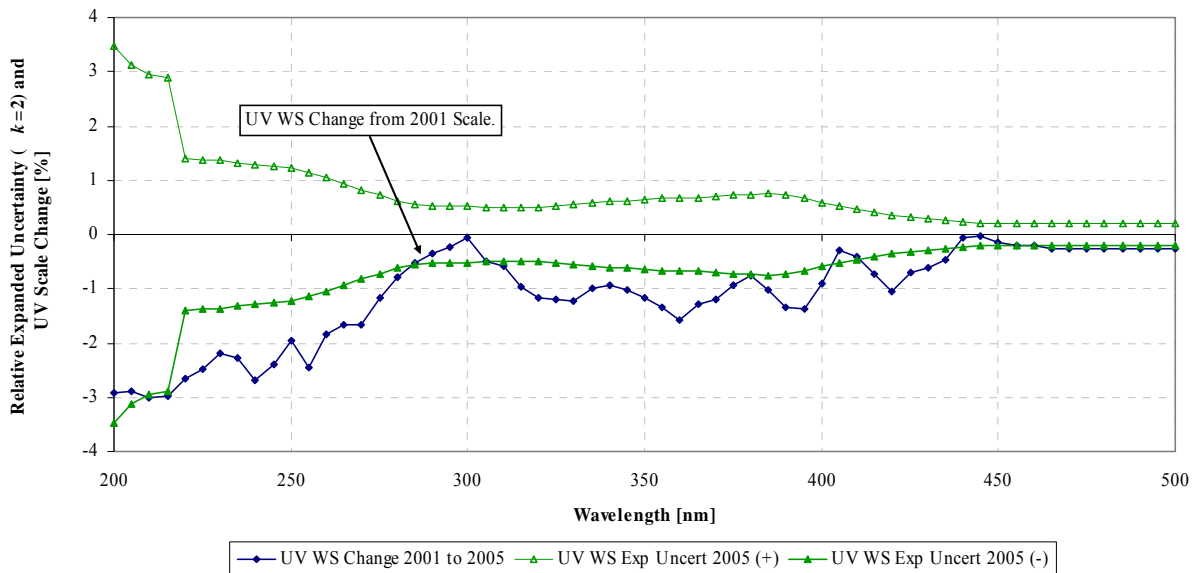


Figure 8.3. Change in the UV spectral power responsivity scale (UV WS) from 2001 to 2005 and expanded uncertainty ($k = 2$).

¹⁰ International Radiation Detectors (IRD), Torrance, CA (<http://www.ird-inc.com/>).

8.3.2 Visible Scale (350 nm to 1100 nm)

The current responsivity scale from 350 nm to 1100 nm for spectral radiant power at the NIST Vis/NIR SCF was realized in 2006. The changes in the Vis WS assigned values from the previous realization in 2005 are shown in Figure 8.4. The uncertainties were significantly reduced beyond 950 nm because of the Ge TS calibrated by SIRCUS. The uncertainty still increases beyond 950 nm mainly due the temperature coefficient of the photodiodes. (See the Vis WS uncertainty Sec. 7.2.1.) New temperature controlled mounts were acquired to keep the Vis WS at a constant temperature which will reduce this uncertainty. The uncertainty beyond 950 nm will still be larger than in the visible region due to the increasing spatial non-uniformity of the diodes as the wavelength approaches the Si bandgap.

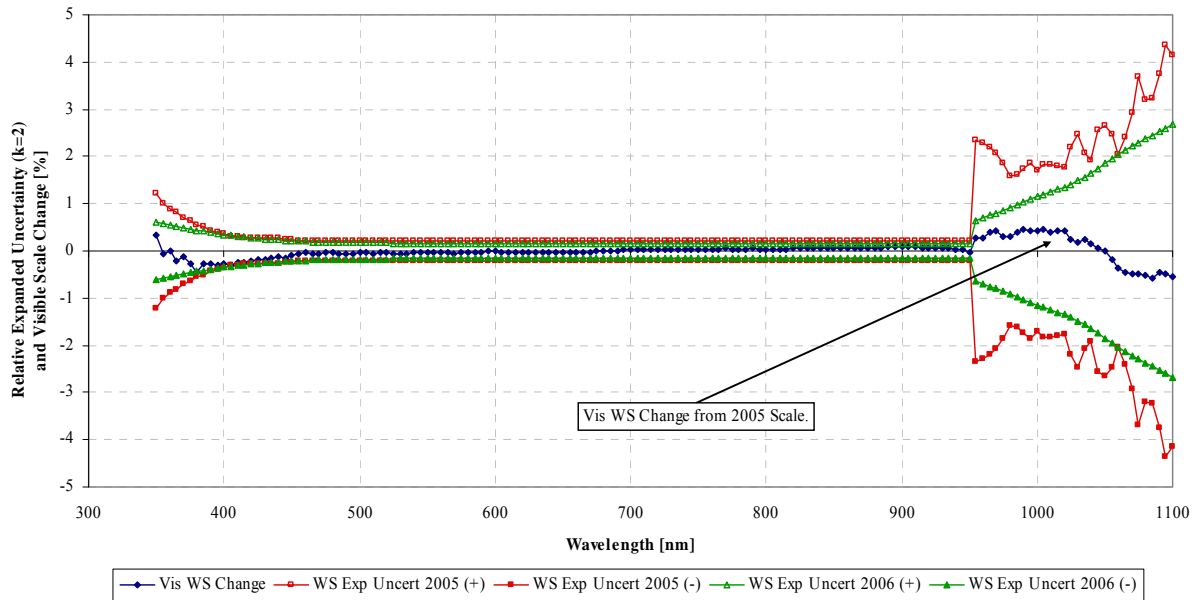


Figure 8.4. Change in the visible spectral power responsivity scale (Vis WS) from 2005 to 2006 and expanded uncertainties ($k = 2$).

8.3.3 NIR Scale (700 nm to 1800 nm)

The NIR spectral radiant power responsivity scale (IGA WS: 700 nm to 1800 nm) at the Vis/NIR SCF was last realized in 2006, except in the 1650 nm to 1800 nm region where scale is still based on the 1999 realization [49]. The previous NIR WS were a group of four Ge WS described in the 1998 edition of this document [46]. The Ge WS and IGA WS were calibrated concurrently in 1999 as described in Sec. 5.4.3. The change of the assigned values of the IGA WS from the previous realization in 1999 (700 nm to 1650 nm) is shown in Figure 8.5. The change of the assigned values to the Ge WS from the realization in 1996 to 1999 is shown in Figure 8.6.

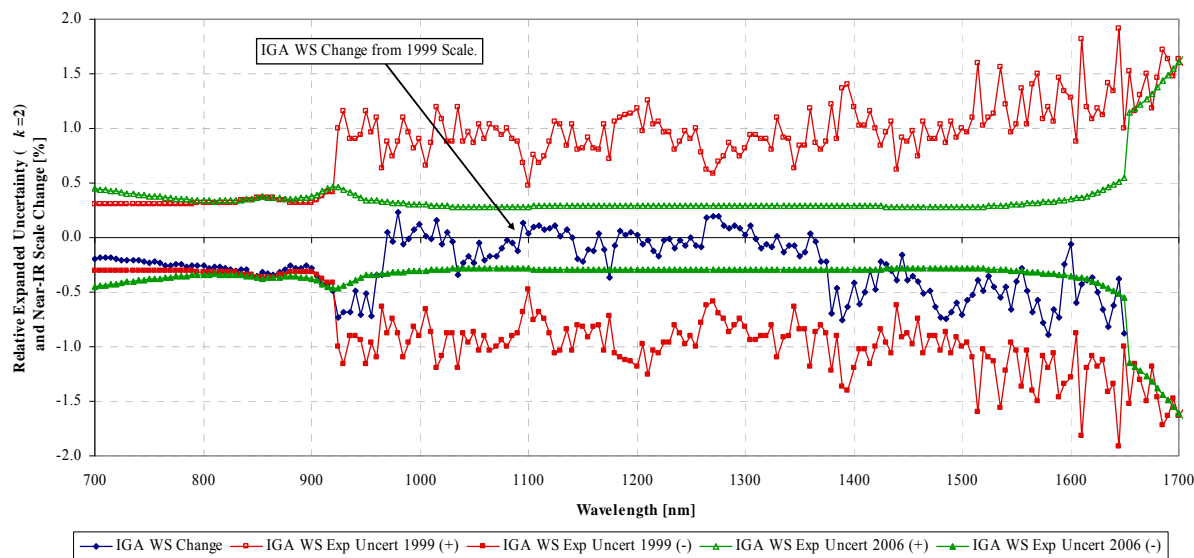


Figure 8.5. Change in the NIR spectral power responsivity scale (IGA WS) from 1999 to 2006 and expanded uncertainties ($k=2$).

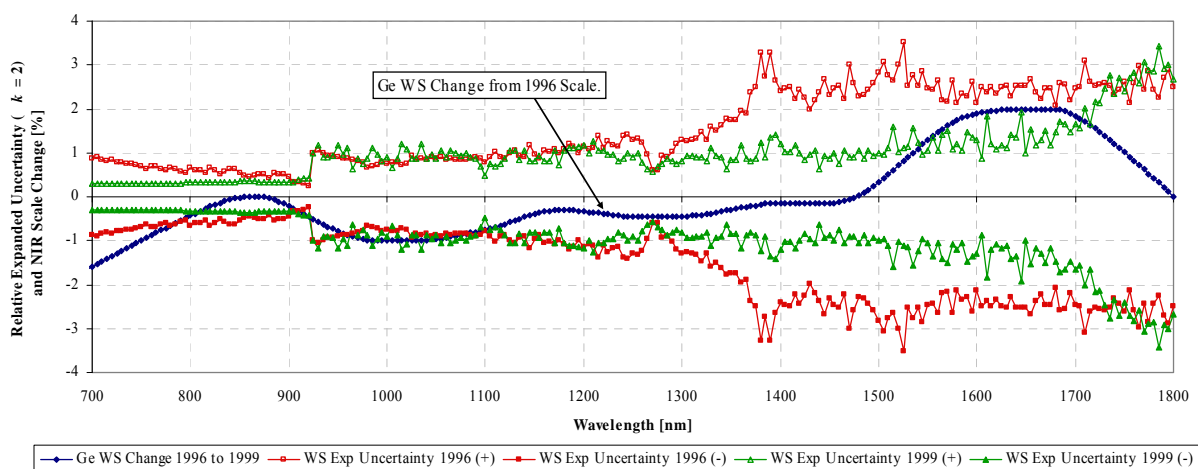


Figure 8.6. Change in the NIR spectral power responsivity scale (Ge WS) from 1996 to 1999 and expanded uncertainties ($k=2$). The current IGA WS were calibrated concurrently with the Ge WS in 1999.

9. Characteristics of Photodiodes Available from NIST

This section describes the characteristics of the silicon photodiodes provided by NIST under Service ID numbers 39071C, 39073C, and 39077C. The physical and electrical characteristics of the photodiodes are discussed and the results of linearity measurements are given.

9.1 Hamamatsu S1337-1010BQ

Hamamatsu S1337-1010BQ silicon photodiodes have been supplied by NIST as spectral radiant power responsivity standards. NIST currently supplies a similar diode, the Hamamatsu S2281 for this purpose under NIST Service ID numbers 39073C and 39077C. The major differences between the S1337-1010BQ and the S2281 photodiodes are how they are packaged and the shape of the active area. The S1337-1010BQ is packaged in a square ceramic package with a square active area. The S2281 is packaged in a round package with a round active area. As mentioned previously, the Hamamatsu S1337 series diode is a popular diode for radiometric standards and it has been extensively characterized [35, 36, 89, 90]. Hamamatsu describes¹¹ the S1337-1010BQ as a p-n diode with a 1 cm x 1 cm active area, a fused quartz window, and a ceramic case. The spectral response range is < 190 nm to 1100 nm with a peak at 960 nm. Changes in spectral responsivity have been noted with the Hamamatsu S1337 and S2281 models when exposed to light < 250 nm [64, 91, 92]. The S1337-1010BQ also has a high shunt resistance (dynamic impedance), with a typical value of 200 M Ω and a minimum value of 50 M Ω ¹¹.

The typical measured spectral responsivity and quantum efficiency are shown in Figure 6.2 and Figure 6.3, respectively. The typical spatial uniformities measured at 500 nm and 1000 nm are shown in Figure 6.4a and b, respectively. Because the responsivity of a photodiode can be affected by temperature, the temperature coefficient of several S1337 series photodiodes were measured using a temperature-controlled fixture. All of the measurements were made following the typical spectral responsivity procedures at temperatures around 25 °C. Figure 9.1 shows the average temperature coefficient of the Hamamatsu S1337 series photodiode. A second common silicon photodiode series, the S1226, is shown for comparison in Figure 9.1 along with the wavelength of peak responsivity for each photodiode.

The linearity of the S1337-1010BQ at 633 nm is shown in Figure 9.2 spanning irradiance level from 0.5 mW/cm² to 6.6 mW/cm². Each data point represents the ratio of the photodiode responsivity at the indicated irradiance to the responsivity at low power. The linearity was measured by using a beamsplitter to irradiate two photodiodes at approximately a 10:1 intensity ratio, with the diode aperture filled and uniformly irradiated [79]. The linearity is dependent on the irradiation geometry and will differ for spot sizes significantly smaller than the aperture size.

¹¹ These values are from the manufacturer's catalog, Photodiodes, Cat. No. KPD 0001E05, Aug. 1996 T, Hamamatsu Photonics K. K., Solid State Division, 1126-1, Ichino-cho, Hamamatsu City, 435-91, Japan

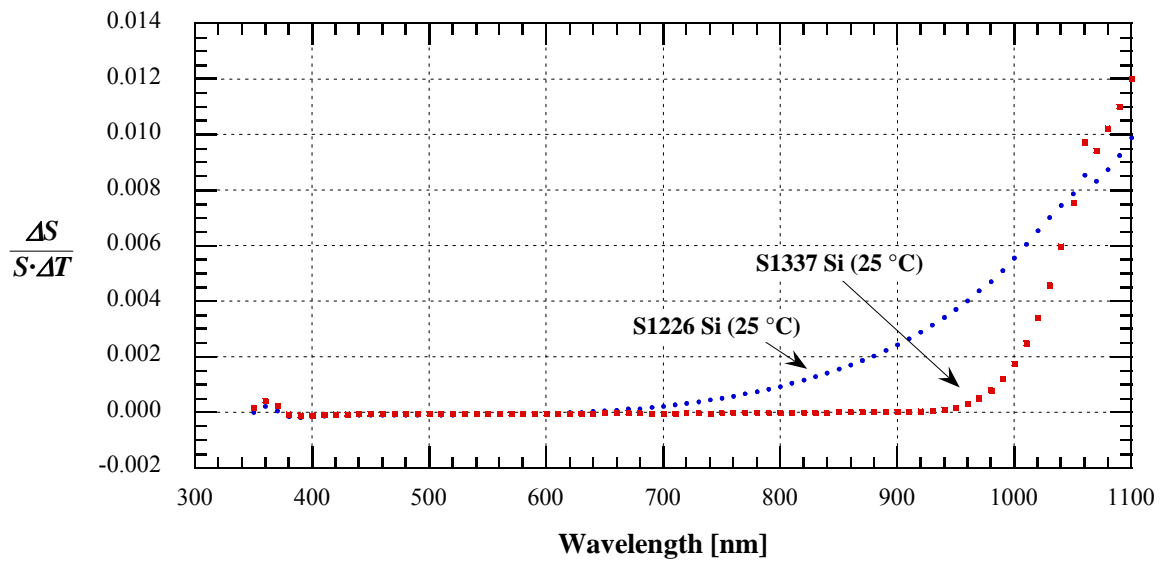


Figure 9.1. Temperature coefficient of silicon Hamamatsu S1226 and S1337 photodiodes.

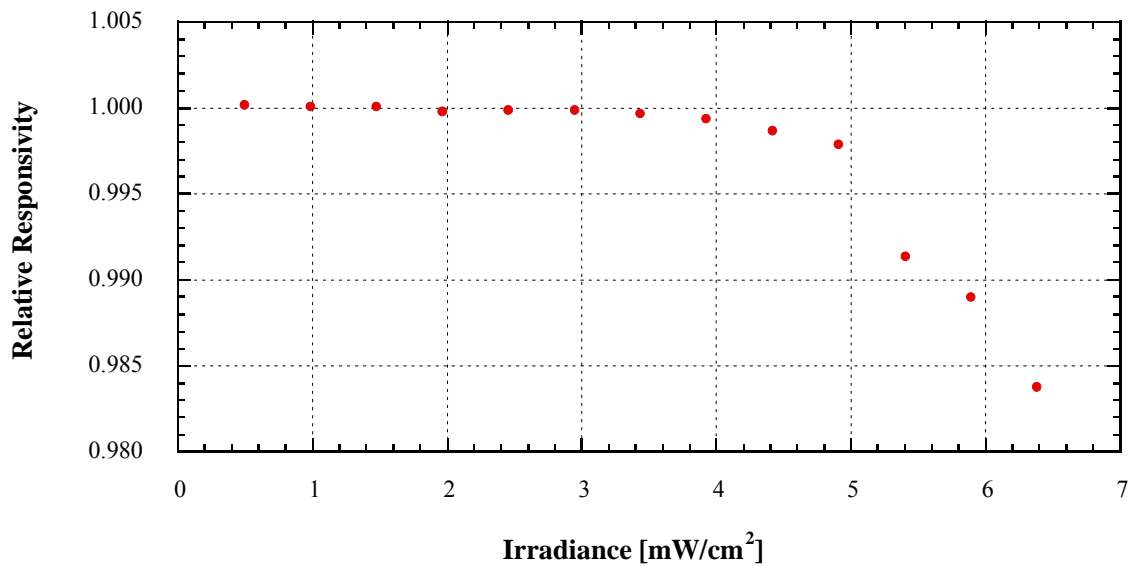


Figure 9.2. Linearity of Hamamatsu S1337-1010BQ at 633 nm.

9.2 Hamamatsu S2281

Hamamatsu S2281 silicon photodiodes are currently provided by NIST as standards of spectral responsivity (NIST Service ID numbers 39073C and 39077C). The characteristics are essentially identical to the S1337-1010BQ. Since the spectral responsivity and quantum efficiency of the S2281 is almost indistinguishable from the S1337, they are not shown in Figure 6.2 and Figure 6.3. The significant differences between the two diode models are that the S2281 has a 1 cm^2 active area that is circular instead of square and it is housed in a metal case with a BNC connector. The BNC case simplifies the photodiode mounting since no electrical wiring is required.

9.3 OSI Optoelectronic UV-100

UDT Sensors UV100 silicon photodiodes have been supplied by NIST as spectral radiant power responsivity standards. UDT Sensors was acquired by OSI Optoelectronics in 1990 and stopped using the name “UDT Sensors, Inc.” around 2004. The OSI Optoelectronics UV-100 silicon photodiodes are currently provided as spectral responsivity standards in the UV (NIST Service ID number 39071C). OSI Optoelectronic literature¹² describes the UV-100 as having an inversion layer structure, excellent UV responsivity, and high shunt resistance. The UV-100 has a quartz window, a 1 cm^2 circular active area, and is housed in a metal case with a BNC connector similar to the Hamamatsu S2281. The spectral response range is from $< 200 \text{ nm}$ to 1100 nm with a peak around 760 nm . The typical shunt resistance value is $10 \text{ M}\Omega$ ¹².

The linearity of the UV-100, shown in Fig. 9.3 at 442 nm , spans irradiance levels from 0.1 mW/cm^2 to 1.1 mW/cm^2 with and without a reverse bias voltage. Each data point represents the ratio of the photodiode responsivity at the indicated irradiance to the responsivity within the linear region. The linearity was measured by using a beamsplitter to irradiate two photodiodes at approximately a 10:1 intensity ratio, with the diode aperture filled and uniformly irradiated [79]. The linearity is dependent on the irradiation geometry and will differ for spot sizes significantly smaller than the aperture size.

The change in the responsivity as a function of bias voltage for this type of photodiode at 442 nm is shown in Figure 9.4. For wavelengths shorter than 450 nm , a 1 V bias can be used to improve the linearity of the photodiode without significantly changing the spectral responsivity. There will however be some dark current and $1/f$ noise introduced which will limit the minimum usable signal.

¹² These values were taken from the OSI Optoelectronics 2007 Optoelectronic Components Catalog (<http://www.udt.com/OSI-Optoelectronics-Catalog-2007.pdf>), OSI Optoelectronics, 12525 Chadron Ave., Hawthorne, CA 90250, USA.

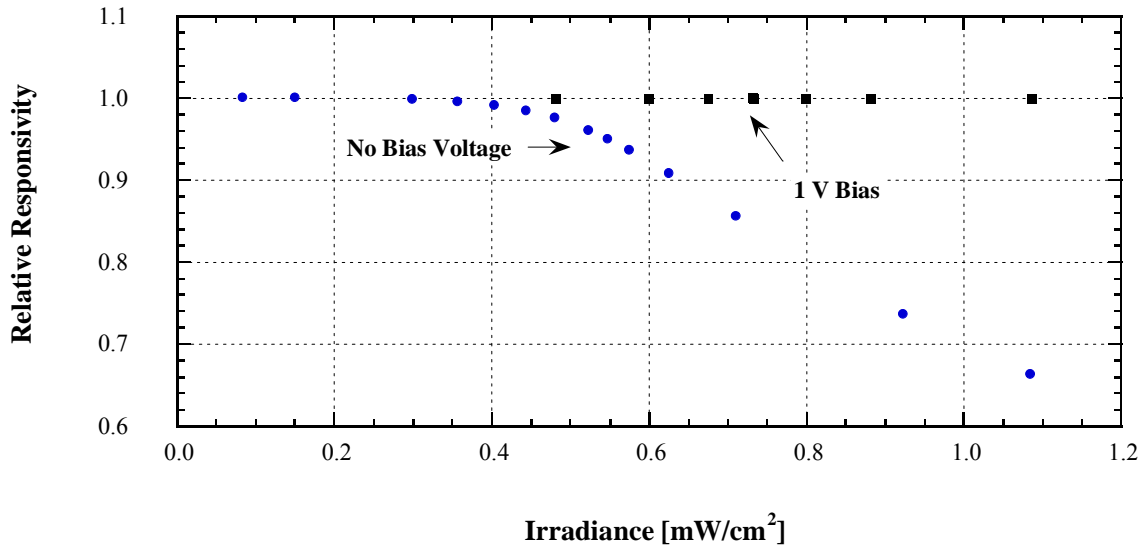


Figure 9.3. Linearity of UDT Sensors UV100 at 442 nm.

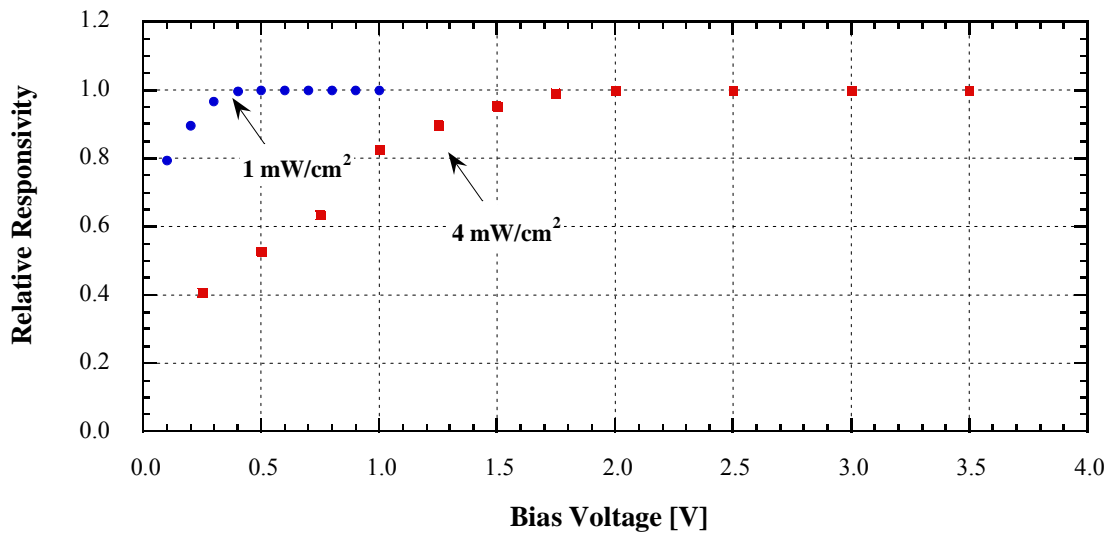


Figure 9.4. Responsivity dependence on bias voltage of UDT Sensors UV100 at 442 nm.

9.4 Detector Mounting Fixture Mechanical Drawings

Note: As stated in the Introduction, this document follows the NIST policy of using the International System of Units (SI). The following mechanical drawings were originally prepared in English units and are presented without converting the values shown to SI units.

The detector mounting fixtures for the Hamamatsu S2281 and the OSI Optoelectronics UV-100 silicon photodiodes are designed for convenient handling and use. The fixture housings are black anodized aluminum and the 5.08 cm diameter was chosen as a convenient size for use with common optical mounts. Most of the fixtures also have a threaded hole (1/4-20: a common English thread size and not shown in drawings) on the side of the fixture for a standard optical table post. Each fixture has an engraved serial number on the back. Black anodized aluminum covers (not shown) were added later to protect the photodiodes during storage and shipment.

The OSI Optoelectronics UV-100 and Hamamatsu S2281 photodiodes are housed in metal cases with BNC outputs. This simplifies the mounting fixture and reduces the construction time since no electrical wiring is required. The mounting fixture mechanical diagram for the UV-100 and S2281 diodes is shown in Figure 9.5.

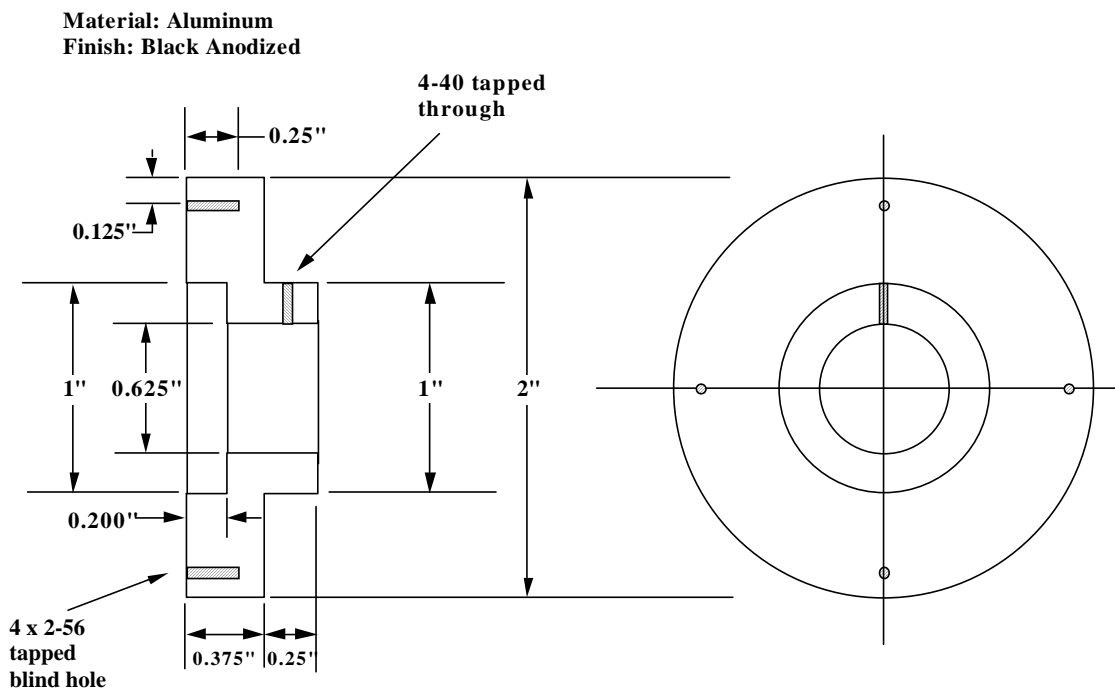


Figure 9.5. Mechanical diagram of OSI Optoelectronics UV-100 and Hamamatsu S2281 mounting fixture.

The detectors NIST issues to customers are supplied in a wooden box with a form-fitting foam insert to hold the photodiode fixture. An anodized aluminum cap is provided to protect the detector when not in use. Figure 9.6 is a photograph of the NIST issued photodiode, fixture, cap, and wooden storage box.



Figure 9.6. Photograph of a sample NIST issued photodiode in mounting fixture, cap, and wooden storage box.

10. Future Work

This section will discuss the future modifications and improvements to the UV and Vis/NIR SCFs. Several publications are planned to describe these modifications and improvements to the SCFs. This publication describing the measurement services offered by the UV and Vis/NIR SCFs will be revised every 3 to 5 years.

In the near future, single element nitrided Si detectors will be used as working standards in the UV. Nitrided silicon photodiodes have been reported with higher responsivities, better spatial uniformity, and a lower sensitivity to UV-induced changes than other Si photodiodes [89-91, 93, 94]. To reduce the uncertainty component due to laboratory temperature fluctuations, temperature-controlled mounts will be used with the Vis WS. New windowless InGaAs photodiodes will be used as transfer standards from the SIRCUS facility to the SCF. These photodiodes are mounted in temperature-controlled housings.

Several major modifications will be made to the UV SCF. A new, higher efficiency UV monochromator (with automated order sorting filters) and larger linear translation stages have been purchased and will be integrated into the UV SCF when the measurement schedule allows. The translation stages will replace the rotating stage and small linear stages that have limited the UV SCF to measuring only one test detector at a time. The new stages will be configured similar to the Vis/NIR SCF stages. Additional imaging mirrors for astigmatism correction will be added to the UV SCF similar to the Vis/NIR SCF. A new prism pre-disperser for the Vis/NIR SCF monochromator made from Supracil 300 will improve the throughput out to 3 μm .

Improvements are being studied in the SCF irradiance measurement method [95] that can reduce the amount of time needed for the calibrations. New methods for irradiance calibration are also being explored [96]. Continued improvements in the calibration procedures will be made by applying the Once-is-Enough model [97] throughout the calibration service.

The ‘Once-is-Enough’ model is really just applying good process control techniques to our calibration services. For example, a transfer artifact is typically thought of as being well characterized, that is, its performance is understood, including its stability. If the same facility and method is used, there is no need to remeasure the artifact’s stability every time it is returned to NIST for calibration. For certain artifacts with limited lifetimes, such as lamps, it is detrimental to take measurements that are in essence redundant.

Also the measurement system must also be ‘under control’, meaning that it too is well characterized and its performance is understood. This means that not only is the system routinely calibrated, but its performance is monitored, for instance, with check standards. If control parameters exceed set limits, calibrations are stopped until the system is brought back under control.

11. Acknowledgments

The development, operation, and evolution of this measurement service have involved several NIST personnel. The major contributors over the past decades have been: Sally Bruce, Chris Cromer, Bob Saunders; Ed Zalewski.

The authors would like to thank Tom Gentile, Jonathan Hardis, Chris Cromer, Chris Classon, George Eppeldauer, Keith Lykke, and Steve Brown for their work with the cryogenic radiometers, silicon trap detectors, and other transfer standard detectors. Additional thanks go to Randy Canfield, Rob Vest, and Ping-Shine Shaw for their work with SURF III and help with UV detector studies and measurements; and to Joel Fowler for providing the transimpedance amplifiers.

Thanks are also given to the staffs of the NIST Measurement Services Division and National Voluntary Laboratory Accreditation Program (NVLAP) of Technology Services and the Statistical Engineering Division of the Information Technology Laboratory for their help with maintaining and improving the measurement service.

12. References

- [1] General Requirements for the Competence of Testing and Calibration Laboratories, ISO, IEC, Geneva, Switzerland (2005).
- [2] F. Hengstberger, Determination of the Spectral Responsivity of Optical Radiation Detectors, Bureau central de la CIE, Paris, France (1984).
- [3] W. Budde, Optical Radiation Measurements, Vol. 4, Physical Detectors of Optical Radiation, Academic Press, New York, NY (1983).
- [4] J. Geist, L. B. Schmidt, and W. E. Case, Comparison of the laser power and total irradiance scales maintained by the national bureau of standards, *Applied Optics* **12** (11), 2773-1776 (1973).
- [5] J. Geist, M. A. Lind, A. R. Schaefer, and E. F. Zalewski, Spectral Radiometry: A New Approach Based on Electro-Optics, NBS Technical Note 954 (1977).
- [6] Preprint of sequel to NBS Technical Note 950 describing the radiometric characteristics of the DRTIP radiometers, Unpublished work, National Bureau of Standards (1980?).
- [7] Guide to the Expression of Uncertainty in Measurement, International Organization for Standardization, Geneva, Switzerland (1995).
- [8] M. S. A. Group, NIST Quality Manual for Measurement Services QM-1, Gaithersburg, MD, National Institute of Standards and Technology (2006).
- [9] B. N. Taylor and C. E. Kuyatt, Guidelines for Evaluating and Expressing the Uncertainty of NIST Measurement Results, NIST Technical Note 1297, 1994 Edition (1994).
- [10] The NIST Reference on Constants, Units, and Uncertainty website, <http://physics.nist.gov/cuu/Uncertainty/index.html>
- [11] E. F. Zalewski and J. Geist, Silicon photodiode absolute spectral response self-calibration, *Applied Optics* **19** (8), 1214-1216 (1980).
- [12] J. Geist, E. F. Zalewski, and A. R. Schaefer, Spectral response self-calibration and interpolation of silicon photodiodes, *Applied Optics* **19** (22), 3795-3799 (1980).
- [13] E. F. Zalewski and C. R. Duda, Silicon photodiode device with 100 % external quantum efficiency, *Applied Optics* **22** (18), 2867-2873 (1983).
- [14] E. F. Zalewski, The NBS Photodetector Spectral Response Calibration Transfer Program, NBS Special Publication 250-17 (1988).
- [15] J. M. Houston and E. F. Zalewski, Photodetector spectral response based on 100% quantum efficient detectors, in *Optical Radiation Measurements II*, J. M. Palmer, ed., Int Soc for Optical Engineering, Bellingham, WA, USA, SPIE 1109 (1989) 268-277.

- [16] C. L. Cromer, A new spectral response calibration method using a silicon photodiode trap detector, Presented at the 1991 Measurement Science Conference, Anaheim, CA (1991).
- [17] N. P. Fox, Trap Detectors and Their Properties, *Metrologia* **28** (3), 197-202 (1991).
- [18] J. Geist, Current status of and future directions in silicon photodiode self-calibration, in *Publ by Int Soc for Optical Engineering*, Bellingham, WA, USA, 1109 (1989) 246-256.
- [19] E. F. Zalewski and C. C. Hoyt, Comparison between Cryogenic Radiometry and the Predicted Quantum Efficiency of Pn Silicon Photodiode Light Traps, *Metrologia* **28** (3), 203-206 (1991).
- [20] N. P. Fox, Radiometry with cryogenic radiometers and semiconductor photodiodes, *Metrologia* **32** (6), 535-543 (1996).
- [21] A. C. Parr, A National Measurement System for Radiometry, Photometry, and Pyrometry Based Upon Absolute Detectors, NIST Technical Note 1421 (1996).
- [22] T. R. Gentile, J. M. Houston, J. E. Hardis, C. L. Cromer, and A. C. Parr, National Institute of Standards and Technology high-accuracy cryogenic radiometer, *Applied Optics* **35** (7), 1056-1068 (1996).
- [23] J. M. Houston and J. P. Rice, NIST reference cryogenic radiometer designed for versatile performance, *Metrologia* **43** (2), S31-S35 (2006).
- [24] T. R. Gentile, J. M. Houston, and C. L. Cromer, Realization of a scale of absolute spectral response using the national institute of standards and technology high-accuracy cryogenic radiometer, *Applied Optics* **35** (22), 4392-4403 (1996).
- [25] T. C. Larason, S. S. Bruce, and C. L. Cromer, The NIST high accuracy scale for absolute spectral response from 406 nm to 920 nm, *Journal of Research of the National Institute of Standards and Technology* **101** (2), 133-140 (1996).
- [26] G. P. Eppeldauer and D. C. Lynch, Opto-mechanical and electronic design of a tunnel-trap Si radiometer, *Journal of Research of the National Institute of Standards and Technology* **105** (6), 813-828 (2000).
- [27] S. W. Brown, G. P. Eppeldauer, and K. R. Lykke, Facility for spectral irradiance and radiance responsivity calibrations using uniform sources, *Applied Optics* **45** (32), 8218-8237 (2006).
- [28] H. J. Kostkowski and F. E. Nicodemus, An Introduction to the Measurement Equation, Chapter 5 in *Self-Study Manual on Optical Radiation Measurements: Part I, Concepts*, NBS Technical Note 910-2 (1978).
- [29] H. J. Kostkowski, The Relative Spectral Responsivity and Slit-Scattering Function of a Spectroradiometer, Chapter 7 in *Self-Study Manual on Optical Radiation Measurements: Part I, Concepts*, NBS Technical Note 910-4 (1979).

- [30] R. Kohler, R. Goebel, R. Pello, and J. Bonhoure, Effects of Humidity and Cleaning on the Sensitivity of Si Photodiodes, *Metrologia* **28** (3), 211-215 (1991).
- [31] F. L. Pedrotti and L. S. Pedrotti, *Introduction to Optics*, Prentice Hall, Englewood Cliffs, NJ (1993).
- [32] E. Hecht and A. Zajac, *Optics*, Addison-Wesley, Reading, MA (1987).
- [33] J. B. Shumaker, Introduction to Coherence in Radiometry, Chapter 10 in *Self-Study Manual on Optical Radiation Measurements: Part I: Concepts*, NBS Technical Note 910-6 (1983).
- [34] J. L. Gardner, Astigmatism Cancellation in Spectroradiometry, *Metrologia* **28** (3), 251-254 (1991).
- [35] F. Lei and J. Fischer, Characterization of Photodiodes in the UV and Visible Spectral Region-Based on Cryogenic Radiometry, *Metrologia* **30** (4), 297-303 (1993).
- [36] R. Kohler, R. Goebel, and R. Pello, Report on the International Comparison of Spectral Responsivity of Silicon Detectors, (CCPR/94-2), Bureau International des Poids et Mesures, Cedex, France, July 27, 1994.
- [37] J. M. Bridges and W. R. Ott, Vacuum Ultraviolet Radiometry—3. Argon Mini-Arc as a New Secondary Standard of Spectral Radiance, *Applied Optics* **16** (2), 367-376 (1977).
- [38] G. Eppeldauer and J. E. Hardis, 14-Decade Photocurrent Measurements with Large-Area Silicon Photodiodes at Room-Temperature, *Applied Optics* **30** (22), 3091-3099 (1991).
- [39] G. P. Eppeldauer, Optical Radiation Measurement with Selected Detectors and Matched Electronic Circuits Between 200 nm and 20 μm , NIST Technical Note 1438 (2001).
- [40] R. Goebel, R. Pello, R. Kohler, P. Haycocks, and N. P. Fox, Comparison of the BIPM cryogenic radiometer with a mechanically cooled cryogenic radiometer from the NPL, *Metrologia* **33** (2), 177-179 (1996).
- [41] R. Kohler, R. Goebel, R. Pello, O. Touayar, and J. Bastie, First results of measurements with the BIPM cryogenic radiometer and comparison with the INM cryogenic radiometer, *Metrologia* **32** (6), 551-555 (1996).
- [42] R. Goebel, R. Pello, K. D. Stock, and H. Hofer, Direct comparison of cryogenic radiometers from the BIPM and the PTB, *Metrologia* **34** (3), 257-259 (1997).
- [43] J. E. Martin, N. P. Fox, and P. J. Key, A cryogenic radiometer for absolute radiometric measurements, *Metrologia* **21** 147-155 (1985).
- [44] L. P. Boivin and K. Gibb, Monochromator-based cryogenic radiometry at the NRC, *Metrologia* **32** (6), 565-570 (1996).

- [45] K. D. Stock, H. Hofer, J. G. S. Romero, L. P. G. Galvan, and W. Schmid, Cryogenic radiometer facility of the CENAM and first international comparison, *Metrologia* **37** (4), 269-271 (2000).
- [46] T. C. Larason, S. S. Bruce, and A. C. Parr, Spectroradiometric detector measurements : part I-ultraviolet detectors and part II-visible to near-infrared detectors, NIST Special Publications 250-41, U.S. Government Printing Office, Washington, DC (1998).
- [47] P. S. Shaw, K. R. Lykke, R. Gupta, T. R. O'brian, U. Arp, H. H. White, T. B. Lucatorto, J. L. Dehmer, and A. C. Parr, Ultraviolet radiometry with synchrotron radiation and cryogenic radiometry, *Applied Optics* **38** (1), 18-28 (1999).
- [48] P. S. Shaw, T. C. Larason, R. Gupta, S. W. Brown, R. E. Vest, and K. R. Lykke, The new ultraviolet spectral responsivity scale based on cryogenic radiometry at Synchrotron Ultraviolet Radiation Facility III, *Review of Scientific Instruments* **72** (5), 2242-2247 (2001).
- [49] P. S. Shaw, T. C. Larason, R. Gupta, S. W. Brown, and K. R. Lykke, Improved near-infrared spectral responsivity scale, *Journal of Research of the National Institute of Standards and Technology* **105** (5), 689-700 (2000).
- [50] R. C. Paule and J. Mandel, Consensus Values and Weighting Factors, *Journal of Research of the National Bureau of Standards* **87** (5), 377-385 (1982).
- [51] S. W. Brown, Personal communication, NIST (2006).
- [52] E. M. Gullikson, R. Korde, L. R. Canfield, and R. E. Vest, Stable silicon photodiodes for absolute intensity measurements in the VUV and soft x-ray regions, *Journal of Electron Spectroscopy and Related Phenomena* **80** 313-316 (1996).
- [53] K. D. Stock, Internal Quantum Efficiency of Ge Photodiodes, *Applied Optics* **27** (1), 12-14 (1988).
- [54] A. R. Schaefer, E. F. Zalewski, and J. Geist, Silicon Detector Nonlinearity and Related Effects, *Applied Optics* **22** (8), 1232-1236 (1983).
- [55] R. Austin, Personal communication, Gamma Scientific (1997).
- [56] T. C. Larason and S. S. Bruce, Spatial uniformity of responsivity for silicon, gallium nitride, germanium, and indium gallium arsenide photodiodes, *Metrologia* **35** (4), 491-496 (1998).
- [57] NIST Policy on Reporting Measurement Uncertainty website, <http://ts.nist.gov/MeasurementServices/Calibrations/policy.cfm#uncertain> (2007).
- [58] E. F. Zalewski, Radiometry and Photometry, Ch. 24 in *Handbook of Optics. vol. 2 : Devices, Measurements, and Properties*, M. Bass, E. W. Van Stryland, and D. R. Williams, eds., McGraw-Hill, New York (1995) Find pages for Ch. 24.

- [59] C. L. Wyatt, Radiometric Calibration: Theory and Methods, Academic Press, New York, NY (1978).
- [60] J. L. Gardner, Uncertainty Estimates in Radiometry, Ch. 6 in Optical Radiometry, A. C. Parr, R. U. Datla, and J. L. Gardner, eds., Elsevier Academic Press, Amsterdam (2005) 291-325.
- [61] G. P. Eppeldauer, G. Sauter, and J. L. Gardner, Uncertainties of Spectral Responsivity Measurements, in Proceedings of the CIE Symposium on Measurement Uncertainty, 2006, A. Sperling, ed., CIE Central Bureau, (2006) 133-138.
- [62] R. D. Saunders and J. B. Shumaker, Apparatus Function of a Prism-Grating Double Monochromator, Applied Optics **25** (20), 3710-3714 (1986).
- [63] N. M. Durant and N. P. Fox, Evaluation of solid-state detectors for ultraviolet radiometric applications, Metrologia **32** (6), 505-508 (1996).
- [64] R. Goebel, R. Kohler, and R. Pello, Some effects of low-power ultraviolet radiation on silicon photodiodes, Metrologia **32** (6), 515-518 (1996).
- [65] G. P. Eppeldauer, Long-Term Changes of Silicon Photodiodes and Their Use for Photometric Standardization, Applied Optics **29** (15), 2289-2294 (1990).
- [66] L. R. Canfield, J. Kerner, and R. Korde, Stability and Quantum Efficiency Performance of Silicon Photodiode Detectors in the Far Ultraviolet, Applied Optics **28** (18), 3940-3943 (1989).
- [67] R. Korde and J. Geist, Quantum Efficiency Stability of Silicon Photodiodes, Applied Optics **26** (24), 5284-5290 (1987).
- [68] R. Korde and J. Geist, Stable, High Quantum Efficiency, UV-Enhanced Silicon Photodiodes by Arsenic Diffusion, Solid-State Electronics **30** (1), 89-92 (1987).
- [69] K. D. Stock, Spectral Aging Pattern of Carefully Handled Silicon Photodiodes, Measurement **5** 141-144 (1987).
- [70] K. D. Stock and R. Heine, On the Aging of Photovoltaic Cells, Optik **71** (4), 137-142 (1985).
- [71] P. S. Shaw, R. Gupta, and K. R. Lykke, Stability of photodiodes under irradiation with a 157-nm pulsed excimer laser, Applied Optics **44** (2), 197-207 (2005).
- [72] U. Arp, P. S. Shaw, R. Gupta, and K. R. Lykke, Damage to solid-state photodiodes by vacuum ultraviolet radiation, Journal of Electron Spectroscopy and Related Phenomena **144** 1039-1042 (2005).
- [73] W. Budde, Multi-Decade Linearity Measurements on Si Photo-Diodes, Applied Optics **18** (10), 1555-1558 (1979).

- [74] J. L. Gardner and F. J. Wilkinson, Response-Time and Linearity of Inversion Layer Silicon Photodiodes, *Applied Optics* **24** (10), 1531-1534 (1985).
- [75] A. L. Migdall and C. Winnewisser, Linearity of a Silicon Photodiode at 30 Mhz and Its Effect on Heterodyne Measurements, *Journal of Research of the National Institute of Standards and Technology* **96** (2), 143-146 (1991).
- [76] H. W. Yoon, J. J. Butler, T. C. Larason, and G. P. Eppeldauer, Linearity of InGaAs photodiodes, *Metrologia* **40** (1), 154-158 (2003).
- [77] K. D. Stock, S. Morozova, L. Liedquist, and H. Hofer, Nonlinearity of the quantum efficiency of Si reflection trap detectors at 633 nm, *Metrologia* **35** (4), 451-454 (1998).
- [78] H.-M. Chen, Beamconjoiner Characteristics and Linearity Measurements of Optical Radiation Detectors, University of Alabama in Huntsville, MSE Thesis (1992).
- [79] R. D. Saunders and J. B. Shumaker, Automated Radiometric Linearity Tester, *Applied Optics* **23** (20), 3504-3506 (1984).
- [80] NIST Quality System website, <http://ts.nist.gov/qualitysystem/> (2007).
- [81] General Requirements for the Competence of Testing and Calibration Laboratories, NCSL International, Boulder, CO (2005).
- [82] T. C. Larason, The Radiometric Physics Division's Efforts at Building a Quality System Based on ISO/IEC Guide 25, Presented at the Asociacion Mexicana De Metrologia, A. C. 1994 Conference, Acapulco, Mexico (1994).
- [83] S. S. Bruce and T. C. Larason, Building a Quality System Based on ANSI/NCSL Z540 1 1994 - An Effort by the Radiometric Physics Division at NIST, Proc. National Conference of Standards Laboratories 1995 Workshop and Symposium, Dallas, TX (1995).
- [84] S. S. Bruce and T. C. Larason, Developing Quality System Documentation Based on ANSI/NCSL Z540-1-1994 -- The Optical Technology Division's Effort, NISTIR 5866 (1996).
- [85] W. Mendenhall and S. Terry, *Statistics for Engineering and the Sciences*, Dellen Pub. Co., San Francisco, CA (1992).
- [86] R. Kohler, R. Goebel, and R. Pello, Results of an international comparison of spectral responsivity of silicon photodetectors, *Metrologia* **32** (6), 463-468 (1996).
- [87] L. P. Boivin and S. S. Bruce, A bilateral comparison of spectral responsivity measurements in the spectral range 250 nm to 1800 nm between the NIST (USA) and the NRC (Canada), *Metrologia* **40** (1), S45-S49 (2003).
- [88] International Bureau of Weights and Measures (BIPM) Key Comparison Database website, <http://kcdb.bipm.org/> (2008).

- [89] P. Kuschnerus, H. Rabus, M. Richter, F. Scholze, L. Werner, and G. Ulm, Characterization of photodiodes as transfer detector standards in the 120 nm to 600 nm spectral range, *Metrologia* **35** (4), 355-362 (1998).
- [90] R. Gupta, K. R. Lykke, P. S. Shaw, and J. L. Dehmer, Characterization of UV-Induced Radiation Damage to Si-Based Photodiodes, in *Ultraviolet Atmospheric and Space Remote Sensing : Methods and Instrumentation II*, G. R. Carruthers and K. F. Dymond, eds., Society of Photo-optical Instrumentation Engineers, SPIE 3818 (1999) 27-33.
- [91] L. Werner, Ultraviolet stability of silicon photodiodes, *Metrologia* **35** (4), 407-411 (1998).
- [92] J. M. Houston and T. C. Larason, Spectral Responsivity Changes in Si Photodiodes Induced by UV Radiation, Unpublished work, National Institute of Standards and Technology (2007).
- [93] P. S. Shaw, T. C. Larason, R. Gupta, and K. R. Lykke, Characterization of UV detectors at SURF III (invited), *Review of Scientific Instruments* **73** (3), 1625-1628 (2002).
- [94] R. Korde, C. Prince, D. Cunningham, R. E. Vest, and E. Gullikson, Present status of radiometric quality silicon photodiodes, *Metrologia* **40** (1), S145-S149 (2003).
- [95] T. C. Larason, S. W. Brown, G. P. Eppeldauer, and K. R. Lykke, Responsivity calibration methods for 365-nm irradiance meters, *IEEE Transactions on Instrumentation and Measurement* **50** (2), 474-477 (2001).
- [96] T. C. Larason and Y. Ohno, Calibration and characterization of UV sensors for water disinfection, *Metrologia* **43** (2), 151-156 (2006).
- [97] G. T. Fraser, C. E. Gibson, H. W. Yoon, and A. C. Parr, "Once is enough" in radiometric calibrations, *Journal of Research of the National Institute of Standards and Technology* **112** (1), 39-51 (2007).

Appendix A: Sample Calibration Report



UNITED STATES DEPARTMENT OF COMMERCE
National Institute of Standards and Technology
Gaithersburg, Maryland 20899

REPORT OF CALIBRATION

NIST Test # 39073C - Spectral Responsivity

for

Hamamatsu Silicon Photodiode Model S2281, S/N H###

Issued to:

Big-time Laboratory
Attn.: Dr. Alyssa Scientist
100 Laboratory Road
Calibration City, CA xxxxx-xxxx

(See your Purchase Order No. ##-###, dated August 10, 2007)

1. Description of Calibration Material

The test photodiode, serial number H###, is a Hamamatsu model S2281 silicon photodiode in a 2 in diameter anodized aluminum mount. The active area of the photodiode is $\approx 1 \text{ cm}^2$.

2. Description of Calibration

The spectral radiant power responsivity of the test photodiode was determined from 350 nm to 1100 nm in 5 nm increments by comparisons to silicon photodiode working standards, H630 and H633, using the monochromator-based NIST Visible to Near-Infrared Spectral Comparator Facility (Vis/NIR SCF) [1]. The spectral comparisons between the test photodiode and working standard photodiodes were performed using a double monochromator illuminated by a quartz-halogen lamp as the tunable monochromatic source. The circular exit aperture of the Vis/NIR SCF monochromator was imaged ($\approx f/9$) on the test photodiode resulting in a beam diameter of 1.1 mm at the diode. The beam was centered on, and underfilled, the photosensitive area.

The wavelength scale of the monochromator was calibrated with several laser and emission lines to within an uncertainty of $\pm 0.1 \text{ nm}$ over the entire spectral range. The bandpass (FWHM) of the monochromator was 4 nm. The short-circuit photocurrent from the test photodiode and each working standard photodiode was measured with a calibrated transimpedance amplifier. Beam power fluctuations were monitored with a beamsplitter and silicon photodiode. The spectral radiant power responsivity scale is based on the NIST reference absolute cryogenic radiometer. The laboratory temperature during this calibration was $23.8 \text{ }^\circ\text{C} \pm 0.5 \text{ }^\circ\text{C}$.

Calibration Date: September 25, 2007
NIST Test No.: 844/#####-07

Page 1 of 8

NIST

The spatial uniformity of the responsivity across the test photodiode photosensitive area was measured at 500 nm using the described comparator facility. The uniformity was measured in 0.5 mm increments using a 1.1 mm diameter beam.

3. Results of Calibration

The spectral radiant power responsivity of the test photodiode is listed in A/W at each wavelength in Table 1 and is plotted in Fig. 1. The uncertainty in the NIST spectral radiant power responsivity scale is described in Ref. 1. The relative expanded uncertainty ($k=2$) for this measurement is listed at each wavelength in Table 1 and plotted in Fig. 1. The uncertainty budget of this spectral power responsivity calibration is summarized in Table 2.

Figure 2a is a plot of the uniformity of the test photodiode at 500 nm showing 0.2 % contours of the deviations from the responsivity at the photodiode center. Figure 2b is a 3-dimensional plot showing the responsivity relative to the center of the photodiode.

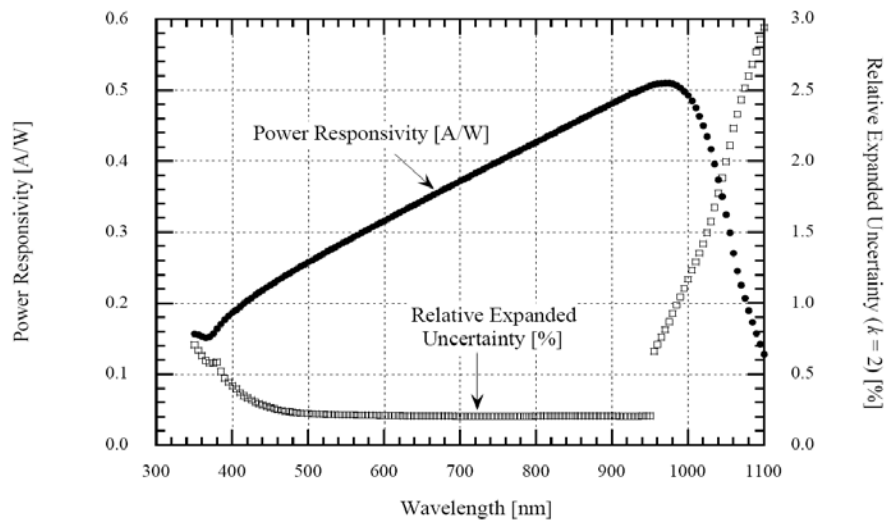


Figure 1. Spectral power responsivity of Hamamatsu silicon photodiode model S2281, S/N H###.

Table 1
Spectral power responsivity of Hamamatsu silicon photodiode model S2281, S/N H###

Wavelength [nm]	Spectral power responsivity [A/W]	Relative expanded uncertainty ($k = 2$) [%]	Wavelength [nm]	Spectral power responsivity [A/W]	Relative expanded uncertainty ($k = 2$) [%]
350	0.1567	0.70	550	0.2876	0.22
355	0.1556	0.66	555	0.2905	0.22
360	0.1533	0.62	560	0.2934	0.22
365	0.1511	0.60	565	0.2962	0.22
370	0.1526	0.58	570	0.2991	0.22
375	0.1572	0.58	575	0.3020	0.22
380	0.1636	0.58	580	0.3049	0.22
385	0.1705	0.52	585	0.3077	0.20
390	0.1769	0.48	590	0.3106	0.20
395	0.1824	0.44	595	0.3134	0.20
400	0.1870	0.42	600	0.3162	0.20
405	0.1908	0.40	605	0.3191	0.20
410	0.1953	0.36	610	0.3219	0.20
415	0.1996	0.34	615	0.3247	0.20
420	0.2037	0.34	620	0.3275	0.20
425	0.2076	0.32	625	0.3303	0.20
430	0.2114	0.30	630	0.3332	0.20
435	0.2151	0.30	635	0.3360	0.20
440	0.2187	0.28	640	0.3387	0.20
445	0.2222	0.28	645	0.3416	0.20
450	0.2257	0.26	650	0.3443	0.20
455	0.2291	0.26	655	0.3471	0.20
460	0.2325	0.24	660	0.3499	0.20
465	0.2358	0.24	665	0.3527	0.20
470	0.2390	0.24	670	0.3555	0.20
475	0.2422	0.24	675	0.3582	0.20
480	0.2454	0.24	680	0.3610	0.20
485	0.2485	0.22	685	0.3638	0.20
490	0.2517	0.22	690	0.3666	0.20
495	0.2548	0.22	695	0.3693	0.20
500	0.2578	0.22	700	0.3721	0.20
505	0.2609	0.22	705	0.3748	0.20
510	0.2639	0.22	710	0.3776	0.20
515	0.2669	0.22	715	0.3804	0.20
520	0.2699	0.22	720	0.3831	0.20
525	0.2729	0.22	725	0.3859	0.20
530	0.2758	0.22	730	0.3886	0.20
535	0.2788	0.22	735	0.3914	0.20
540	0.2817	0.22	740	0.3941	0.20
545	0.2847	0.22	745	0.3968	0.20

Table 1 (cont.)
Spectral power responsivity of Hamamatsu silicon photodiode model S2281, S/N H###

Wavelength [nm]	Spectral power responsivity [A/W]	Relative expanded uncertainty (<i>k</i> = 2) [%]	Wavelength [nm]	Spectral power responsivity [A/W]	Relative expanded uncertainty (<i>k</i> = 2) [%]
750	0.3996	0.20	925	0.4951	0.20
755	0.4023	0.20	930	0.4969	0.20
760	0.4050	0.20	935	0.4993	0.20
765	0.4078	0.20	940	0.5020	0.20
770	0.4105	0.20	945	0.5040	0.20
775	0.4133	0.20	950	0.5057	0.20
780	0.4160	0.20	955	0.508	0.66
785	0.4187	0.20	960	0.509	0.70
790	0.4215	0.20	965	0.510	0.76
795	0.4242	0.20	970	0.510	0.82
800	0.4269	0.20	975	0.510	0.86
805	0.4297	0.20	980	0.509	0.92
810	0.4324	0.20	985	0.507	0.98
815	0.4351	0.20	990	0.503	1.0
820	0.4378	0.20	995	0.499	1.1
825	0.4406	0.20	1000	0.493	1.2
830	0.4433	0.20	1005	0.485	1.2
835	0.4460	0.20	1010	0.475	1.3
840	0.4487	0.20	1015	0.464	1.4
845	0.4515	0.20	1020	0.450	1.4
850	0.4542	0.20	1025	0.435	1.5
855	0.4569	0.20	1030	0.417	1.6
860	0.4597	0.20	1035	0.396	1.7
865	0.4623	0.20	1040	0.374	1.8
870	0.4650	0.20	1045	0.350	1.9
875	0.4678	0.20	1050	0.325	2.0
880	0.4704	0.20	1055	0.299	2.2
885	0.4732	0.20	1060	0.271	2.2
890	0.4759	0.20	1065	0.245	2.4
895	0.4786	0.20	1070	0.226	2.4
900	0.4814	0.20	1075	0.207	2.6
905	0.4841	0.20	1080	0.190	2.6
910	0.4868	0.20	1085	0.173	2.6
915	0.4895	0.20	1090	0.157	2.8
920	0.4923	0.20	1095	0.142	2.8
			1100	0.128	3.0

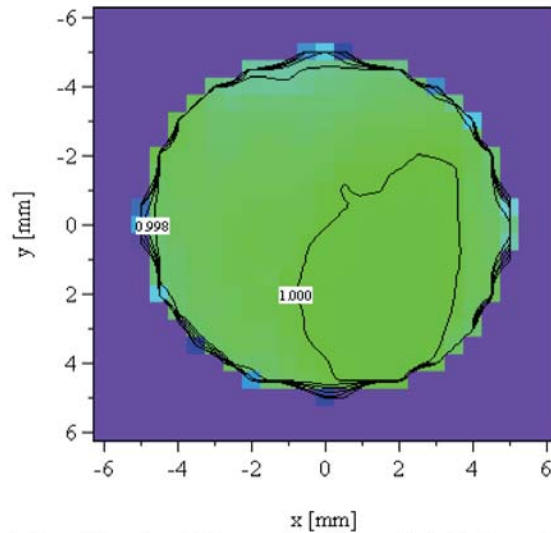


Figure 2a. Responsivity uniformity of Hamamatsu silicon photodiode model S2281, S/N H###: 0.2 % contours at 500 nm; 1.1 mm resolution; 0.5 mm/Step.

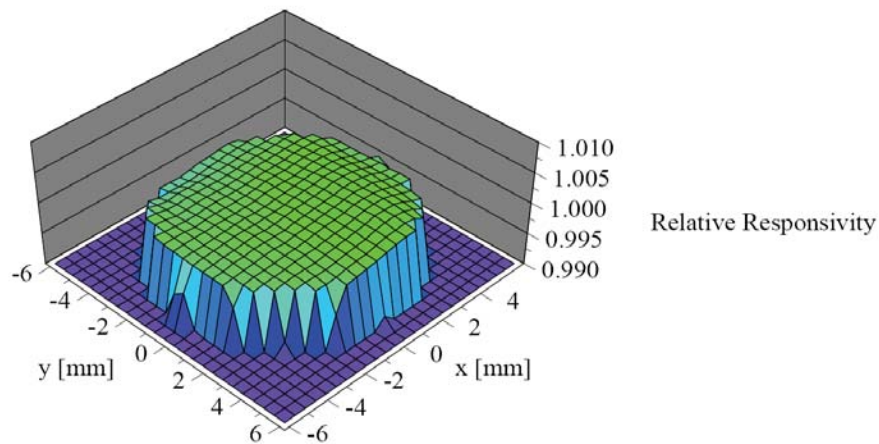


Figure 2b. Surface plot of the responsivity relative to the center of photodiode for Hamamatsu silicon photodiode model S2281, S/N H### at 500 nm; 0.5 mm/Step.

Table 2
Spectral power responsivity uncertainty budget summary for Hamamatsu model S2281, S/N H###

Wavelength [nm]	Uncertainty contribution from each component of uncertainty [%]							Relative combined uncertainty [%]	Relative expanded uncertainty (k = 2) [%]
	Vis WS calibration 2006	Customer- to-monitor ratio noise	Vis WS-to- monitor ratio noise	Customer & Vis WS amplifier calibration	Monochro- mator wavelength	Bandpass error	Reproduci- bility and other components		
	Type B	Type A	Type A	Type B	Type B	Type B	Type A		
350	0.30	0.03	0.04	0.06	0.01	0.02	0.17	0.35	0.70
375	0.25	0.01	0.01	0.06	0.09	0.01	0.10	0.29	0.58
400	0.18	0.00	0.01	0.06	0.06	0.01	0.05	0.21	0.42
425	0.14	0.00	0.00	0.06	0.04	0.00	0.03	0.16	0.32
450	0.11	0.00	0.00	0.06	0.03	0.00	0.01	0.13	0.26
475	0.10	0.00	0.00	0.06	0.03	0.00	0.01	0.12	0.24
500	0.09	0.00	0.00	0.06	0.03	0.00	0.01	0.11	0.22
525	0.09	0.00	0.00	0.06	0.02	0.00	0.01	0.11	0.22
550	0.08	0.00	0.00	0.06	0.02	0.00	0.01	0.11	0.22
575	0.08	0.00	0.00	0.06	0.02	0.00	0.01	0.11	0.22
600	0.08	0.00	0.00	0.06	0.02	0.00	0.01	0.10	0.20
625	0.08	0.00	0.00	0.06	0.02	0.00	0.01	0.10	0.20
650	0.08	0.00	0.00	0.06	0.02	0.00	0.01	0.10	0.20
675	0.08	0.00	0.00	0.06	0.02	0.00	0.01	0.10	0.20
700	0.08	0.00	0.00	0.06	0.02	0.00	0.01	0.10	0.20
725	0.08	0.00	0.00	0.06	0.01	0.00	0.01	0.10	0.20
750	0.08	0.00	0.00	0.06	0.01	0.00	0.01	0.10	0.20
775	0.08	0.00	0.00	0.06	0.01	0.00	0.01	0.10	0.20
800	0.08	0.00	0.00	0.06	0.01	0.00	0.01	0.10	0.20
825	0.08	0.00	0.00	0.06	0.01	0.00	0.01	0.10	0.20
850	0.08	0.00	0.00	0.06	0.01	0.00	0.01	0.10	0.20
875	0.08	0.00	0.00	0.06	0.01	0.00	0.01	0.10	0.20
900	0.08	0.00	0.00	0.06	0.01	0.00	0.01	0.10	0.20
925	0.08	0.00	0.00	0.06	0.01	0.00	0.01	0.10	0.20
950	0.08	0.00	0.00	0.06	0.00	0.00	0.01	0.10	0.20
975	0.43	0.00	0.00	0.06	0.01	0.01	0.04	0.43	0.86
1000	0.57	0.00	0.00	0.06	0.05	0.01	0.09	0.58	1.2
1025	0.70	0.00	0.00	0.06	0.11	0.02	0.21	0.75	1.5
1050	0.91	0.00	0.00	0.06	0.15	0.02	0.37	1.0	2.0
1075	1.1	0.00	0.00	0.06	0.17	0.02	0.49	1.3	2.6
1100	1.3	0.00	0.00	0.06	0.19	0.03	0.58	1.5	3.0

REPORT OF CALIBRATION

NIST Test # 39073C - Spectral Responsivity
Big-time Laboratory

Manufacturer: Hamamatsu
Model #: S2281
Serial #: H###

4. General Information

The uncertainty of the spectral radiant power responsivity will be larger than reported in Sec. 3 if the irradiation geometry is significantly different from the test conditions described in Sec. 2. The uncertainty will also increase if the ambient temperature is significantly different from reported in section 2 (The temperature coefficient of this photodiode is typically less than 0.01 % / °C in the 380 nm to 900 nm region and increases outside this region.). Such uncertainty components should be evaluated by the customer. The spectral responsivity of photodiodes is subject to drift over time. Periodic calibration is recommended.

The appendix provides operating instructions for the test photodiode.

This report shall not be reproduced, except in full, without the written approval of NIST.

Prepared by:

Reviewed by:

Jeanne M. Houston
Optical Technology Division
Physics Laboratory
(301) 975-2327

Thomas C. Larason
Optical Technology Division
Physics Laboratory
(301) 975-2334

Approved by:

Yoshihiro Ohno
For the Director,
National Institute of Standards and Technology
(301) 975-2321

References:

- [1] T. C. Larason and J. M. Houston, Spectroradiometric detector measurements: part I-ultraviolet detectors and part II-visible to near-infrared detectors, Natl. Inst. Stand. Technol., Spec. Publ. 250-41 2007 revision (2007).

Calibration Date: September 25, 2007
NIST Test No.: 844/#####-07

Page 7 of 8

REPORT OF CALIBRATION
NIST Test # 39073C - Spectral Responsivity
Big-time Laboratory

Manufacturer: Hamamatsu
Model #: S2281
Serial #: H###

Appendix: OPERATING INSTRUCTIONS FOR NIST PHOTODIODE

The NIST characterized photodiode consists of a silicon photodiode with a quartz window and a BNC connector.

- A. The photodiode should be rigidly mounted on a dual-axis tilt mount such that the photodiode can be tilted about two orthogonal axes. The photodiode should be adjusted to be perpendicular to the incident radiation.
- B. The incident beam of radiation should be smaller than the active area, and should be centered in the photodiode active area.
- C. The photodiode should be connected with a BNC cable to an electrometer grade amplifier (transimpedance amplifier) which measures the current from the photodiode.
- D. The diode window can be cleaned with lens tissue and spectral grade solvent.

Calibration Date: September 25, 2007
NIST Test No.: 844/#####-07

Page 8 of 8

Appendix B: Bibliography

Optics

E. Hecht, *Optics*, 2nd edition, Addison-Wesley Publishing Company, 1987.

F. L. Pedrotti and L. S. Pedrotti, *Introduction to Optics*, 2nd edition, Prentice Hall, Englewood Cliffs, NJ, 1993.

F. A. Jenkins and H. E. White, *Fundamentals of Optics*, 4th edition, McGraw-Hill, New York, NY, 1976.

M. Born and E. Wolf, *Principles of Optics*, 6th (corrected) edition, Pergamon Press, Oxford, England, 1993.

Applied Optics and Optical Engineering, Vol. V, Optical Instruments, R. Kingslake, editor, Academic Press, San Diego, CA, 1969.

D. C. O'Shea, *Elements of Modern Optical Design*, Wiley, New York, NY, 1985.

W. J. Smith, *Modern Optical Engineering*, 2nd edition, McGraw-Hill, New York, NY, 1990.

Military Handbook 141, Optical Design, U. S. Department of Defense, Washington, D. C., 1962.

Handbook of Optics, Vol. I and II, 2nd edition, M. Bass, editor-in-chief, McGraw-Hill, New York, NY, 1995.

The Optics Problem Solver, Research and Education Association, Piscataway, NJ, 1990 revision.

E. Hecht, *Schaum's Outline of Theory and Problems of Optics*, McGraw-Hill, New York, NY, 1975.

Detectors and Amplifiers

Determination of the Spectral Responsivity of Optical Radiation Detectors, CIE Publication 64 (Commission Internationale de l'Eclairage, Paris, 1984). Available for sale on-line through the International Commission on Illumination (CIE) website, <http://www.cie.co.at/cie/>.

E. L. Dereniak and D. G. Crowe, *Optical Radiation Detectors*, Wiley, New York, NY, 1984.

E. L. Dereniak and G. D. Boreman, *Infrared Detectors and Systems*, Wiley, New York, NY, 1996.

G. H. Rieke, *Detection of Light: from the Ultraviolet to the Submillimeter*, Cambridge University Press, New York, NY, 1994.

J. D. Vincent, *Fundamentals of Infrared Detector Operation and Testing*, Wiley, New York, NY, 1990.

- T. M. Frederiksen, *Intuitive Operational Amplifiers*, McGraw-Hill, New York, NY, 1988.
- J. G. Graeme, *Photodiode Amplifiers: Op Amp Solutions*, McGraw-Hill, New York, NY, 1996.
- D. L. Terrell, *Op Amps: Design, Application, and Troubleshooting*, Butterworth-Heinemann, Newton, MA, 1996.
- P. Horowitz and W. Hill, *The Art of Electronics*, 2nd edition, Cambridge University Press, New York, NY, 1989.
- S. M. Sze, *Physics of Semiconductor Devices*, 2nd edition, Wiley, New York, NY, 1981.
- S. M. Sze, *Semiconductor Devices, Physics and Technology*, Wiley, New York, NY, 1985.

Radiometry

- Optical Radiometry*, A. C. Parr, R. U. Datla, and J. L. Gardner, editors, Elsevier Academic Press, New York, NY, 2005.
- Reliable Spectroradiometry*, H. J. Kostkowski, Spectroradiometry Consulting, La Plata, MD (1997).
- The Self-Study Manual on Optical Radiation Measurements (NBS 910-1 through 910-8) website, <http://physics.nist.gov/Divisions/Div844/manual/studymanual.html> (2007).
- Optical Radiation Measurements*, F. Grum and C. J. Bartleson, editors, *Vol. 1: Radiometry*, F. Grum and R. J. Becherer; *Vol. 4: Physical Detectors of Optical Radiation*, W. Budde. Academic Press, San Diego, CA, Vol. 1: Vol. 4: 1983.
- Absolute Radiometry: Electrically Calibrated Thermal Detectors of Optical Radiation*, F. Hengstberger, editor, Academic Press, San Diego, CA, 1989.
- C. L. Wyatt, *Radiometric Calibration: Theory and Methods*, Academic Press, San Diego, CA, 1978.
- C. L. Wyatt, *Electro-Optical System Design: For Information Processing*, McGraw-Hill, New York, NY, 1991. Expanded and revised version of the author's *Radiometric System Design*.
- W. R. McCluney, *Introduction to Radiometry and Photometry*, Artech House, Norwood, MA, 1994.
- R. W. Boyd, *Radiometry and the Detection of Radiation*, Wiley, New York, NY, 1983.
- R. H. Kingston, *Optical Sources, Detectors, and Systems: Fundamentals and Applications*, Academic Press, San Diego, CA, 1995.
- R. H. Kingston, *Detection of Optical and Infrared Radiation*, Springer-Verlag, New York, NY, 1978.

New Developments and Applications in Optical Radiometry III, *Metrologia* **28** (3) 1991.
New Developments and Applications in Optical Radiometry IV, *Metrologia* **30** (4) 1993.
New Developments and Applications in Optical Radiometry V, *Metrologia* **32** (6) 1996.
New Developments and Applications in Optical Radiometry VI, *Metrologia* **35** (4) 1998.
New Developments and Applications in Optical Radiometry VII, *Metrologia* **37** (5) 2000.
New Developments and Applications in Optical Radiometry VIII, *Metrologia* **40** (1) 2003.
New Developments and Applications in Optical Radiometry IX, *Metrologia* **43** (2) 2006.

Statistics/Error Analysis/Uncertainties

P. R. Bevington, *Data Reduction and Error Analysis for the Physical Sciences*, McGraw-Hill, New York, NY, 1969.

J. R. Taylor, *An Introduction to Error Analysis: The Study of Uncertainties in Physical Measurements*, University Science Books, Mill Valley, CA, 1982.

ANSI/NCSL Z540-2-1997, American National Standard for Expressing Uncertainty-U.S. Guide to the Expression of Uncertainty of Measurement. Available for sale on-line through the NCSL International website, <http://www.ncsli.org/>.

National Conference of Standard Laboratories (NCSL) Secretariat, 1800 30th Street, Suite 305B, Boulder, CO 80301.

B. N. Taylor and C. E. Kuyatt, Guidelines for Evaluating and Expressing the Uncertainty of NIST Measurement Results, Natl. Inst. Stand. Technol. (US), Tech. Note 1297 (1994 ed.). Also available on-line, <http://physics.nist.gov/Document/tn1297.pdf>.

W. Mendenhall and T. Sincich, *Statistics for Engineering and the Sciences*, 3rd edition, Dellen Publishing Company, San Francisco, CA, 1992.

NBS Handbook 91, Experimental Statistics, Natl. Bur. Stand. (U.S.), NBS HDBK 91, 1963.

Precision Measurement and Calibration, Harry Ku, editor, Natl. Bur. Stand. (U.S.), Spec. Publ. 300, Vol. 1, 1969.

Quality and Laboratory Accreditation

ANSI/ISO/IEC 17025:2005, General Requirements for the Competence of Testing and Calibration Laboratories. Available for sale on-line through the NCSL International website, <http://www.ncsli.org/>.

NIST Handbook 150, National Voluntary Laboratory Accreditation Program Procedures and General Requirements, C. D. Faison, J. Horlick, W. R. Merkel, V. R. White, Editors, 2006. Available on-line at <http://ts.nist.gov/Standards/214.cfm>.